UNIVERSITEIT VAN PRETORIA
UNIVERSITY OF PRETORIA
YUNIBESITHI YA PRETORIA

Suspension forces on a tri-axle air suspended semi-trailer

by

Cor-Jacques Kat

Submitted in partial fulfilment of the requirements for the degree

Master of Engineering

in the Faculty of

Engineering, Built Environment and Information Technology

University of Pretoria, Pretoria

February 2009

100
1908 - 2008

UNIVERSITEIT VAN PRETORIA
UNIVERSITY OF PRETORIA
YUNIBESITHI YA PRETORIA

Suspension forces on a tri-axle air suspended semi-trailer

Author: Cor-Jacques Kat
Supervisor: Prof. P.S. Els
Department: Mechanical and Aeronautical Engineering
Degree: Master of Engineering

Keywords: validated trailer model, validated air spring model, rough road, force correlation.

Abstract

The aim of this study is to investigate the use of multi-body vehicle simulation models to predict the suspension forces acting on the chassis of the vehicle, in order to perform durability analyses.

Traditionally, durability of vehicles is evaluated with proving ground tests. This implies that a physical prototype of the vehicle is required before its durability can be evaluated. If we were able to evaluate the durability of the vehicle without any physical part or a full prototype of the vehicle available, great cost and time savings may be gained. These possible gains have lead to the use of computer aided engineering (CAE) tools. These tools have supplemented the proving ground durability test by using historical measured data and/or predicted data from vehicle simulation models, as input to the durability analyses i.e. Finite Element Analyses (FEA). The usefulness of the historical test data is limited and many of the vehicle simulation models that are used to predict the input data, have not been validated.

In this study a validated mathematical model of a 40 ton flat bed tri-axle semi-trailer, able to predict the suspension forces, is created. The validation of the full vehicle model includes correlations for displacements, velocities, accelerations and forces of various vehicle parameters. A validated mathematical model of the air springs, that includes mass transfer and flow effects for use in full vehicle dynamic simulations, is also developed.

The results obtained indicate that the air spring model, integrated into the full vehicle model, is able to give relative accurate predictions of displacements, velocities, accelerations and forces of various vehicle parameters, over a discrete road event and over a rough road.

Suspensiekragte op ’n drie-as luggeveerde semi-sleepwa

Outeur: Cor-Jacques Kat
Studieleier: Prof. P.S. Els
Departement: Meganiese en Lugvaartkundige Ingenieurswese
Graad: Magister in Ingenieurswese

Sleutelwoorde: gevalideerde sleepwa model, gevalideerde lugveermodel, rowwe pad, kragte korrelasie.

Opsomming

Die doel van die studie is om die gebruik van voertuigsimulasiemodelle vir die voorspelling van die suspensiekragte wat inwerk op die onderstel van die voertuig, te ondersoek met die oog op gebruik in uithouvermoë analises.

Die uithouvermoë van voertuie word tradisioneel geëvalueer aan die hand van padtoetse. Hierdie prosedure impliseer dat ’n fisiese prototipe van die voertuig benodig word voordat die voertuig se uithouvermoë geëvalueer kan word. As dit moontlik was om die voertuig se uithouvermoë te evalueer, sonder dat enige fisiese onderdele of ’n volledige prototipe van die voertuig beskikbaar is, kan noemenswaardige koste-en tydbesparings verkry word. Hierdie moontlike voordele het gelei tot die gebruik van rekenaargesteunde ingenieurshulpmiddels. Hierdie hulpmiddels het die padtoetse aangevul deur historiese gemete data, en/of voorspelde data verkry vanaf voertuig simulasie modelle, te gebruik om die insetdata te bekom wat benodig word vir uithouvermoë analises o.a. Eindige Element Analises. Die bruikbaarheid van die historiese data is beperk en baie van die voertuig simulasiemodelle wat gebruik word om die data te voorspel, is nie gevalideer nie.

In hierdie studie word ’n gevalideerde wiskundige model van ’n 40 ton platbak drie-as semi-sleepwa, met die vermoë om die kragte te voorspel, geskep. Die validasie van die voertuig simulasiemodel sluit in korrelasie van verplasings, snelhede, versnellings en kragte van verskillende voertuig parameters. ’n Gevalideerde wiskundige model van die lugvere, wat massa-oordrag en die vloei-effekte insluit vir gebruik in dinamiese voertuig simulasiemodelle, is ook ontwikkel.

Die resultate dui daarop dat die lugveermodel, geïntegreer met die voertuigmodel, daartoe in staat is om relatiewe akkurate voorspellings te maak van die verplasings, snelhede, versnellings en kragte van verskillende voertuig parameters, oor ’n diskrete hindernis en oor ’n rowwe pad.

Table of Contents

Abbreviations

ADAMS	Automatic Analysis of Mechanical Systems
BIW	Body-in-White
CAD	Computer Aided Design
CAE	Computer Aided Engineering
FE	Finite Element
FEA	Finite Element Analysis
FFT	Fast Fourier Transform
GPS	Global Positioning System
MBS	Multi-Body Simulation
rms	Root-Mean-Squared
SUV	Sports Utility Vehicle
VPG	Virtual Proving Ground

List of symbols

A	Area
A_1	Area at state 1
A_2	Area at state 2
b	Width of cross section
d	Diameter
E	Young's modulus of elasticity
F	Force
F_{as}	Force exerted by air spring
$F_{\text{Left front}}$	Force exerted by left front air spring
$F_{\text{Left middle}}$	Force exerted by left middle air spring
$F_{\text{Left rear}}$	Force exerted by left rear air spring
$F_{\text{Right front}}$	Force exerted by right front air spring
$F_{\text{Right middle}}$	Force exerted by right middle air spring
$F_{\text{Right rear}}$	Force exerted by right rear air spring
F_1	Force exerted by stand-alone air spring at state 1
F_2	Force exerted by stand-alone air spring at state 2
f	Darcy friction factor
f_s	Sample frequency
G	Shear modulus of elasticity
g	Earth's gravitational constant (= 9.81m/s^2)
h	Height of cross section
h_f	Head loss
I_P	Polar moment of inertia
$I_{P,inner}$	Polar moment of inertia of inner area
$I_{P,outer}$	Polar moment of inertia of outer area
k_T	Torsional stiffness
L	Length
m	Mass
m_e	Mass entering or exiting the control surface
P	Pressure
P_1	Pressure of the stand-alone air spring at state 1
P_2	Pressure of the stand-alone air spring at state 2
${}_{sys}P$	Pressure of interconnected system
${}_{sys}P_1$	Pressure of interconnected system at state 1

$_{sys}P_2$	Pressure of interconnected system at state 2
$_{sys2}P_{1,j}$	Pressure of the front-middle-rear interconnected system at state 1
$_{sys2}P_{2,j}$	Pressure of the front-middle-rear interconnected system at state 2
$_{sys3}P_{1,k}$	Pressure of the left-right interconnected system at state 1
$_{sys3}P_{2,k}$	Pressure of the left-right interconnected system at state 2
Δp	Pressure difference
Q	Summation of volume flow in the three branches
q	Volume flow
R	Gas constant
Re_d	Reynolds number
T	Temperature
V	Volume
V_1	Volume of stand-alone air spring at state 1
V_2	Volume of stand-alone air spring at state 2
$_{sys}V$	Volume of the interconnected system
$_{sys}V_1$	Volume of the interconnected system at state 1
$_{sys}V_2$	Volume of the interconnected system at state 2
$_{sys2}V_1$	Volume of the front-middle-rear interconnected system at state 1
$_{sys2}V_{2,j}$	Volume of the front-middle-rear interconnected system at state 2
$_{sys3}V_1$	Volume of the left-right interconnected system at state 1
$_{sys3}V_{2,k}$	Volume of the left-right interconnected system at state 2
ΔV	Change in volume of a stand-alone air spring
ΔV_{sys}	Change in volume of the interconnected system
$\Delta V_{sys2,j}$	Change in volume of the front-middle-rear interconnected system for the j^{th} axle
$\Delta V_{sys3,k}$	Change in volume of the left-right interconnected system
v	Velocity
Δt_{inner}	Inner loop time step
x	Relative displacement of air spring
x_1	Relative displacement of air spring at state 1
x_2	Relative displacement of air spring at state 2
x_{o1}	Non-geometrical length of air spring at state 1
x_{o2}	Non-geometrical length of air spring at state 2
Δx	Relative deformation of the air spring

Greek symbols

ε	Roughness value for ducts
ρ	Density
ν	Poison ratio

List of figures

Figures in Chapter 1

Figures in Chapter 2

Figures in Chapter 3

Figures in Chapter 4

Figures in Appendix A

Figures in Appendix B

Figures in Appendix C

List of figures

Figures in Chapter 1

Figures in Chapter 2

Figures in Chapter 3

Figures in Chapter 4

Figures in Appendix A

Figures in Appendix B

Figures in Appendix C

Figures in Appendix D

Figures in Appendix E

Figures in Appendix F

Figures in Appendix G

Figures in Appendix D

Figures in Appendix E

Figures in Appendix F

Figures in Appendix G

Chapter 1

Introduction

The ever increasing demand for new and improved products in the vehicle industry has decreased the time available for the development of new vehicles, but at the same time the demands on quality, reliability and mass that are set for the vehicle, by both the consumer and the manufacturer, are becoming ever more stringent. These requirements have lead to the investigation of procedures and methodologies that will reduce the development time of a new vehicle without inhibiting the quality, durability or mass of the vehicle.

To address the demand for faster, better and cheaper vehicle development and the current design drivers like lightweight vehicular structures and improved durability, computer aided design (CAD) and computer aided engineering (CAE) tools have been used extensively through the years and their role in the development phase is on the increase. These tools enable the evaluation of the vehicle's characteristics such as ride, handling, durability, etc. at a very early stage of the vehicle's development even without any physical parts or the vehicle being available. There is a clear advantage in using these tools in the development of new vehicles, as the design engineer is now enabled at an early stage of development to identify possible shortfalls in the design that may cause the vehicle not to perform as required. This avoids expensive iterations using physical prototypes or sending a sub-quality vehicle into the field.

One of the main advantages of being able to evaluate the vehicle without having the physical vehicle available for tests, is that the evaluation can be done early on in the development life cycle. This may eliminate a costly iteration of one or all of the processes preceding the evaluation process. An example of such an iteration is shown in Figure 1.1 and Figure 1.2. In this example the vehicle can only be evaluated after it has been manufactured. If the vehicle does not pass the evaluation, the problem has to be analysed to determine why it occurred and to which process in the development life cycle has to be returned to fix this problem (see Figure 1.1). If, for argument's sake, the problem was a design error, the next iteration starts at the design process but with a cost offset. It would therefore be advantageous if the evaluation process could be done at an earlier stage to detect design errors and thus minimising the total development cost of the vehicle by reducing the cost offset of each development life cycle iteration.

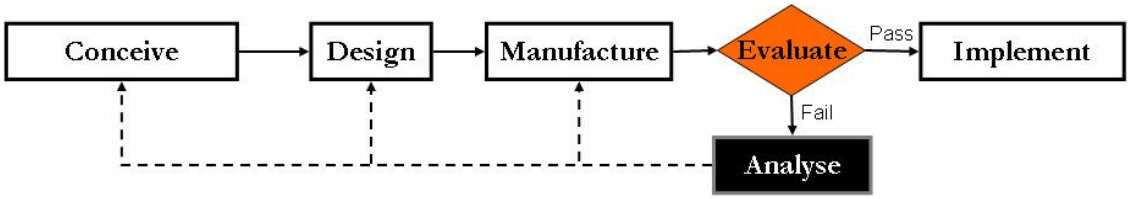

Figure 1.1. Typical product development life cycle.

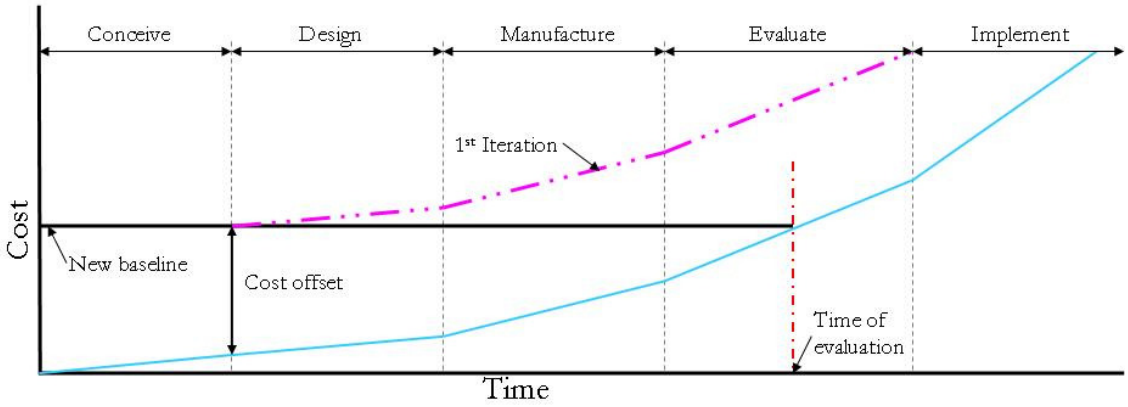

Figure 1.2. Typical product development life cycle cost.

From the above example it is clear that there are considerable gains to be obtained from enabling the design engineer to evaluate vehicle characteristics in the concept phase of the development life cycle. However, the design engineer will not have the physical vehicle available for evaluation at this early stage of the development. The solution to this problem is to make use of computerised mathematical models, also called Multi-Body Simulation (MBS) models that are mathematical representatives of the physical vehicle. The MBS model can then be used to predict vehicle characteristics and aid in the evaluation of the vehicle.

The following section will look at some other reasons why MBS models are used and the roles they have played in previous work.

1.1 Literature study

The literature study will serve as a brief introduction to this field of study, and from the literature study the problem statement and aim of this particular study will be derived. The literature study is divided into three sections explaining why we want to use MBS models, how MBS models have been used in previous studies and then the importance of validating the MBS models before using it for making key engineering and business decisions.

1.1.1 Why use MBS models?

Kuo and Kelkar (1995) states that traditionally the automotive industry has relied heavily on physical proving ground tests for the detection of vehicle body structural durability failures. But, when a vehicle passes durability tests, it is very difficult to identify if there

are areas that have been over-designed. Furthermore, as previously mentioned, being able to evaluate the vehicle's characteristics early on in the development life cycle has the advantage of reducing time and cost of vehicle development. Being able to predict ride, handling, durability, etc. of a vehicle and performing sensitivity studies on the vehicle characteristics due to changes in the design of certain components, makes the use of MBS models very attractive. If MBS models are able to predict loads it will imply that one of the crucially needed input parameters, namely loading, to the structural analysis methods can be determined early on in the development phase of the vehicle.

Fatigue problems are generally solved by addressing the three major aspects of the phenomenon namely material properties, the effects of geometry, and the input load histories. The material properties, geometry, and loading histories are the required input data for fatigue analysis. Wannenburg (2007) and others (Broek (1988), Svensson (1997), Dressler and Kottgen (1999), Socie and Pompetzki (2004)) indicate that defective structural designs are mostly caused by insufficient knowledge of the input data, rather than inadequate analysis or testing methods. Wannenburg (2007) also states that "of the input data required, geometry is usually well-defined. In some cases, notably with fatigue crack initiation and propagation analysis, the accuracy of material properties presents difficulties. In the vast majority of practical applications, however, the major concern involves the determination of input loading". Figure 1.3 shows the framework for the summary of Fatigue Design Methods (adapted from Wannenburg (2007)). This summary shows the importance of the input loads as it forms the basis for Fatigue Design Methods. When the time load histories are known, quasi-static or dynamic finite element analysis (FEA) can be performed. Vehicles (and these include motor vehicles, airplanes, ships, spacecraft etc.) are one of the many fields where structures are found to be under considerable dynamic loading and this may possibly lead to the violation of certain assumptions of the quasi-static method. It will therefore be advantageous, when designing these structures, to be able to include the loading due to the dynamic conditions and to evaluate the structure's response to these dynamic loads.

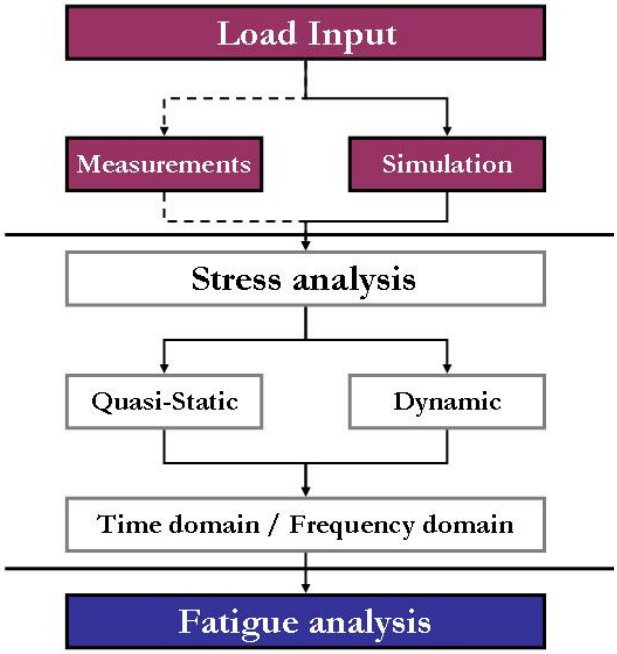

Figure 1.3. Framework for summary of Fatigue Design Methods. (Adapted from Wannenburg (2007)).

Loads associated with automotive and transport structures are nontrivial to quantify. These input loads can be obtained through measurement but this then places the restriction of not being able to perform durability analysis on a vehicle body-structure early on in the development life cycle of the vehicle. This restriction might be avoided by making use of MBS models to predict the input loading. Conle and Chu (1997) states that at the time, loads could not be predicted reliably from full vehicle simulations. As will be stated later, this will be one of the main aims of our current study.

1.1.2 Role of MBS models in previous studies

Simulation of commercial vehicles started in the 1950's with mathematical modelling applied to various aspects of vehicle directional response, but computer analysis of the models did not become a realistic possibility until the 1960's. Bernard and Shannan (1990) give a history of the simulation of commercial vehicles. They start with the early models used in the 1950's and progress to the multi-body models of the late 1980's. With computers becoming ever more powerful as hardware and software improve, the use of MBS models has been playing an increasingly important role in the prediction of vehicle characteristics.

MBS models have been used to predict vehicle characteristics like ride, handling, durability, etc. They have also been used in the optimisation of various of these vehicle characteristics in studies by Chandrasekaran *et al* (2002), Edara and Shih (2004), Uys *et al* (2007), Els *et al* (2006) and Haiba *et al* (2003). Mousseau *et al* (1999) state in their study that, "it has become common practice to use computer modelling to evaluate vehicle dynamics performance. This approach has proved to be very effective for predicting the handling performance of vehicles; however, it has proved less successful for predicting the vehicle response at frequencies that are of interest in ride harshness and durability applications". They contribute the lack in correlation between theory and experiment partially to tyre models that are inadequate for rough road simulation. They addressed this tyre problem in their study by modelling the tyre using nonlinear finite element methods and their combined tyre and vehicle simulation model was able to predict the vertical spindle forces, for a mid-size automobile, very accurately when driving through a pot hole. This seems to be in contradiction as the tyre model was developed for rough road simulation but was only validated over a discrete obstacle. A similar remark towards the tyre model is made by Anderson *et al* (2001) in their development of an ADAMS multi-body dynamics model of a tractor semi-trailer for use as a predictive tool in evaluating ride quality design improvements. Results from the simulations with the axle motions driven by test data were compared to measured accelerations collected on the test vehicle over various terrains and show good correlation for the vertical accelerations. This method of exciting the model for correlation purposes was selected for reasons having to do with some of the inherent difficulties associated with the tyre representations in MBS models. The extremely important effect of the tyre model on the predictions of the MBS model will also be shown later in this study.

In the study by Ferry *et al* (2002) they describe a project to model a compact sport utility vehicle (SUV) so as to mirror as closely as possible the behaviour of the physical vehicle for it to be used for the following:

- To assist in determining the vehicles' durability characteristics under varying road conditions,

- to assess vehicle responses by using different suspension components or payloads and,
- to observe potential issues associated with the vehicle structure, suspension components or payload positioning through simulation prior to performing physical tests.

It is also stated in this study that this process has the potential to reduce vehicle development cost and time. Their virtual dynamic vehicle model was created in ADAMS. The vertical, lateral and longitudinal displacements and longitudinal and lateral forces are inputs to the virtual model at each spindle point on the axles. It seems that the drawback of the way the vehicle was modelled, is that to simulate the response of the vehicle over different roads the physical vehicle has to drive over these roads first as to obtain the vertical, lateral and longitudinal displacements and longitudinal and lateral forces as inputs to the virtual model. At the time the article was published only accelerations of the virtual and physical model had been compared.

The proposed modelling of the MBS model as in Anderson *et al* (2001), using the method of driving the axle motions of the model by test data, imposes similar constraints on the use of the MBS model as in the study of Ferry *et al* (2002). Both these MBS models first need experimentally measured data before they can be used, which implies that a physical prototype of the trailer is needed before the MBS model can be used. This eliminates the possibility of using the MBS model in the concept design phase of the vehicle.

In a study by Chen *et al* (2006) they apply the virtual proving ground (VPG) approach for vehicle durability load prediction for a minivan over three different road events. The road events consisted of two short events (pothole and curb island), and one long event (resonance road). Correlation between the left and right front spindle forces and the left, front and rear, and the right rear sub-frame body mounting forces were shown and relatively good correlation was obtained.

Edara *et al* (2005) conducted a study also using VPG simulation studies to predict the durability performance of a trailer suspension frame. They state, similarly to Chen *et al* (2006), that “accurate loads at the early stage of product development will help to reduce the number of design changes and thereby shortening of the product development time and cost. Traditionally, the structural durability studies are carried out using generic load cases or based on the measurements from the previous vehicle”. This provides preliminary guidance for the design engineer, but errors and inaccuracies in this data may add uncertainty to the prediction and the resulting design decisions made based on these results. Edara *et al* (2005) also used VPG to predict the stress- and strain time histories, spindle loads and the component fatigue life for a given road input. The road inputs used in the study of Edara *et al* (2005) were discrete events namely staggered bumps, potholes and calibrated bumps. The VPG simulation model was validated only against vertical displacement and acceleration of the wheel spindles. The predicted spindle loads were not correlated with the measured loads in this study as the spindle loads were yet to be measured using wheel force transducers.

In a study by Gopalakrishnan and Agrawal (1993) they state the need for identifying durability problems in automotive body structures, due to road loads, early in the design process. This needs to be done in order to reduce the design, engineering, manufacturing, tooling and prototype cost and timing. Furthermore, automotive industries have developed

many durability requirements which have to be met before they go into production. The vehicles are usually tested by driving them over a predefined durability track consisting of many events; each event corresponding to a predefined road profile. They state that this "find and fix" testing process is very expensive and time consuming. To help expedite the process and reduce cost, simulation should be used. Dynamic simulation can then also be used to solve for the high number of loads acting on the body attachment locations overcoming the practical difficulties in measuring these loads. The loads on the passenger car Body-In-White (BIW) were generated with an ADAMS model. It was found that the predicted loads did not compare well with previously measured data and scale factors were used to correct the load levels.

In the study of Huizinga *et al* (2002), they state that the fatigue life of a car is traditionally verified by performing endurance tests. These tests have two major drawbacks: 1) they are generally time consuming, and 2) they require the availability of physical parts or even complete cars. The use of computed loads to enable a fatigue analysis has the obvious advantage that no physical parts or vehicle is needed. Loads predicted with their MBS model of the car and the physical measured loads in a link arm seem to correlate quite well. This was the only correlation shown in this study.

In a similar study by Cosme *et al* (1999), a multi-body dynamics model of a full truck and trailer was created to simulate handling, roll stability, ride performance, and durability loading. The model was used to evaluate the effect of design changes to the truck frame, but the simulation model was not yet validated against the physical vehicle.

Dietz *et al* (1998) state that lightweight vehicles are more likely to be faced with vibrational and fatigue life problems. They show the benefits of a new method to predict fatigue lifetime by using a bogie frame of a freight locomotive. They compute the dynamic loads that act on the bogie by a multi-body simulation model. These loads are then transferred to a FE-code that calculates the stresses and based on these stresses the fatigue life prediction is carried out. None of these loads or stresses had been verified against measured results. Various similar studies (Kuo and Kelkar (1995), Haiba *et al* (2002), Zhang *et al* (2005) and Chase (2001)) have looked at fatigue life prediction in automotive structures and components, but either used measured loads or loads obtained from MBS models that have not been verified against measured results.

Luque and Mántaras (2003) propose a three-dimensional model of a tri-axle air suspended semi-trailer to evaluate the dynamic response of heavy vehicle combinations common in Europe. They modelled the air springs using the effective length as an input variable and then give the force as output. Their model of the air springs did not include the interconnection between the air springs and thus the air springs were modelled as stand-alone units. The effect of modelling the air spring as stand-alone units will be discussed later in Chapter 3 of the current study. Their model of the heavy vehicle combinations were not validated against measured results.

In each of the studies discussed above, we noted what had been done with respect to validation of the MBS models. This was mentioned intentionally as this is a very important topic in the world of simulation and its importance is discussed in more detail in the next section.

1.1.3 Importance of validation of MBS models

It has been mentioned numerous times, and also pointed out by McBeath (2000), that virtual prototyping is considerably faster than the 'traditional' physical methods. But the process still requires physical validation if it is to be meaningful as a design verification tool. This may imply that physical testing may never be eliminated, but the number of tests and costly redesign cycles over the vehicle's development life cycle can be reduced. A similar remark is made by Huizinga *et al* (2002) namely that incorporating CAE for predicting vehicle characteristics and simultaneously replacing physical tests is not without risk. Underpinning the process purely with CAE predictions, without performing any physical tests, can result in an unpredictable shortcoming in the design.

Validation, as defined by Bernard and Clover (1994), is the process of gaining confidence that the calculations yield useful insights into the behaviour of the simulated vehicle. In Heydinger *et al* (1990) they state that a computerised mathematical model of a physical system will be considered to be valid if, within some specified operating range[1] of a system, a simulation's predictions of a system's responses of interest to specified input(s)[2] agree with the actual physical system's responses to the same input(s) to within some specified level of accuracy. Two points that may impose limits on the validity of the use of the simulations model are 1) operating range and 2) input(s).

1) Heydinger *et al* (1990) state that a simulation model's predictions will, in general, only be correct within some portion of the system's operating range. They give the obvious example of a vehicle dynamics simulation model's predictions being correct for low lateral acceleration manoeuvres but may become progressively worse as lateral acceleration increases and non-linear effects become more important.
2) Similarly, a simulation model's predictions may only hold for certain inputs. This, for example, may refer to the frequency content of the inputs. As many vehicle simulations may be valid for steady state and slowly varying input conditions but have problems with fast transients that contain high frequencies.

A general simulation validation methodology, similar to the methodology used in this study, is given in Heydinger *et al* (1990) and shown here in Figure 1.4. This figure shows the flow of information through two processes that make up the validation process; the experimental and the simulation process. Each sub-process (a-g) in the flow chart is briefly described here.

The experimental process starts with obtaining measurements of the behaviour of the physical system through experimental testing (sub-process a). The data reduction in sub-process b includes transforming measured electrical signals into engineering units, digital filtering and other signal processing operations may be performed at this stage. In the sub-process c the ensemble averaging of the repeated test runs are calculated. The measurements on the physical system in sub-process d are to obtain the physical system's parameters. These parameters include mass, inertia, damping, geometry, etc. To be able to validate the simulation model's predictions against the physical system's characteristics it is important to subject the simulation model to the same inputs. In this study the inputs to the simulation model is the road profiles and vehicle speed. The road profiles are obtained through measurements (in sub-process a) or by other means in sub-process e. When the physical system's parameters and the road profiles are known, the simulation can be performed in sub-process f to obtain the simulation predictions. The simulation data can

then be reduced in sub-process g in order to perform qualitative and/or quantitative comparisons with the experimental data.

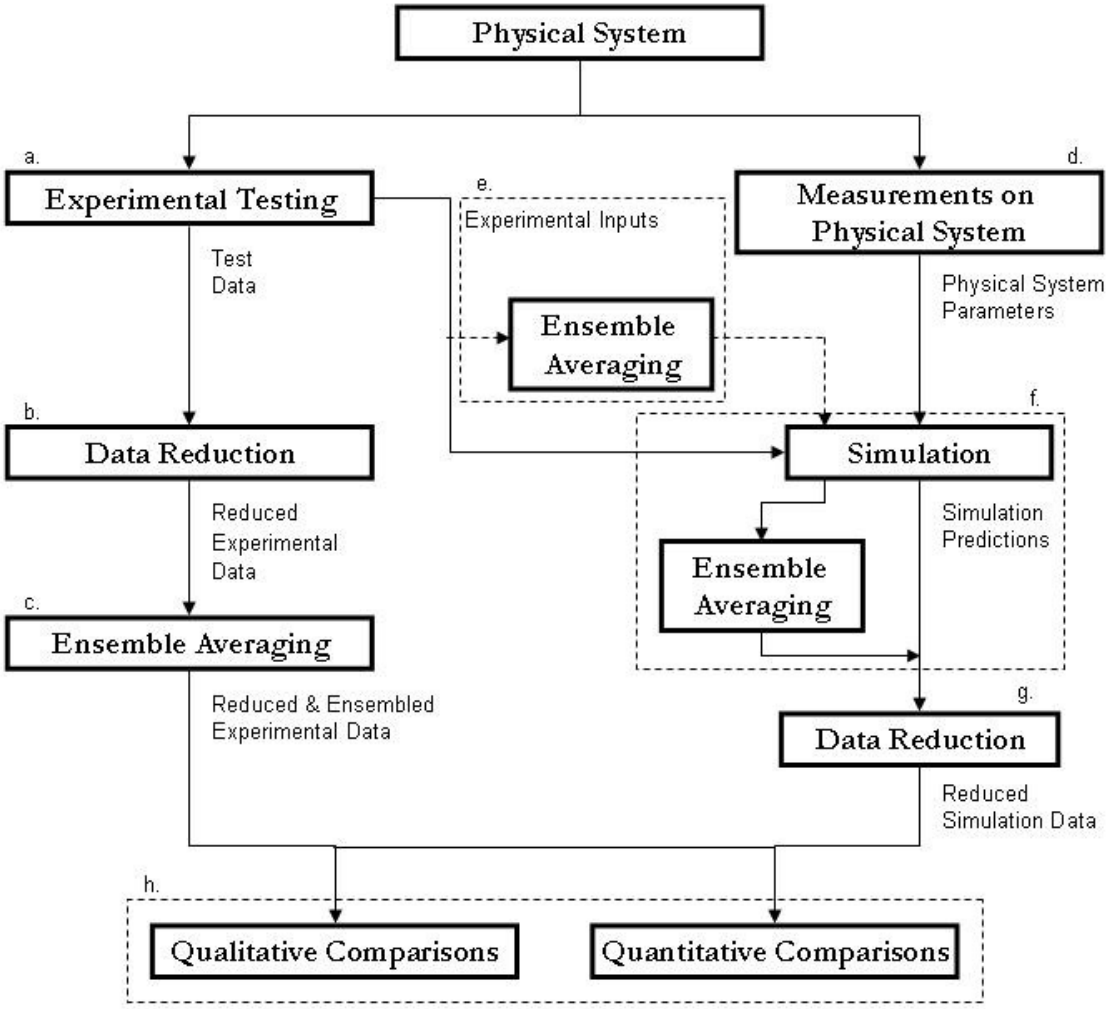

Figure 1.4. Simulation validation process data flow. (Heydinger *et al* (1990))

Bernard and Clover (1994) made the remark that using vehicle test data to validate the model may lead to certain shortfalls of the simulation model not being detected. They demonstrate this point by using the example of a vehicle doing a severe J-turn with the assumption that measured yaw rate and lateral acceleration are available from vehicle tests, but measured normal loads on the tyres are not. They then compare the simulated yaw rate and lateral acceleration of two models of the same vehicle with the difference that the centre of gravity height of one of the models is 10 percent higher. Comparing the yaw rate and lateral acceleration the models seem to be giving similar results, but comparing the lateral load transfer it becomes clear that there is some discrepancy between the two models. This illustrates the point that the simulation model may seem to be behaving correctly when compared to a specific set of test data, but may be behaving incorrectly when compared to a different set of test data. This seems to indicate that it would be very risky to validate one's model against accelerations alone and then to use that model to predict, for example, forces in the suspension.

After the mathematical models of sub-systems such as the suspension unit and critical elements such as the springs, dampers, tyres, etc. have been validated, any trailer with the same suspension unit, tyres and dampers, can be modelled with good reliability as the other parameters can be obtained accurately from CAD.

1.2 Problem definition and aim

It is clear from the preceding introduction and literature study that the use of Multi-Body Simulation models in vehicle development has the potential to reduce the development time and cost, and enable the early evaluation and improvement of the vehicle's characteristics like handling, ride, durability, etc. However, it is very important to validate the MBS model, and to validate the model using the parameters that are to be predicted

In this study the objective will be to create a validated MBS model of the vehicle dynamics of a 40 ton flat bed tri-axle air suspended semi-trailer with the main aim for the model to be used to predict suspension forces. Because the MBS model is to be used for the prediction of forces and to address the shortfalls of using test data to validate the model as mentioned in Bernard and Clover (1994), the validation will be done for numerous vehicle parameters including forces. The limitations of the validity of the MBS model, to certain inputs set out by Heydinger *et al* (1990), will be addressed by comparing data measured on the physical trailer to the data generated by the MBS model over discrete road events and rough roads.

The study is divided into 5 chapters. A graphical representation of the breakdown of this study is shown in Figure 1.5. The first chapter served as an introduction into this field of study. From this the relevant problem was identified and the problem definition and aim of this study were stated.

Chapter 2 discusses the experimental work that consists of two parts: 1) obtaining vehicle parameters and, 2) vehicle testing. In the first part certain vehicle parameters will be obtained that will be required in the construction of the MBS model. The second part will consist of the vehicle tests that were performed to obtain the experimental data that will be used in validating the MBS model in Chapter 4.

Chapter 3 describes the process of the development of a mathematical model for the air suspension unit used on the trailer, and the validation thereof.

Chapter 4 will look at the creation of the Multi-Body Simulation model and the comparison of various sets of predicted data with the measured data. This is done for a discrete symmetric and asymmetric obstacle as well as a rough road. The validation procedure that was followed in this study is also stated in this chapter.

In Chapter 5 the final conclusions are drawn and possible future work and recommendations are made.

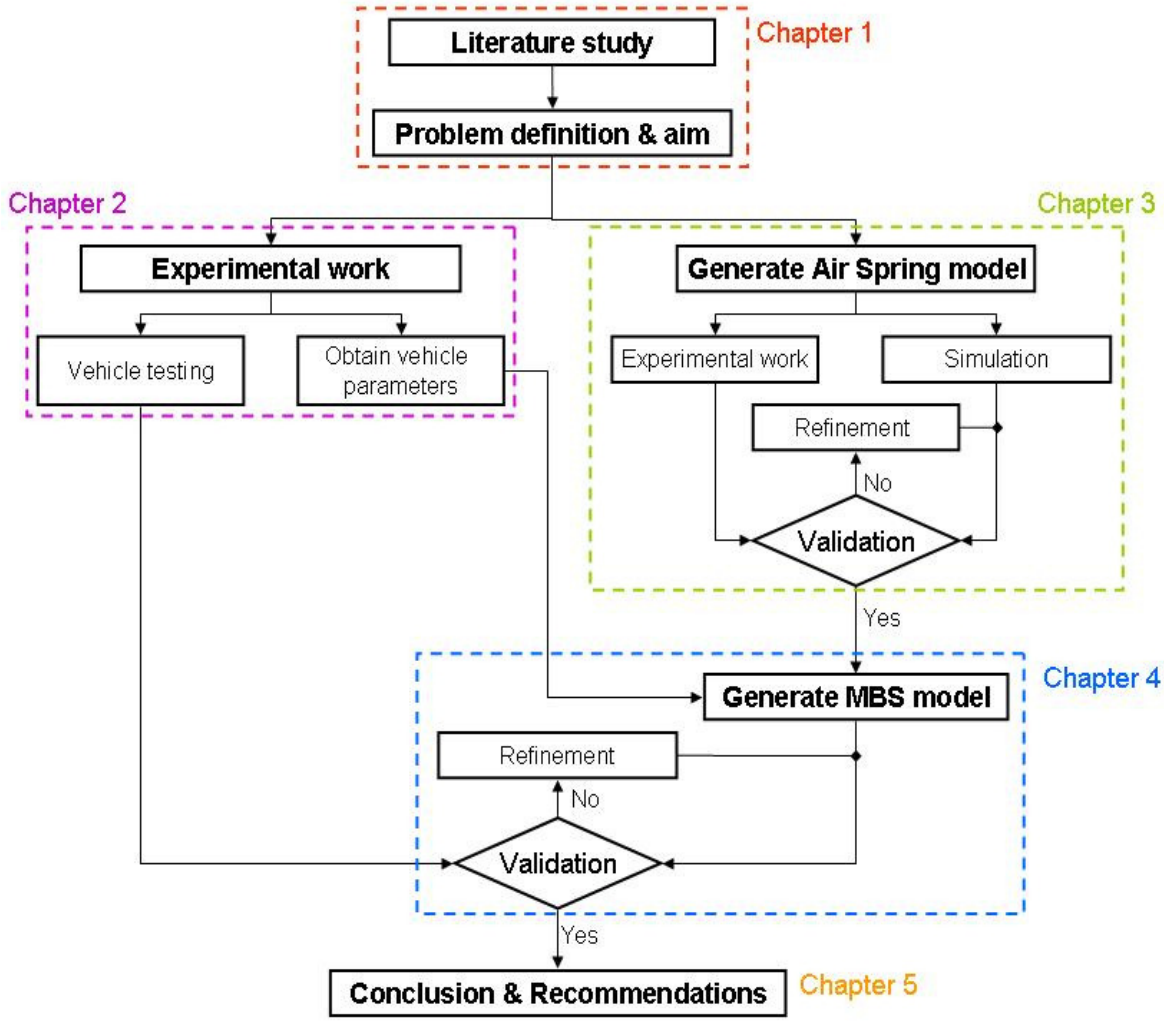

Figure 1.5. Breakdown of study.

Chapter 2

Experimental work

The experimental work set out in this chapter consists of two parts: 1) obtaining vehicle parameters and 2) testing of the experimental trailer. The vehicle parameters that need to be obtained include the characteristics of the dampers, air springs, tyres and the mass, moments of inertia and centre of gravity position of all the components. These vehicle parameters are required when the multi-body simulation model is created. Calibration of some of the suspension components are also discussed in this chapter, as these components will serve as measuring instruments. The second part of the experimental work will be concerned with road testing of the trailer. During these tests, data will be measured that will be used later to validate the MBS model. These two parts of the experimental work are described in more detail in the following two sections.

2.1. Obtain vehicle parameters

In order to build a mathematical model of a physical vehicle, certain parameters of the vehicle need to be determined. Parameters such as mass, moments of inertia and the position of the centre of gravity of all the components can be obtained from CAD software. Other parameters need to be obtained experimentally if the supplier cannot supply the data. In this study the following force elements need to be characterised:

- dampers,
- air springs,
- bump stops and,
- tyres.

The air springs will not be included in this chapter as the whole Chapter 3 is dedicated to the characterisation of the air springs and the development of a validated air spring model. The characterisation of each of the remaining force elements will be discussed in this chapter as well as the conversion of the dampers into measuring equipment.

2.1.1. Dampers

The experimental setup for the damper characterisation is shown in Figure 2.1. A 160kN Schenck actuator is used and a triangular displacement input with various frequencies is played through the actuator. The displacement as well as the force is measured. These data

sets of displacement and force for the various frequencies are then processed to obtain force vs. velocity characteristics. To compare the characteristic we have obtained with the characteristics obtained from the manufacturer, we take the average of the six measured damper characteristics and compare it with the manufacturer's data. The experimentally obtained characteristics compare very well with that of the manufacturer and are shown in Figure 2.2.

Figure 2.1. Experimental setup for damper characterisation and calibration.

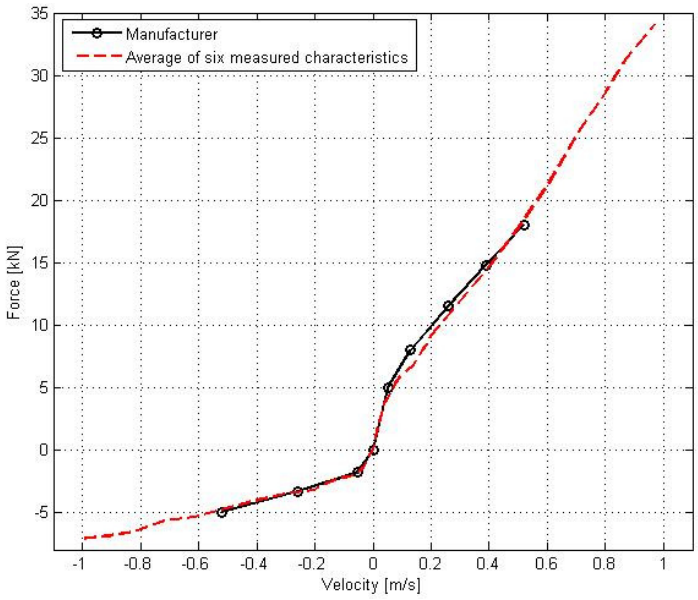

Figure 2.2. Comparison between averaged experimentally obtained damper characteristics and manufacturer data.

In order to measure damper forces during vehicle tests, the rods of the six dampers were instrumented with strain gauges. To calibrate the strain gauge bridge and to obtain a calibration factor that will relate strain to damper force, the same test setup is used as for the damper characterisation. The strain gauge bridge used on the damper rod is a full bridge configuration with two active gauges which cancels bending. The time histories of strain as well as the load cell force are measured. From the measured data the calibration factor is then determined. Figure 2.3 compares the forces measured by the strain gauge[1] and the load cell, respectively. It can be seen from this figure that at higher frequencies the correlation between the two sets, especially for the tension forces in the damper, are not good. This was found to be true for all six dampers. The calibration factor was therefore determined based on good correlation for the compression forces in the damper. The rationale, for this approach, is based on the fact that these high tension forces obtained experimentally will not be achieved once the dampers are implemented on the vehicle, since then the only contribution to the tension forces will be the unsprung mass. The resulting calibrations give very good correlation for compression.

Considering only the correlation of the compression force in the damper, the calibration factors for the six dampers were determined and are given in Table 2.1. Figure 2.4 shows the correlation between the compression forces, as measured by the strain gauge[1] and the load cell for the right rear damper. From this figure it can be noted that the maximum deviation of the strain gauge measurement, from that of the load cell, is 763 N. Deviation between the compression force measured by the strain gauge and the load cell for all six dampers is summarised in Table 2.2. Table 2.2 gives the percentage deviation as well as the deviation in terms of force. These deviations are acceptable and it can be concluded that the force measurement gained through the strain gauge will be accurate enough. Graphical representation of the correlation of the other dampers can be found in Appendix A.

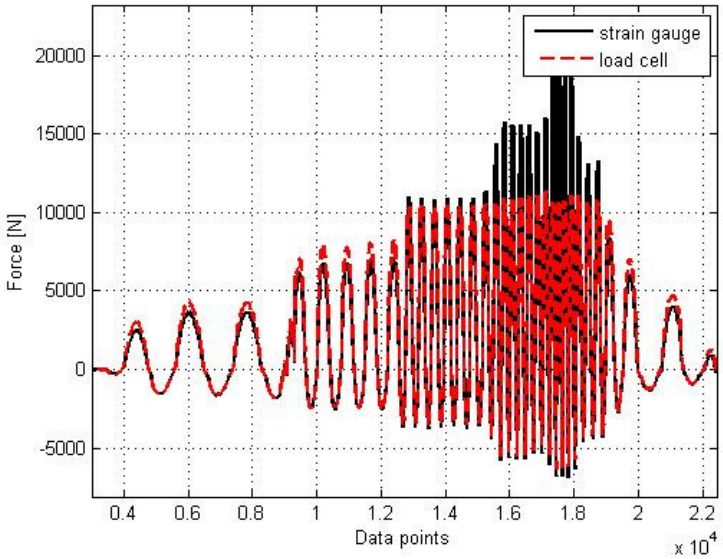

Figure 2.3. Comparison of strain gauge data with load cell data.

[1] The force is not measured directly by the strain gauge. The force is obtained from the measured strain after it is converted to Newton by multiplying it by the calibration factor given in Table 2.1.

Table 2.1. Calibration factors for each damper.

Damper	Calibration factor [N/με]
Left front	54.94
Left middle	57.42
Left rear	45
Right front	64.75
Right middle	41.14
Right rear	54.8

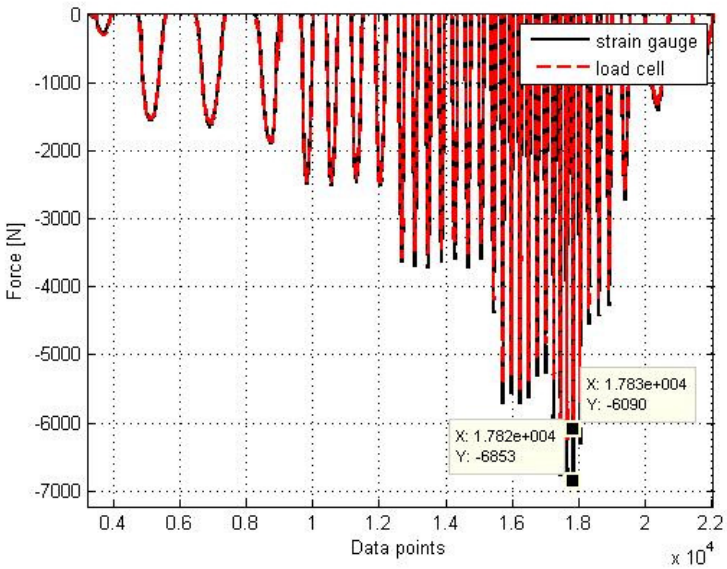

Figure 2.4. Comparison of compression forces as measured by strain gauge and load cell for right rear damper.

Table 2.2. Deviation between compression forces measured by strain gauge and load cell.

Damper	Percentage deviation [%]	Deviation [N]
Left front	6.4	323
Left middle	4.7	253
Left rear	12.3	480
Right front	7.3	398
Right middle	15.7	395
Right rear	12.5	763
Mean	**9.82**	**435.33**
Standard deviation	**4.29**	**177.90**

2.1.2. Bump stops

The experimental setup for obtaining the characteristics for the bump stop inside the air spring is shown in Figure 2.5. While performing the tests on the bump stop the air spring was ventilated to atmosphere so as to determine the net force vs. displacement of the bump stop without any contribution from the force of the air spring. The measured values of

force and displacement from the tests are plotted to give the bump stop characteristics and is shown in Figure 2.6. The hysteresis present in the rubber of the bump stops is ignored. The fit to the data that will be used as the characteristic of the bump stop is shown in Figure 2.6.

Figure 2.5. Experimental setup for characterising the bump stops.

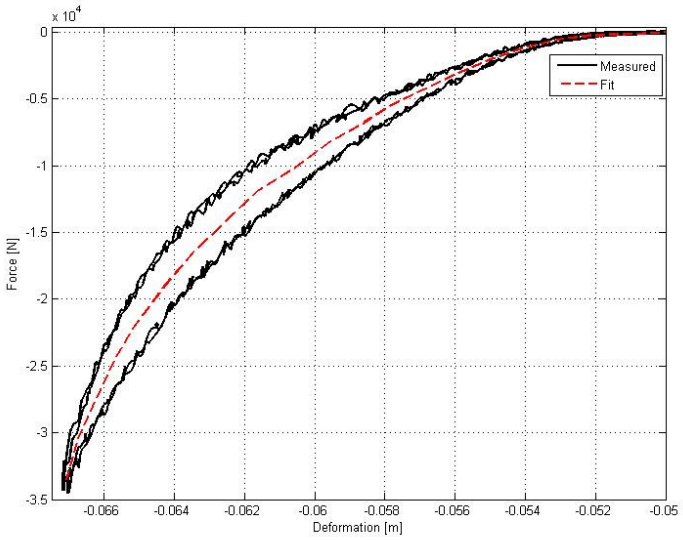

Figure 2.6. Characteristics of bump stop.

2.1.3. Tyres

Tyres are one of the most important components on a vehicle, as it is one of the paths for two of the main sources of external force that acts on a vehicle. The tyre is also the path for many of the forces that act on the suspension components and the chassis of the vehicle. The tyre plays the same critical role in the simulation environment, and it is therefore necessary to make sure that the tyre's characteristics are accurate.

Many of the difficulties in obtaining accurate predictions of vehicle characteristics are due to the tyre models. Analytical tyre models are described by Captain *et al* (1979) and tyre modelling by finite element methods is discussed by Faria *et al* (1992). In studies by Anderson *et al* (2001) and Gopalakrishnan and Agrawal (1993) they mention difficulties in predicting forces with the MBS model due to the tyre model used.

The tyre model that was used in this study is the Pacejka '89 handling tyre model (ADAMS/Tire (2007)). In the ADAMS/Tire help documentation, a list of the applications for each of the available tyre models are given. The application range of two of the available tyre models are given here in Table 2.3. Although FTire is the most suitable tyre model for our situation when ride and durability are considered, the Pacejka '89 handling tyre model was used. Various factors such as license issues and the data required in order to parameterise the tyre for FTire, lead to the use of the Pacejka '89 handling tyre model, but the primary reason for its use was the author's unawareness of the limitations of the Pacejka '89 tyre model. Its limitations of not being able to function above 8Hz were observed in the predictions of our MBS model, during the validation process. This observation lead us to investigate the tyre model and to the discovery of its limitations. The effect of this limitation on the predictions of the MBS model of the present study will be shown and discussed in Chapter 4.

Table 2.3. Typical applications of the Pacejka '89 and FTire tyre models. (Adapted from ADAMS/Tire (2007))

MD Adams	Event / Maneuver	ADAMS/Handling Tyre Pacejka '89[1]	Specific Models Ftire
Handling	Stand still and start	Better	Best
	Parking (standing steering effort)	Not possible/Not realistic	Best
	Standing on tilt table	Best	Best
	Steady state cornering	Better	Better
	Lane change	Better	Better
	ABS braking distance	Better	Best
	Braking/power-off in a turn	Possible	Better
	Vehicle roll-over	Possible	Best
	On-line scaling tire properties	Not possible/Not realistic	Possible
Ride	Cornering over uneven roads*	Possible	Better
	Braking on uneven road*	Possible	Best
	Crossing cleats/obstacles	Not possible/Not realistic	Best
	Driving over uneven road	Not possible/Not realistic	Best
	4 post rig (A/Ride)	Better	Better
Chassis Control	ABS braking control	Possible	Best
	Shimmy[2]	Possible	Best
	Steering system vibrations	Possible	Best
	Real-time	Not possible/Not realistic	Not possible/Not realistic
	Chassis control system > 8 Hz	Not possible/Not realistic	Best
	Chassis control with ride	Not possible/Not realistic	Best
Durability	Driving over curb	Not possible/Not realistic	Better
	Driving over curb with rim impact	Not possible/Not realistic	Better
	Passing pothole	Not possible/Not realistic	Better
	Load cases	Not possible/Not realistic	Better

In this study we are interested in the vertical dynamics of the vehicle and thus imply that we need to be sure that the vertical tyre properties are correct. In order to parameterise the vertical behaviour of the tyre for the Pacejka '89 tyre model, only the vertical stiffness and damping is needed. Values for both the vertical stiffness and damping were obtained from the tyre manufacturer and are shown in Table 2.4. The vertical stiffness as given by the tyre manufacturer compares well to the vertical stiffness obtained experimentally and is shown in Figure 2.7. The experimental setup to determine the tyre vertical stiffness is shown in Figure 2.8.

Table 2.4. Tyre manufacturer values for vertical stiffness and damping.

Vertical stiffness	1.2 kN/m
Vertical damping	3%

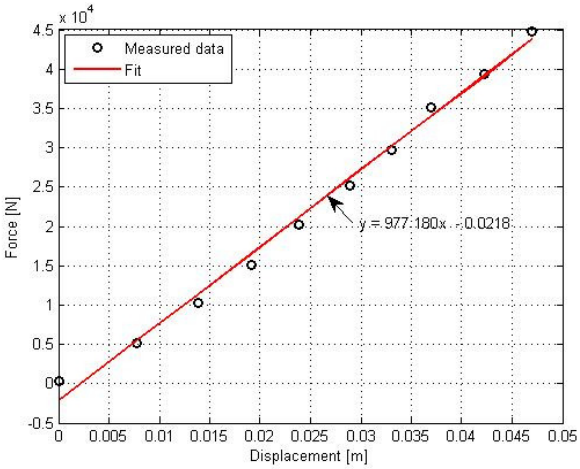

Figure 2.7. Experimental tyre stiffness.

Figure 2.8. Experimental setup to determine tyre stiffness.

The lateral characteristics of the tyre are described in the Pacejka '89 tyre model by a formula that is capable of describing all the characteristics of the tyre's, side force, brake force and self aligning torque, with great accuracy (Bakker *et al* (1989)). In this particular study we only included the side force characteristics of the tyre. From the given side force vs. slip angle data obtained from the tyre manufacturer, the lateral coefficients to be used in the Pacejka '89 tyre model were calculated and are given in Table 2.5. The fit of the Pacejka '89 tyre model to the given data for the vertical load of 6750 kg is shown in Figure 2.9. The data given by the manufacturer was only for the slip angle range of -1° to 1°. This is sufficient as the lateral data is not very important for the present study.

Table 2.5. Lateral coefficients for use in Pacejka '89 tyre model.

Lateral coefficients	Value	Description
a0	1.3	Shape factor
a1	0	Load dependency of lateral friction
a2	0.85	Lateral friction level
a3	6200	Maximum cornering stiffness
a4	66.2175	Load at maximum cornering stiffness
a5	0	Camber sensitivity of cornering stiffness
a6	0	Curvature factor
a7	0	Curvature factor
a8	0	Horizontal shift
a9	0	Horizontal shift
a10	0	Horizontal shift
a11	0	Vertical shift
a12	33.5948	Vertical shift
a13	-457.0175	Vertical shift

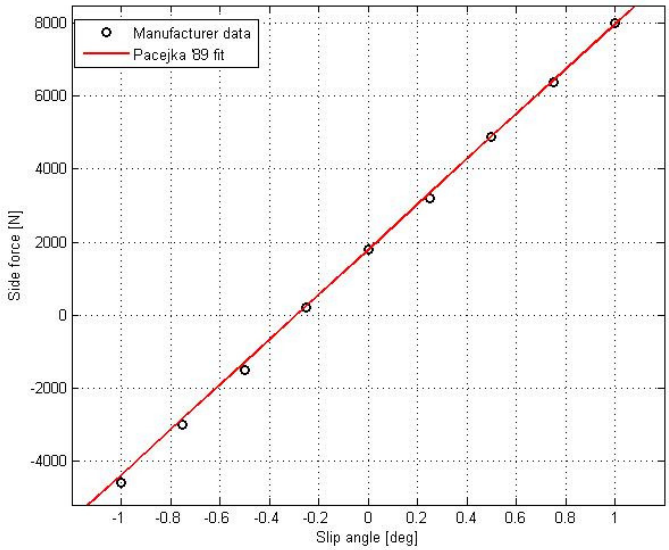

Figure 2.9. Comparison between manufacturer data and Pacejka '89 tyre model for vertical load of 6750 kg.

2.2. Testing of trailer

The main aim of the experimental tests is to obtain the experimental data to validate the MBS model. The experimental data that will be measured consists of displacements, accelerations, angular velocities, vehicle speed and forces. These measured data will be used in the validation process to verify if the MBS model can indeed predict these parameters accurately.

The tests were performed at Gerotek Test Facilities (Gerotek (2008)). Gerotek is a vehicle test facility designed for heavy vehicles. The facility has different, well maintained tracks for testing different vehicle characteristics. These include tracks such as the suspension track, handling track, high speed track etc. Performing the tests at Gerotek Test Facilities enabled us to ensure that the tests took place over repeatable, known road surfaces. It is of the utmost importance to have the tests performed over road surfaces that are known in order for the MBS model to go over the same road surface and thus enabling us to compare data in the validation process. The data required to validate the MBS model was obtained over two types of roads: 1) a discrete obstacle and 2) a rough road (Belgian paving).

2.2.1. Instrumentation of physical trailer

To obtain the required experimental data, the trailer was instrumented with the equipment as shown in Table 2.6. The equipment's position on the trailer is shown in Figure 2.10 to Figure 2.14. Figure 2.10 shows the position of the four pressure transducers that were mounted on four of the six air springs. This figure also shows the rope displacement transducers that were placed parallel to all six dampers to measure their displacement. The accelerometers measuring the acceleration on the three axles are shown in Figure 2.10 and Figure 2.11. The two accelerometers mounted on the body of the trailer can be seen in Figure 2.12. The position and orientation of the GPS antenna and the gyroscopes measuring the vehicle speed, roll velocity, pitch velocity and yaw velocity are shown in Figure 2.13. Another speed measurement is taken by an optical sensor that measures the rotational speed of one of the wheels and is shown in Figure 2.14.

Table 2.6. Test equipment.

Measurement parameter	**Equipment**
Vehicle speed	Somat e-DAQ GPS
Wheel speed (2nd axle left-hand)	Turck MS25 frequency to voltage converter with optical sensors
Wheel speed (2nd axle right-hand)	
Air spring pressure (1st axle left)	Wika pressure transducer
Air spring pressure (2nd axle left)	
Air spring pressure (3rd axle left)	
Air spring pressure (2nd axle right)	
Damper displacement (1st axle left)	Penny and Giles rope displacement transducer
Damper displacement (2nd axle left)	
Damper displacement (3rd axle left)	

Measurement parameter	**Equipment**
Damper displacement (1st axle right)	
Damper displacement (2nd axle right)	
Damper displacement (3rd axle right)	
Vertical acceleration (1st axle at centre)	Crossbow tri-axial accelerometer
Vertical acceleration (3rd axle at centre)	Crossbow tri-axial accelerometer
Longitudinal acceleration (2nd axle)	Crossbow tri-axial accelerometer
Lateral acceleration (2nd axle)	
Vertical acceleration (2nd axle)	
Roll velocity	CRS-03 Solid state gyroscopes
Pitch velocity	
Yaw velocity	
Longitudinal acceleration (on body above 2nd axle)	Crossbow tri-axial accelerometer
Lateral acceleration (on body above 2nd axle)	
Vertical acceleration (on body above 2nd axle)	
Longitudinal acceleration (on body on front)	Crossbow tri-axial accelerometer
Lateral acceleration (on body on front)	
Vertical acceleration (on body on front)	

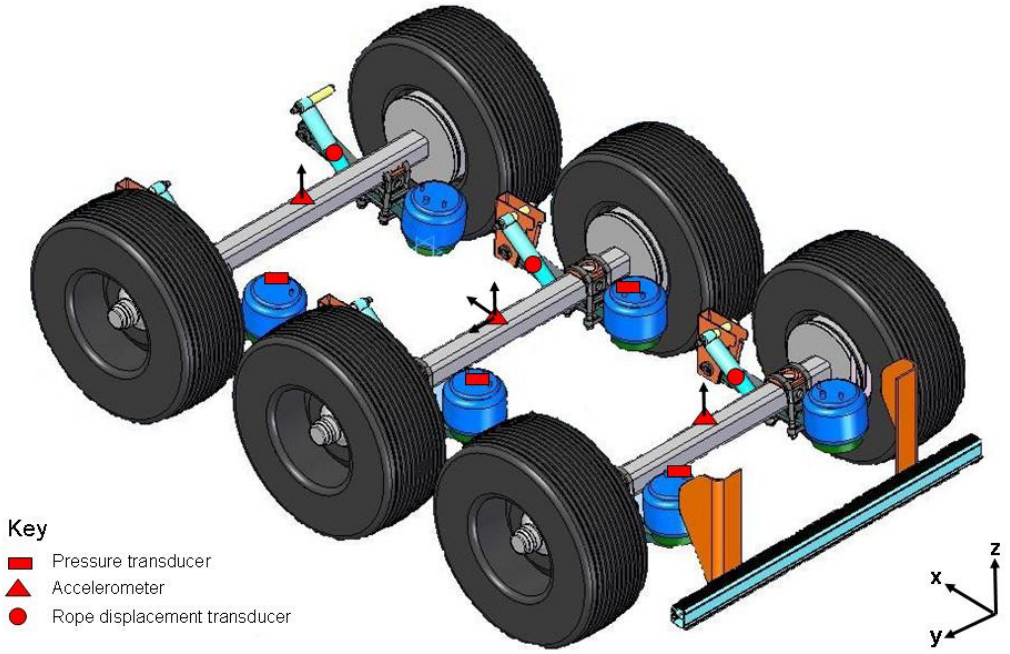

Figure 2.10. Position of pressure transducers and axle accelerometers.

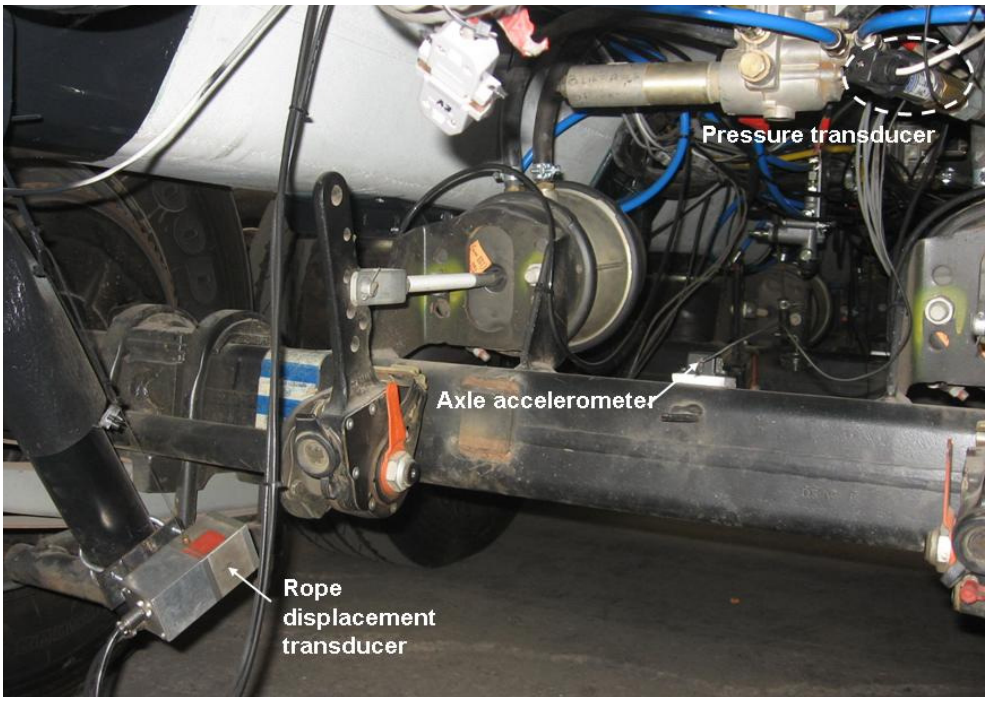

Figure 2.11. Rope displacement transducer, axle accelerometer and pressure transducer on trailer.

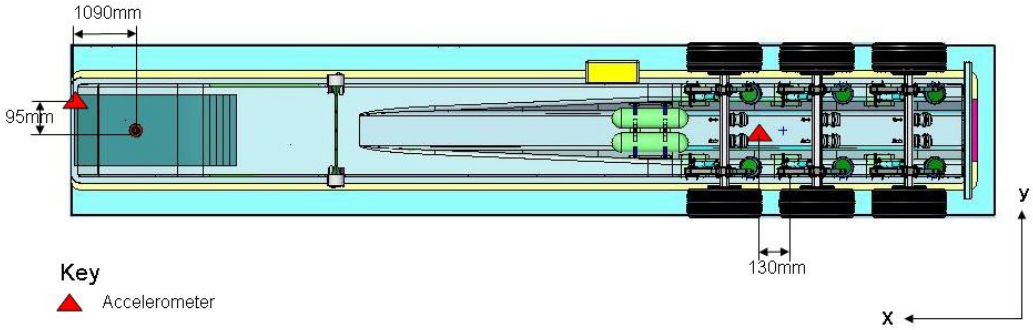

Figure 2.12. Position of body accelerometers.

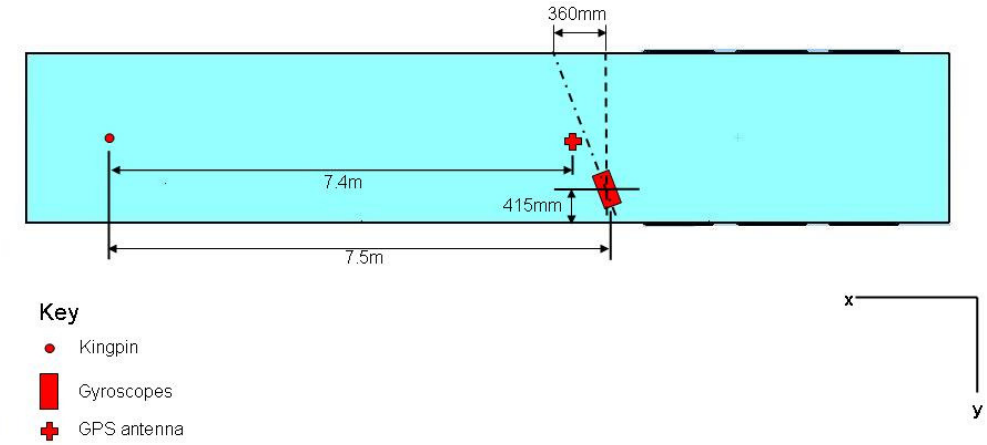

Figure 2.13. Position of gyroscopes.

Figure 2.14. Optical sensor for speed measurement.

2.2.2. Load cases

With the trailer instrumented as above the trailer was tested over the discrete obstacle and rough road with three different load cases. The load distribution and the axle load of the trailer for each load case is given in Figure 2.15 and in Table 2.7 respectively. The tyre pressures were measured for each load case and varied between 7.1bar and 7.4bar. The tyre pressures were not changed for the different load cases.

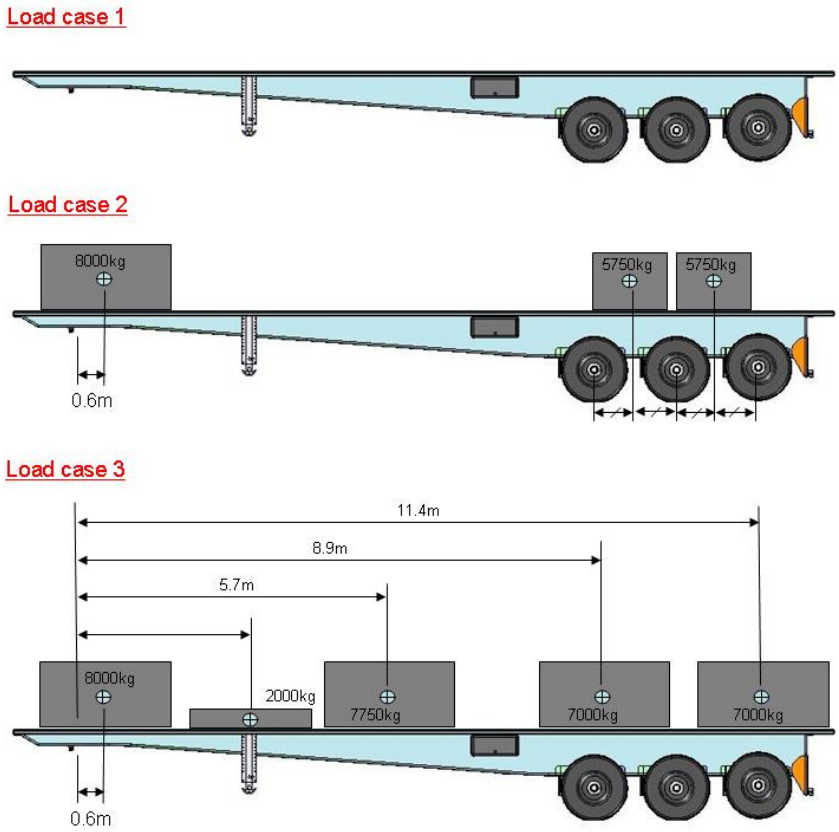

Figure 2.15. Load distribution for the three load cases.

Table 2.7. Axle load distribution of trailer.

	Average of left (kg)	Average of right (kg)	Total (kg)
Load case 1			
Trailer 1st axle	540	510	1050
Trailer 2nd axle	590	525	1115
Trailer 3rd axle	620	515	1135
Total/side	**1750**	**1550**	**3300**
Load case 2			
Trailer 1st axle	2420	2545	4965
Trailer 2nd axle	2535	2395	4930
Trailer 3rd axle	2570	2400	4970
Total/side	**7525**	**7340**	**14 865**
Load case 3			
Trailer 1st axle	3660	3825	7485
Trailer 2nd axle	3745	3705	7450
Trailer 3rd axle	3750	3710	7460
Total/side	**11 155**	**11 240**	**22 395**

2.2.3. Performed tests

The experimental tests were performed on the trailer in order to obtain data that will be used in the validation of the MBS model. The experimental trailer is driven over two types of road events in order to validate the MBS model for a wider operating range. The road events used are:

- a discrete obstacle and,
- a rough road.

The first road event, the discrete obstacle, can be described as a trapezoidal speed bump. This type of road event is used because it generates effects in the data that are easily recognisable in the time domain compared to a rough road. This makes comparisons between the measured data and the predicted data easier. The discrete obstacle is also used, as speed bumps are very common on South African city roads and represents an important load case because the full vehicle load is carried on one axle. Tests over the discrete obstacle will include driving over an asymmetric and symmetric trapezoidal speed bump configuration which includes speed bumps of different heights. The configuration of the discrete obstacles is shown in Figure 2.16, with a picture of the trailer going over the asymmetric discrete obstacle in Figure 2.17.

Chapter 3

The Air Spring Model

In the previous chapter we obtained all the vehicle parameters that are needed to create the Multi Body Simulation (MBS) model of the trailer, except for the air spring characteristics. In creating the MBS model it is necessary to find a compromise between complexity (accuracy) and simplicity (computational efficiency) of the MBS model for its intended use. Therefore, a few assumptions are made at the start to simplify the modelling of some of the physical characteristics of the trailer. The assumptions are:

- all bodies are rigid bodies,
- the air springs are not interconnected and,
- inputs from the truck towing the trailer are ignored.

As will be seen later, some or all of these assumptions may have to be discarded in the validation process in order to obtain better accuracy in the predictions of the MBS model. The assumption we will be looking at in this chapter is the assumption of the air springs. It was initially thought that the flow of air between the air springs, during driving conditions, would not have a substantial effect on the behaviour of the air suspension unit. It was assumed that the air springs are not connected and thus functioned as stand-alone units. During validation of the MBS model bad correlation between the measured and predicted pressures of the air springs, lead us to believe that this assumption may not be valid.

In this chapter the different mathematical models that were used for the air suspension unit are discussed and compared. The discussion of the different air spring models serves as an introduction and motivation of the importance of the air spring model and the need for a more accurate model. The aim of this chapter is to develop a validated mathematical model of the air suspension unit that can be used in full vehicle dynamic simulations.

The details of the MBS model will be discussed in Chapter 4.

3.1. Introduction

All vehicle suspensions are designed with one main aim in mind, to isolate the chassis from the vibrations caused by the tyre following the road surface. Other aims include keeping the wheels in contact with ground for traction, braking, etc. Air suspensions are no different and have certain advantages over mechanical suspensions. Some of these advantages include:

- Adjustable carrying capacity

- Reduced weight
- Reduced structurally transmitted noise
- Variability of ride height

The air suspension unit under consideration in this study consists of six rolling diaphragm (rolling-lobe) air springs (shown in Figure 3.1), which are all connected through pipes. The pneumatic circuit diagram of the suspension unit used in this study is shown in Figure 3.2. The three air springs on both sides respectively, are directly connected. When the trailer is driving the height control valve is in the third setting, and if we assume that during driving conditions the levelling valve is also in its third position the left-hand and right-hand air springs are connected through an orifice.

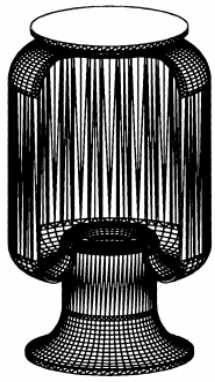

Figure 3.1. Rolling diaphragm type air spring.

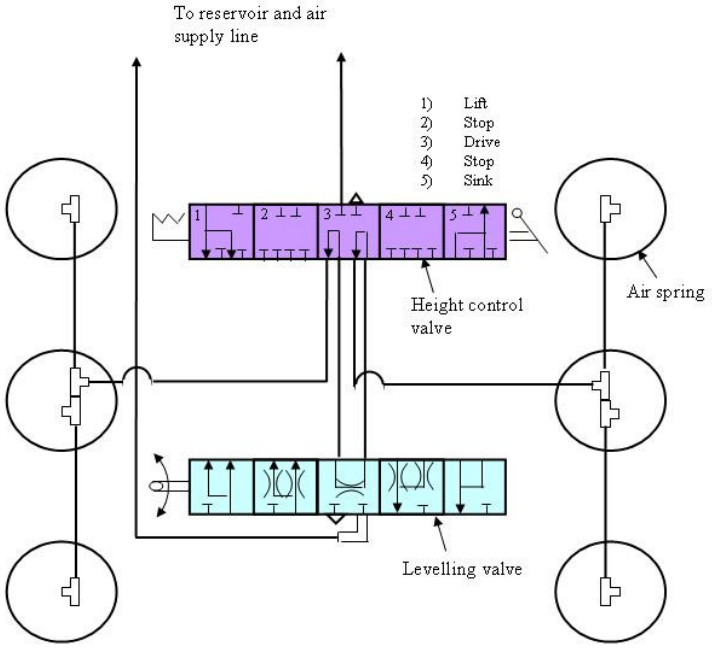

Figure 3.2. Pneumatic circuit diagram of air suspension unit.

3.2. Objective of the air spring model

The aim of this air spring model is to obtain a validated mathematical model of the air suspension unit that can be used in full vehicle dynamic simulations. Thus, the air spring model will be modelled as a sub model that gets, as input, the deformation of each air spring from a dynamic analysis program, in this case ADAMS. The air spring model then calculates the force in each air spring and returns this information to the dynamic analysis program. The data flow as described above is shown in Figure 3.3. ADAMS and MATLAB SIMULINK operate through the ADAMS/controls interface.

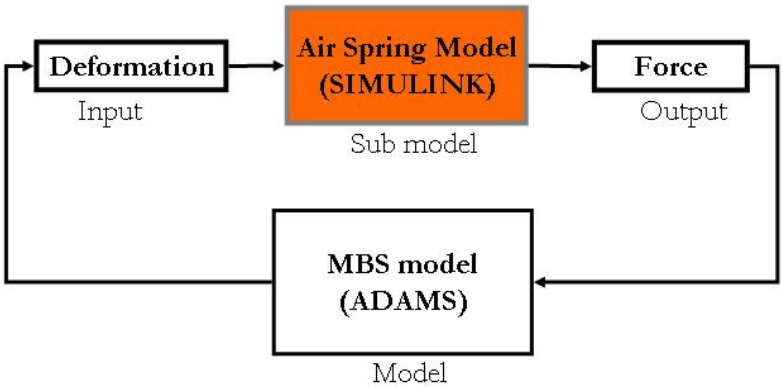

Figure 3.3. Data flow through air spring model.

Before we start looking at the different air spring models, we first have to look at two physical aspects of the air springs. The first aspect concerns the area characteristic of the air spring, and the second concerns the pressure transducer measurements.

3.3. Area characteristic of the air spring

The force of the air spring is related to the pressure in the air spring through the area A.

$$F = PA$$

This relationship will be used later to convert the forces predicted by the air spring model to pressures in order to compare it with the measured pressures. The area A is known as the effective area which is a non-constant imaginary area over which the spring's relative internal pressure acts. As this area is not a geometrical defined value, it is usually calculated by means of a constant internal pressure test (Nieto *et al* (2008)) in which the force is measured while varying the deformation of the air spring. The area is then obtained as a function of the deformation (Δx) of the spring relative to the ride height and the internal pressure (P).

$$A = A(\Delta x, P)$$

As an approximation we assume that the area stays constant and that neither the internal pressure nor the deformation of the air spring has an effect on the area. To check the validity of this assumption we use the experimental setup as shown in Figure 3.4 which consists of three air springs connected with each other through a pipe. The pipe lengths and pressure transducer mounting positions are the same as used during the test on the

experimental trailer described in Chapter 2. The middle and rear air spring is clamped in at the ride height position. The front air spring is mounted on an actuator so that the relative displacement can be changed as required. Underneath each of the air springs is a load cell and a pressure transducer is connected to each air spring.

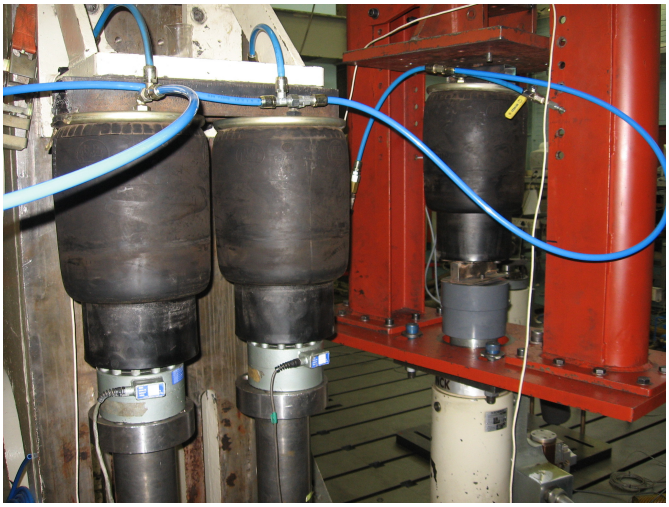

Figure 3.4. Experimental setup of the air springs.

The system is then slowly inflated from atmospheric pressure to a gage pressure of 4.5bar and then deflated back to atmospheric pressure while pressure and force are measured. The system is deflated and inflated slowly so that effects due to flow losses are minimised. It is assumed that the deformation of the test rig is negligible and that the deformation of the air spring (Δx) stays constant. Figure 3.5 shows the area sensitivity to internal pressure at the ride height position. When looking at this figure it seems that the area changes dramatically when the pressures in the air springs go below 0.5bar (gage pressure). This effect is not a physical effect but rather a numerical error that starts to develop when the pressures approach zero. This test was repeated for four different deformations from the ride height position. A histogram of area vs. pressure, for each of the air springs, is shown in Figure 3.6 to Figure 3.8. These histograms include the data of all five deformations.

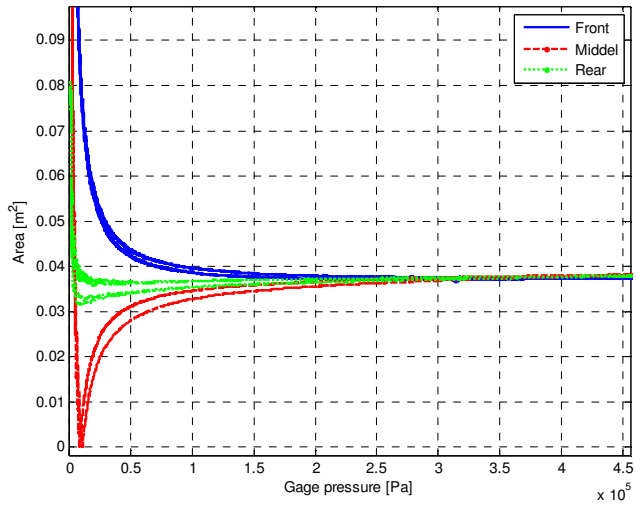

Figure 3.5. Area sensitivity to pressure at ride height position.

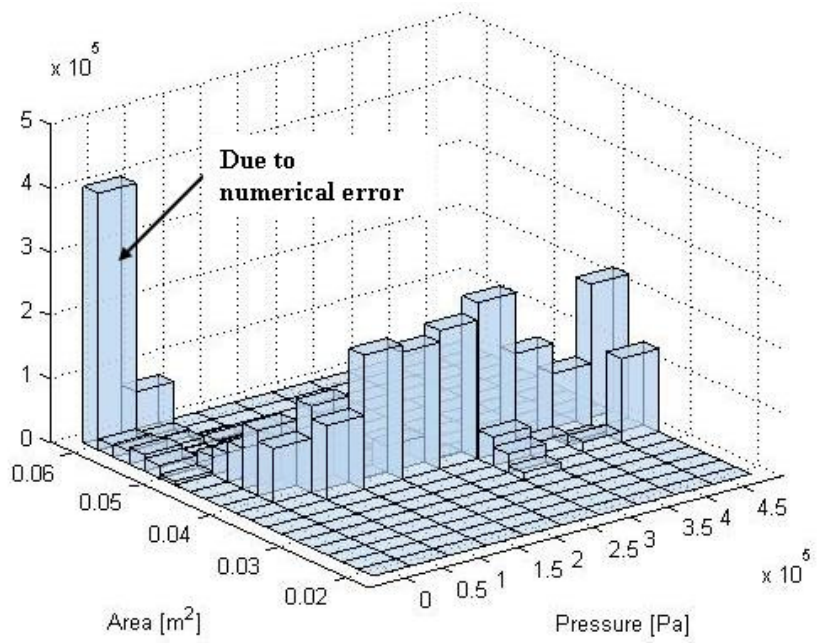

Figure 3.6. Histogram of area vs. pressure for front air spring.

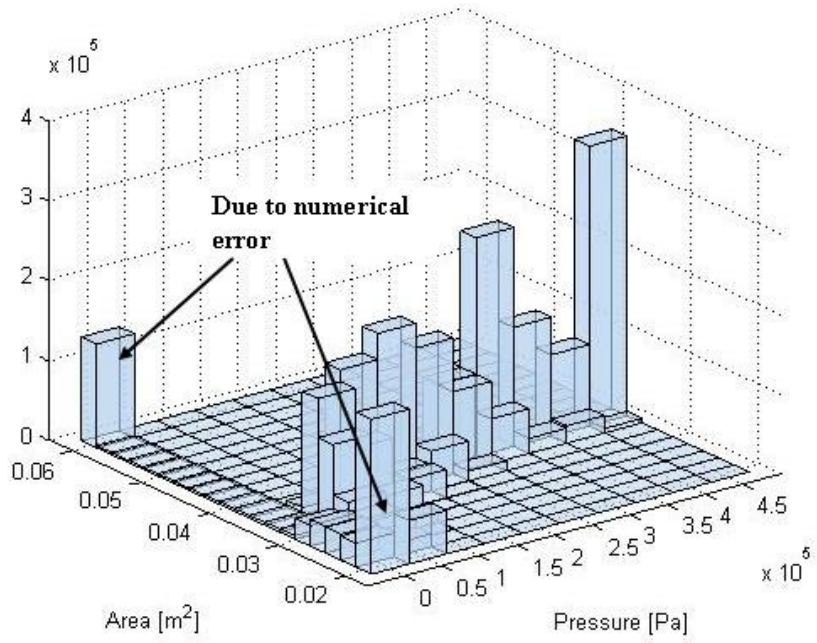

Figure 3.7. Histogram of area vs. pressure for middle air spring.

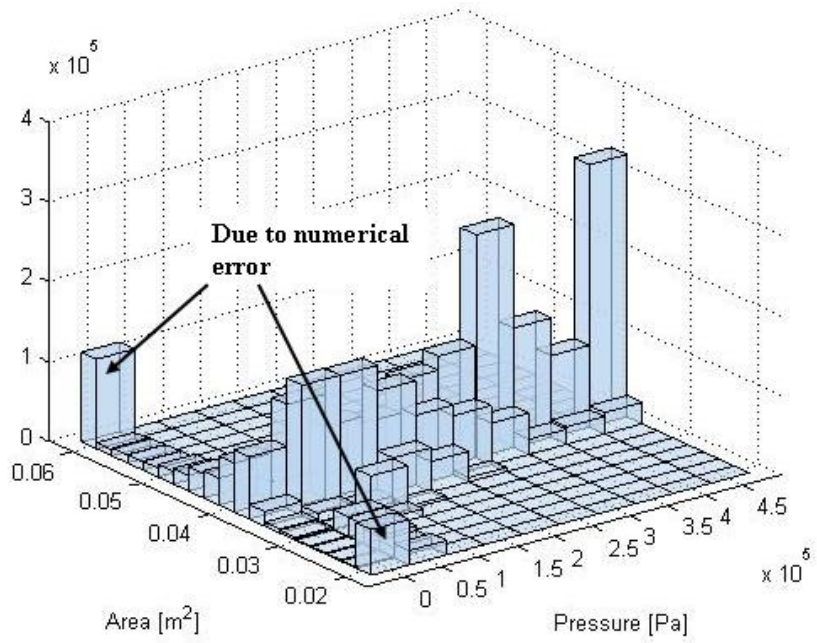

Figure 3.8. Histogram of area vs. pressure for rear air spring.

It can be observed from the three histograms that all three have a higher density around $0.04m^2$. To obtain the mean and the standard deviation of the areas of the three air springs, the area data is filtered to obtain only the data that fall between $0.03m^2$ and $0.05m^2$. This was done to get rid of the numerical error that was mentioned earlier. The results are given in Table 3.1. This indicates that the area of the air spring throughout its travel does not vary greatly and imply that the assumption made that the area does not change significantly with internal pressure or with deformation of the air spring, is valid.

Table 3.1. Statistical values of area data.

	Front air spring	**Middle air spring**	**Rear air spring**
Mean	0.038 m^2	0.036 m^2	0.037 m^2
Standard deviation	0.0032 m^2	0.0021 m^2	0.0022 m^2

3.4. Pressure transducer measurements

During the validation process doubt arose over the correctness of the pressure sensor measurements taken during vehicle tests. To check the reliability of the pressure measurements, the same experimental setup as in section 3.3 was used. The pressure transducer measurements were compared to the pressure in each air spring calculated from the force measurements using the constant area. The results indicate that the pressure transducers made an error in measuring the pressure inside the air springs (shown in Figure 3.9). This effect may be attributed to flow losses in the pipes that connected the pressure transducer to the air spring and the compressibility of the air.

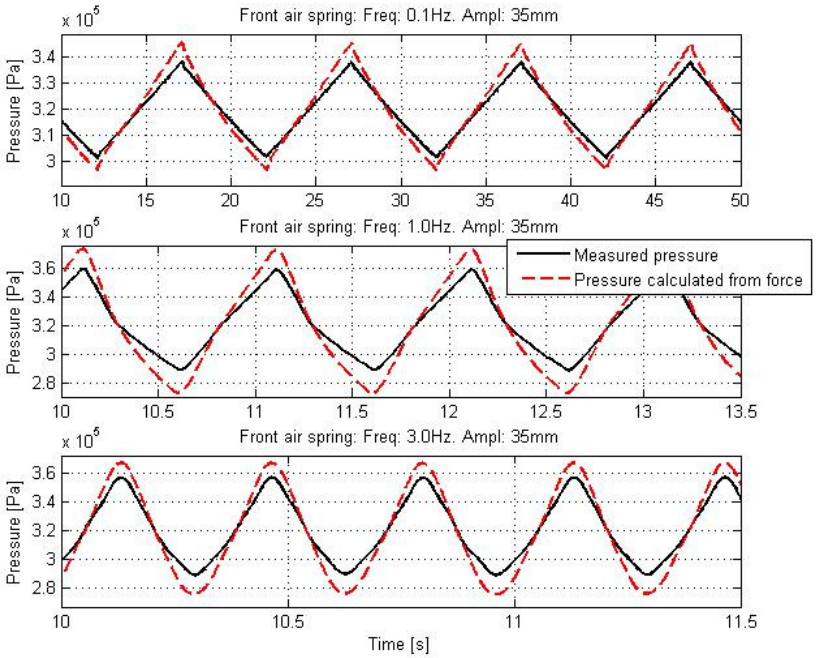

Figure 3.9. Error in the pressure transducer measurements.

In an attempt to try and compensate for these effects, the transfer function between the measured pressure and the pressure obtained from the force measurements was calculated using the MATLAB function *tfestimate*. In calculating the transfer function, it implicitly assumes that we take the relationship between the measured pressure and force to be linear. The pressure transmissibility is obtained by exciting the system with a constant displacement amplitude sine sweep. Three sine sweeps were used, differing in bandwidth and amplitude. The pressure transmissibility for the three sine sweeps are shown in Figure 3.10. This figure shows both the magnitude and phase. The phase stays fairly constant over the frequency range but the magnitude is highly dependent on the frequency. The magnitude is not dependent on the amplitude of the excitation frequency and indicates that the assumption made that the relationship between the measured pressure and force is linear, is valid. The biggest error (40%) occurs at low frequencies in the range where biggest suspension activity is expected due to the sprung mass natural frequency range. The trendline indicates the line on which the transfer function was based. This transfer function will serve as a filter through which the measured pressures will be passed before they are compared to the pressures calculated from the force measurements. Figure 3.11 and Figure 3.12 show the greatly improved correlation after the measured pressures have been filtered with the transfer function. Correlation between the filtered measured pressures and the pressure obtained from the measured force for a random input is shown in Figure 3.13. From this point forward the measured pressures in the air springs will be filtered with this transfer function before they are used.

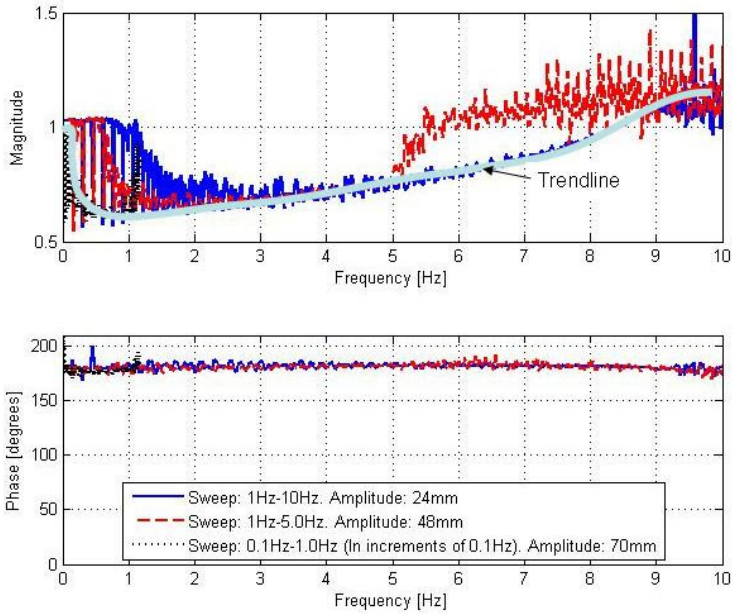

Figure 3.10. Pressure transmissibility.

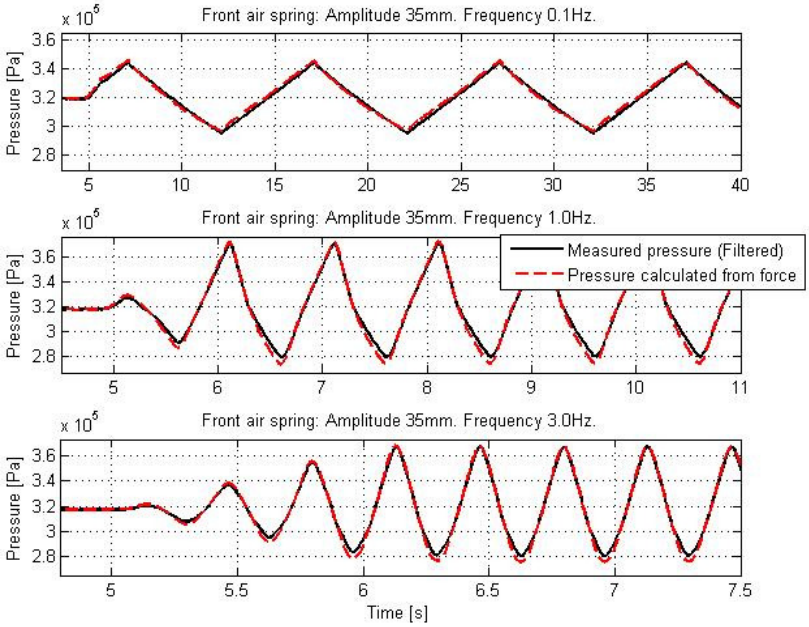

Figure 3.11. Comparison between the filtered measured pressure and the pressure obtained from the measured force.

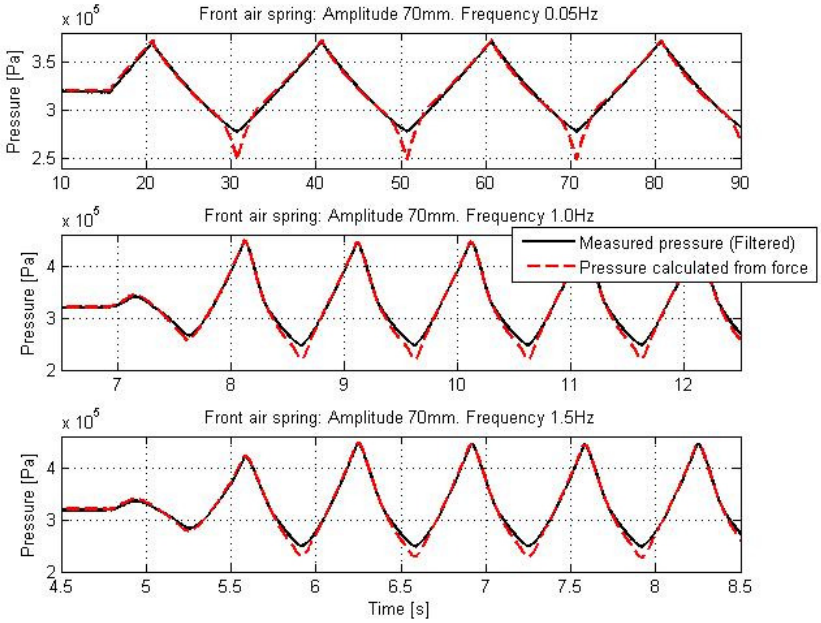

Figure 3.12. Comparison between the filtered measured pressure and the pressure obtained from the measured force for larger amplitudes.

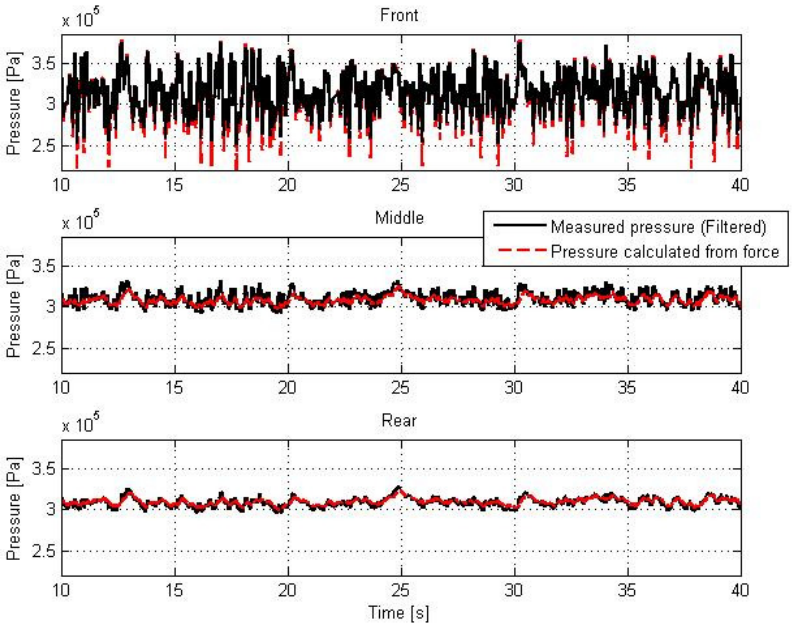

Figure 3.13. Comparison of measured pressures with pressure obtained from measured forces, for a random input with 30mm rms amplitude and 5Hz bandwidth.

3.5. Comparison of different air spring models

During the early part of the validation process of the MBS model, the author struggled to obtain correlation between the pressures predicted by the model and the pressures measured on the physical trailer. After numerous sensitivity studies it was concluded that the problem was most likely with the air springs. One of the assumptions made at the beginning of the study was that the air springs were not connected and thus acted as stand-alone units.
In this section we will look at the errors that resulted from this assumption and discuss the other models that were used to represent the air suspension unit. These models are compared and the final conclusions are drawn at the end of this section. The three air spring models that will be looked at are: 1) Not-connected, 2) interconnected and 3) left-right connected.

3.5.1. Not-connected

The assumption made at the start of this study assumes that the air springs are not connected. In other words it is assumed that there is no flow of air between the individual air springs, also used as such in Luque and Mántaras (2003). This assumption was made because it was believed that the air flow, if any, would not have a substantial effect on the behaviour of the air springs during driving conditions.

The air spring model is required to give the force, due to the deformation of the air spring, as output. The force is obtained by using a lookup table that consists of the force-displacement characteristics of the air spring. The experimental setup for obtaining the force-displacement characteristics is shown in Figure 3.14. In this experiment the air spring is displaced and the resulting force is measured. This is done for total travel of 0.19m at an excitation frequency of 0.002Hz. This process is then repeated for different static internal pressures. This is done because the static pressure of the air suspension unit will change depending on the load on the trailer. Another way of representing the stand-alone rolling-lobe air spring is by using the semi-empirical mathematical model as proposed by Fox *et al* (2007).

The force-displacement characteristics for a static pressure of 3.9bar (gage pressure) can be seen in Figure 3.15. The force-displacement characteristic of the air spring, with the force measured by the load cell, is represented by the graph labelled *Measured force*. Also plotted in Figure 3.15 are the force-displacement characteristics (where the force was obtained from the measured pressures) and two graphs that show the air spring characteristics obtained analytically. The analytical expressions are derived in Appendix B. It's also shown in Appendix B that the isothermal gas compression process gives better correlation than the adiabatic gas compression process. Nieto *et al* (2008) monitored the suspension air temperature during working conditions and their results supported the hypothesis of an isothermal process. Therefore for all analytical derivations, an isothermal gas compression process will be assumed. The comparison between the force-displacement characteristic, as measured by the load cell and the analytically obtained characteristics are good except for when the air spring is in rebound. This can be attributed to the carcass stiffness of the rubber of the air spring that comes into play when the air spring is in rebound, and the possible deviation from the constant area as the rebound limit is approached.

Figure 3.14. Experimental setup for characterising the air spring.

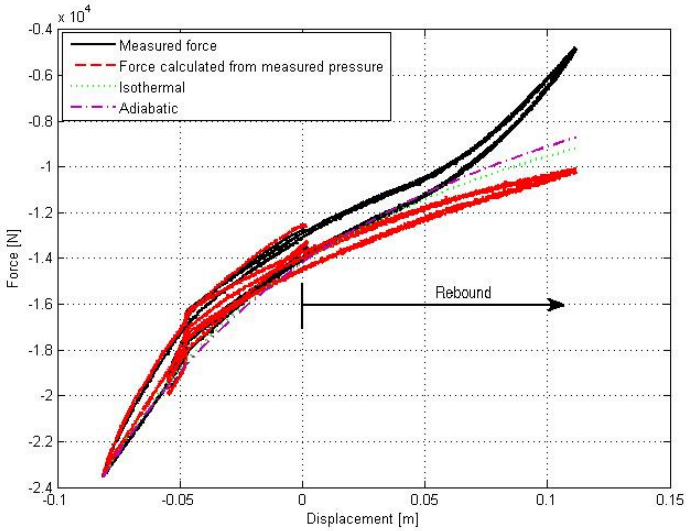

Figure 3.15. Characteristics of the air spring at a gage static pressure of 3.9bar.

This air spring model was integrated with the MBS model of the trailer (described in Chapter 4) and the comparison of the pressures in the air springs are shown in Figure 3.16. This figure shows the data for load case 2 driving over the symmetric discrete obstacle at 8 km/h. It is clear that the predicted pressures are more than double the measured pressures for one of the peaks. This peak takes place when the axle goes over the discrete obstacle. Except for this one peak the trend of the two sets of pressure data correlate well. From this it seems that the spring force predicted by the air spring model may be higher than the actual spring force on the trailer. If the air springs were to be connected with each other it may effectively lower the stiffness of the air springs and improve the predictions. This is investigated in the next paragraph.

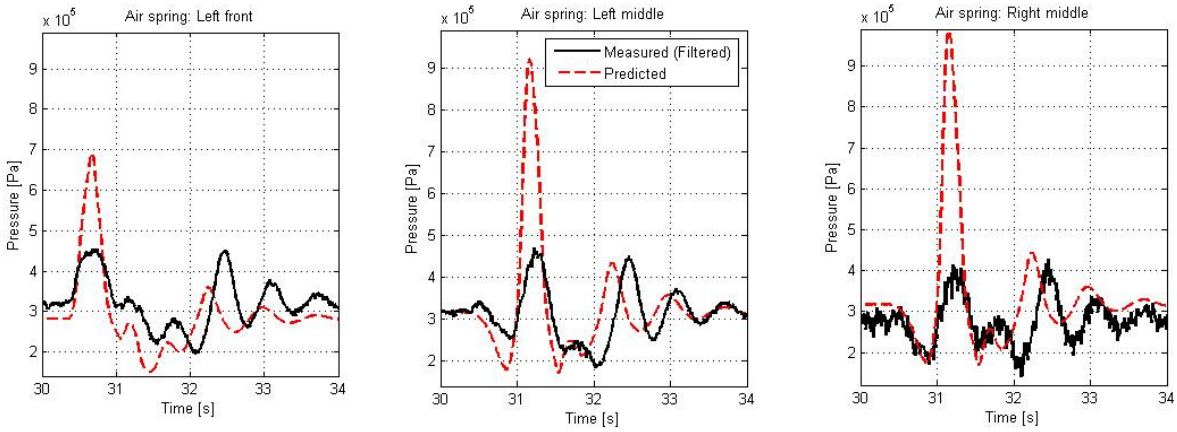

Figure 3.16. Correlation of air spring pressures for the not-connected air spring model.

3.5.2. Interconnected

In the previous paragraph it was indicated that the initial assumption that the air springs are not connected may be incorrect. It seems that when the air springs are modelled as stand-alone units, the predicted pressures are too high. In this paragraph we will model the six air springs as connected, to see if this has the desired effect of lowering the predicted pressures.

To model the six interconnected air springs, the ideal gas law is used and the gas compression process assumed to be isothermal. Any frictional flow losses in the pipes interconnecting the air springs are ignored as well as their volumes. Thus, the pipes are effectively ignored. Starting from the ideal gas law we will derive an analytical expression that is able to describe the characteristics of the interconnected air springs that will give as output the force of each individual air spring. The control surface is chosen in such a manner that it has a control mass as result. This means that the volume of the six individual air springs are now included into one mutual volume. Figure 3.17 shows a schematic representation of the six interconnected air springs. In Figure 3.18, two of the six interconnected air springs at two different states are shown.

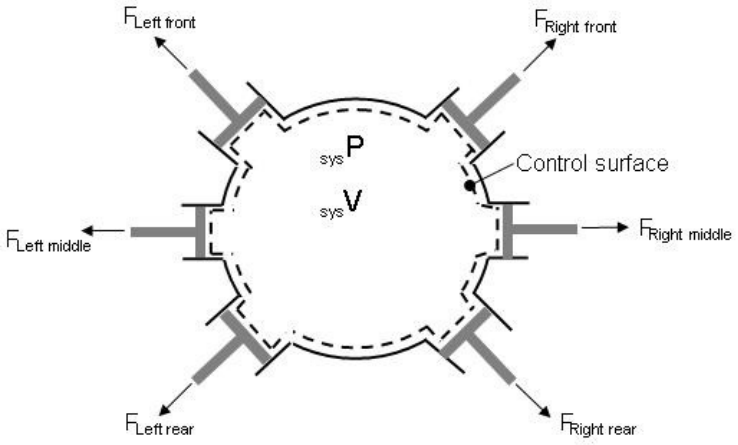

Figure 3.17. Schematic diagram of interconnected system.

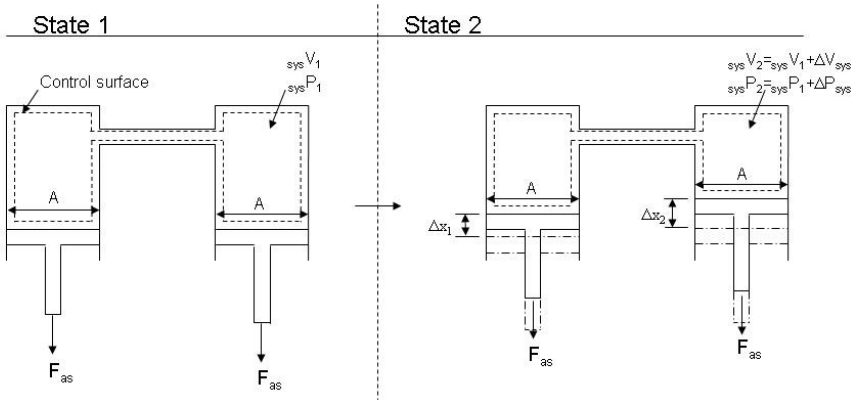

Figure 3.18. Interconnection between two air springs.

The ideal gas law for the interconnected air spring system shown in Figure 3.17 is:

$$\boxed{{}_{sys}P_1\,{}_{sys}V_1 = {}_{sys}P_2\,{}_{sys}V_2} \qquad \{3.1\}$$

where subscript *1* denotes state 1 and subscript *2* denotes state 2, as shown in Figure 3.18. If we substitute ${}_{sys}V_2$ with:

$${}_{sys}V_2 = {}_{sys}V_1 + \Delta V_{sys}$$

we obtain an expression for calculating the pressure of the system at state 2:

$${}_{sys}P_2 = \frac{{}_{sys}P_1\,{}_{sys}V_1}{{}_{sys}V_1 + \Delta V_{sys}}$$

The change in volume of the system, ΔV_{sys}, is calculated as follows:

$$\Delta V_{sys} = \sum_{i=1}^{6} A_i(\Delta x_i, {}_{sys}P).\Delta x_i$$

Where *i* represents each of the six air springs. This equation is for the general case where the area is a function of both the deformation of the air spring, as well as the internal pressure. We now assume that the constant area characteristic derived in section 3.3 holds true. Thus *A* = constant and the equation simplifies to:

$$\Delta V_{sys} = \sum_{i=1}^{6} A\Delta x_i$$

Substituting this equation into the equation for ${}_{sys}P_2$ gives:

$$\boxed{{}_{sys}P_2 = \frac{{}_{sys}P_1\,{}_{sys}V_1}{{}_{sys}V_1 + \sum_{i=1}^{6} A\Delta x_i}} \qquad \{3.2\}$$

The variables on the right hand side of the equation now need to be obtained in order to calculate ${}_{sys}P_2$. The area *A* has already been assumed to be constant. Δx_i is the input to the air spring model that is received from the MBS model. ${}_{sys}P_1$ is the static pressure of the air suspension unit and was measured on the physical trailer. The only variable that is left to

be determined is ${}_{sys}V_1$. This variable represents the volume of the system, made up out of the six air springs, when the trailer is at its ride height position and static equilibrium.

To calculate ${}_{sys}V_1$ we again start with the ideal gas law and assume an isothermal process, but this time we only consider one air spring as a stand-alone unit. The ideal gas law for the stand-alone air spring is:

$$P_1V_1 = P_2V_2$$

With:

$$V_2 = V_1 + \Delta V$$

we substitute this into the ideal gas law and obtain:

$$P_1V_1 = P_2(V_1 + \Delta V)$$

Rearranging the above equation for V_1:

$$V_1 = \frac{P_2\Delta V}{P_1 - P_2} \qquad \{3.3\}$$

With:

$$P_1 = \frac{F_1}{A_1} \qquad \{3.4\}$$

$$P_2 = \frac{F_2}{A_2} \qquad \{3.5\}$$

Substituting equations {3.3} and {3.4} into equation {3.5} and after some manipulation and rearrangement we obtain the following equation for V_1:

$$V_1 = \frac{F_2 \Delta V}{\frac{F_1 A_2}{A_1} - F_2} \qquad \{3.6\}$$

The change in volume, ΔV, is calculated with the following formula:

$$\Delta V = A\Delta x$$

Substituting the equation for ΔV into equation {3.6} and cancelling out A_1 and A_2 (because A_1=A_2=*constant*), the equation for calculating V_1 is given here as equation {3.7}:

$$\boxed{V_1 = \frac{F_2 A\Delta x}{F_1 - F_2}} \qquad \{3.7\}$$

Where $\Delta x = x_2 - x_1$. The variables on the right side of equation {3.7} need to be obtained. To obtain the value of these variables we need to use the Force vs. Deformation characteristics of the air spring we obtained in paragraph 3.5.1 for the stand-alone unit. From the Force vs. Deformation characteristic, at the specific static pressure, we can read off the values for F_1, F_2, x_1 and x_2 from the air spring characteristic, for the present static pressure, as shown in Figure 3.19.

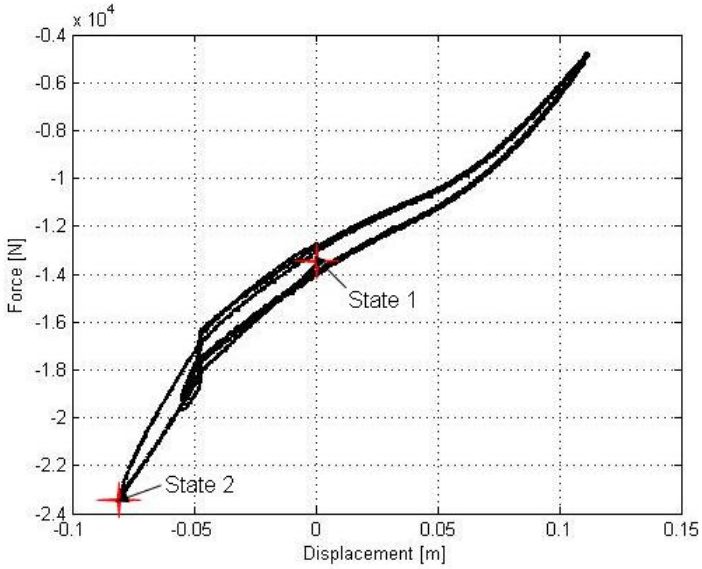

Figure 3.19. Air spring characteristic at a gage static pressure of 3.9bar. Values read off for the variables at state 1 and state 2.

The static volume, V_1, in equation {3.7} is for a single air spring. Thus an approximation for the static volume of the system is made and is denoted as ${}_{sys}V_1$:

$$ {}_{sys}V_1 = 6 \times V_1 $$

With the static volume of the system now known the pressure of the system at state 2 for the system of the six interconnected air springs can now be calculated from equation {3.2}. And with the static pressure of the system at state 2 known, the force in each air spring can be calculated:

$$ \boxed{F_i = {}_{sys}P_2 A} \qquad \text{for i = 1,2 ,…,6} \qquad \{3.8\} $$

Where *i* represents each of the six air springs. The forces calculated in the above equation are sent to the MBS model as the air spring's forces.

The implementation of this air spring model, in the MBS model, has an enormous effect on the correlation between the measured and predicted data. This effect can clearly be seen in Figure 3.20 which compares the predicted pressures, for both the interconnected and not-connected models, to the measured pressures. It is evident that the interconnected spring model now predicts much lower pressures in the air springs. It is also worth noting that the pressures predicted by the air spring model are the same for al six air springs. This is because this model assumes that all three air spring share the same accumulator and all six air springs share the same pressure which is the system pressure. This effect can easily be observed in equation {3.8} from which the forces of each air spring is calculated. This means that the force in all the springs are the same regardless of the displacement of each individual spring.

At the outset of deriving this model, we wanted to lower the effective spring stiffness and thus try and lower the predicted forces. From Figure 3.20 it is clear that the predicted pressures have indeed been lowered, but the trends has now worsened. For completeness we present the effect of assuming an adiabatic process in Appendix C. It can be observed from the results in Appendix C that the difference between the adiabatic and isothermal

gas compression process is minimal. The predicted forces and trends of the interconnected model are still not satisfactory and a more accurate air spring model is required. To try and improve these two aspects we will now look at the next model.

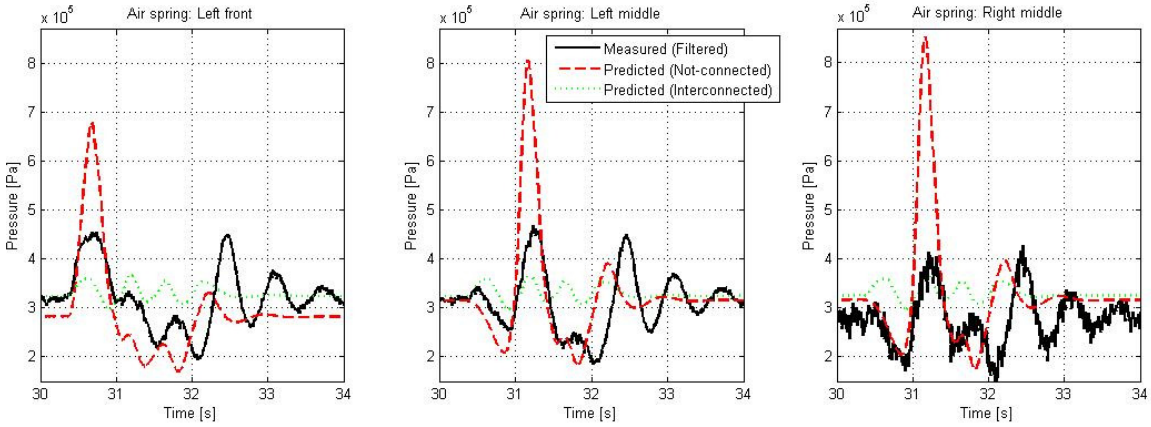

Figure 3.20. Comparison of air spring pressures over discrete symmetrical obstacle for load case 2.

3.5.3. Left-right interconnected

In the previous paragraph we looked at the interconnected air spring model which assumed that all six the air springs are interconnected. The pressures predicted by the interconnected model are too low and the trends are not good. To try and address the problems of the interconnected model we will assume in the next model that the orifice in the levelling valve as described in section 3.1, connecting the left-and right-hand side air springs, restricts the flow so that there is negligible flow between the two sides. The schematic representation of this scenario is shown in Figure 3.21.

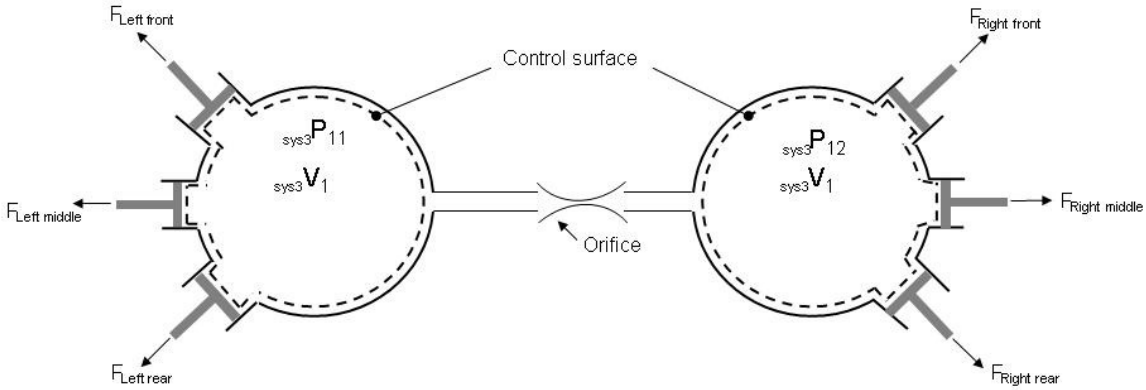

Figure 3.21. Schematic diagram of left-right interconnected system.

We again use the ideal gas law and assume an isothermal gas compression process:

$$ {}_{sys3}P_{1,k}\ {}_{sys3}V_1 = {}_{sys3}P_{2,k}\ {}_{sys3}V_{2,k} \qquad \text{for k = 1,2} $$

Where k represents the two systems consisting of the three air springs on each side respectively. If we substitute ${}_{sys3}V_{2,k}$ with:

$$_{sys3}V_{2,k} = {}_{sys3}V_1 + \Delta V_{sys3,k}$$

we obtain an expression for calculating the pressures in the two systems:

$$_{sys3}P_{2,k} = \frac{_{sys3}P_{1,k}\ {}_{sys3}V_1}{_{sys3}V_1 + \Delta V_{sys3,k}}$$

The change in volume of each system, $\Delta V_{sys3,k}$, is calculated as follows:

$$\Delta V_{sys3,k} = \sum_{i=1}^{3} A\Delta x_{ik}$$

Where *i* represents each of the three air springs, on each of the two sides. Substituting this equation into the equation for $_{sys3}P_{2,k}$ gives:

$$\boxed{_{sys3}P_{2,k} = \frac{_{sys3}P_{1,k}\ {}_{sys3}V_1}{_{sys3}V_1 + \sum_{i=1}^{3} A\Delta x_{ik}}} \qquad \{3.9\}$$

The variables on the right-hand side of the equation {3.9} now need to be obtained in order to calculate $_{sys3}P_{2,k}$. The area A has already been assumed to be constant. Δx_{ik} is the input to the air spring model and is received from the MBS model. $_{sys3}P_{1,k}$ is the static pressure of the air suspension unit and was measured on the physical trailer. The only variable that is still unknown is $_{sys3}V_1$. This variable represents the volume of the system consisting of three air springs, when the trailer is at its ride height position and at static equilibrium. $_{sys3}V_1$ is equal to three times the volume of one of the air springs:

$$_{sys3}V_1 = 3 \times V_1$$

V_1 is calculated from equation {3.7} that was derived in paragraph 3.5.2. With all the variables known the pressure of the two systems at state 2 can now be calculated from equation {3.9}. And with the static pressure $_{sys3}P_{2,k}$ known, the force in each air spring can be calculated:

$$\boxed{F_{ik} = {}_{sys3}P_{2,k}A} \qquad \text{for i = 1,2,3. and k = 1,2.}$$

This air spring model gives the same predictions as the interconnected air spring model over a symmetrical obstacle as shown in Figure 3.22. The left-right interconnected model gives different predictions than the interconnected model when it drives over an asymmetric obstacle as shown in Figure 3.23 although the trends differ, the left-right interconnected model was clearly not successful in improving on the shortfalls of the interconnected model.

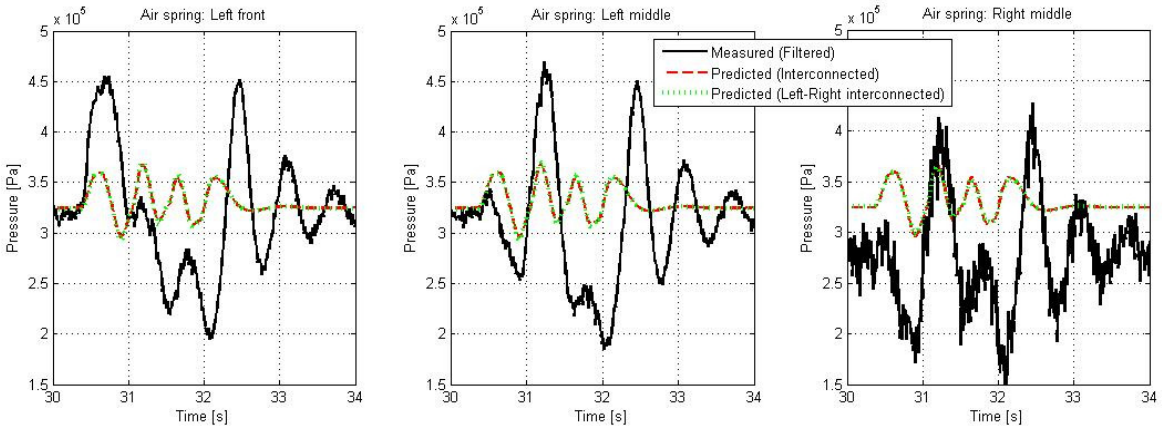

Figure 3.22. Comparison of air spring pressures over discrete symmetrical obstacle.

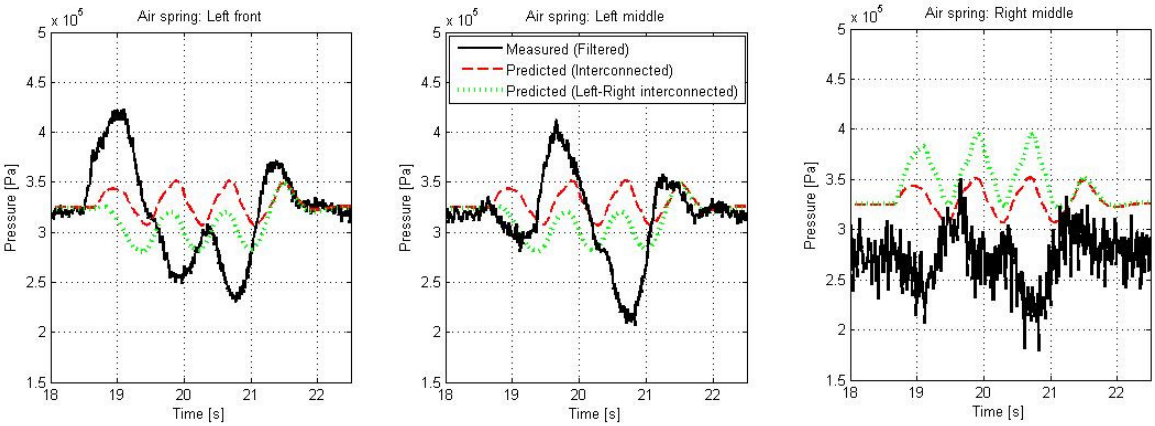

Figure 3.23. Comparison of air spring pressures over discrete asymmetrical obstacle.

3.5.4. Conclusion

It is clear from the previous three paragraphs that the predictions made by the MBS model are strongly dependent on the type of air spring model that is used. The air spring model has a large effect on the predicted pressures. It also has an effect, but to a lesser extend, on other parameters such as the damper force predictions. Because the predictions of the pressure, and indirectly the forces, are dependent on how accurately the air spring model can mimic the physical suspension unit, it is of great importance to be sure that the air spring model is indeed capable of this.

None of the air spring models developed in the previous paragraphs could give satisfactory predictions of the pressures in the air springs. Figure 3.24 and Figure 3.25 shows the pressures predicted by the different air spring models over a discrete symmetric and asymmetric obstacle respectively. The two models that give the worst prediction are the interconnected and left-right interconnected models. Both these models have extremely bad trends. This was attributed to the fact that the pressures in the air springs are calculated from the total system pressure and with the area of the air spring assumed to be constant these calculated pressures are equal. The left-right interconnected model tried to correct this by having the three air springs on each side connected but isolated from the other side. This model did not improve the predictions at all and predicted exactly the same pressures

over the symmetric obstacle, but did predict different pressures over the asymmetric obstacle. The not-connected model, which was the model first used, did not give very accurate prediction in terms of absolute values, but the trend of this model is far better than the interconnected and left-right interconnected models. The problem with the not-connected model seems to be that the effective spring stiffness of the suspension unit is higher than what it physically is. This was one of the reasons for going to the interconnected system and to see if this would lower the spring stiffness. The interconnected model did seem to lower the spring stiffness and its predictions were lower, but the trends were extremely bad. It seemed that this was a step in the right direction if we could only improve the trends. Another modelling approach of the air suspension unit was investigated in Appendix D. In this model it was assumed that the two air springs on each axle are connected, but there is no physical interconnection between the air spring on different axles of the physical vehicle. The mathematical derivation of this model is given in Appendix D. This model shows good trends over both the symmetric and asymmetric obstacles and also reduced the predicted pressure (results indicated in Figure 3.24 and Figure 3.25) but cannot be justified based on the physical layout on the trailer.

From the above discussion it seems that the best model is the front-middle-rear interconnected air spring model. However, it seems that there is some kind of combined effect that lies between the air springs being connected and not-connected. In all of the air spring models considered up to now, none of them have included any flow of air between the air springs or the effects due to flow in the pipes. What will the effects be of this flow of air between the air springs? As stated by Nieto *et al* (2008), when the suspension dynamics are slow and the pipe that connects the air springs is open, we will have the interconnected state. On the other hand, if the suspension dynamics are very fast the pressure waves will not have time to reach the other air spring. This will lead to the air suspension behaving as if the air springs were isolated from each other (the not-connected case). Including the flow of air between the air springs in our model may enable us to capture these effects. In the next section we will look at how we can include the flow of air between the air springs and hopefully obtain a more accurate model for the air suspension unit.

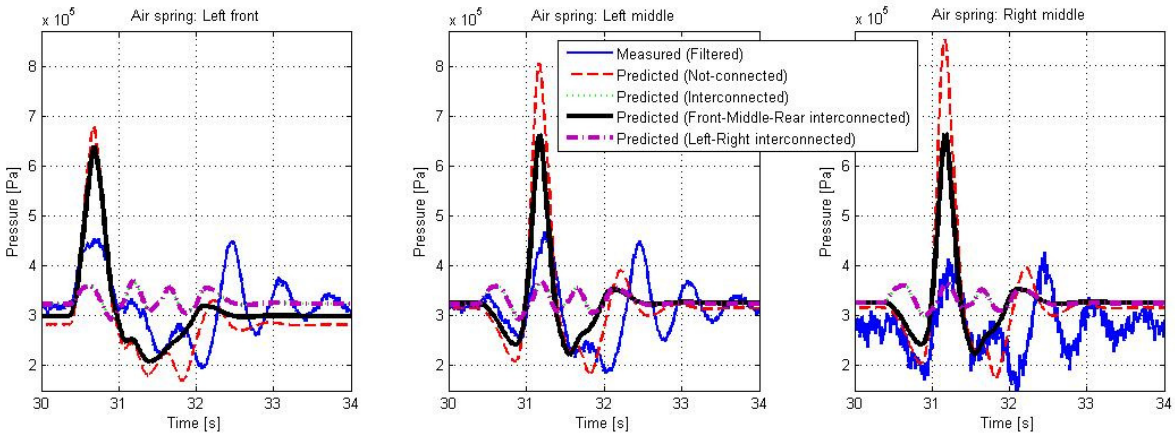

Figure 3.24. Comparison of air spring models over discrete symmetric obstacle.

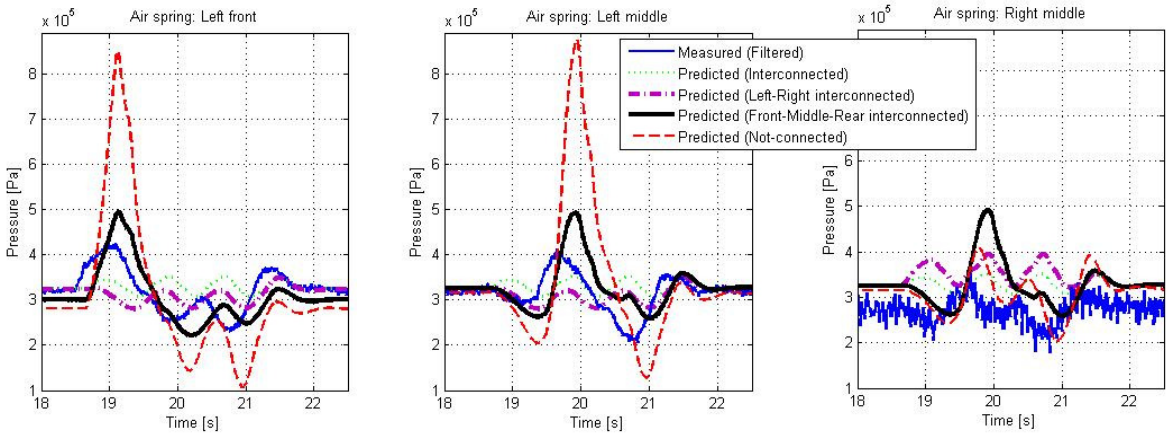

Figure 3.25. Comparison of air spring models over discrete asymmetric obstacle.

3.6. Improved air spring model

It is clear from the previous section that the predictions made by the MBS model are strongly dependent on the type of air spring model that is used. It is for this reason that it was decided to take the air springs in isolation and validate the air spring model before it is integrated into the full vehicle model. To validate the mathematical model of the air springs, the same experimental setup was used as detailed in section 3.3. This setup enable us to give the actuator different inputs and compare the measured forces and pressures, to the forces and pressures predicted by the mathematical air spring model subjected to the same inputs. In all the previous air spring models some of the assumptions made may have simplified the model too much and inhibited the accuracy of these models. All the previous models ignored flow losses and any mass transfer between the air springs. The air spring model derived in this section will try and address these shortfalls.

The modelling of air springs has been the subject of many studies. Nieto *et al* (2008) looked at the modelling of an air suspension system which consists of three principle parts: the air spring, an auxiliary tank, and a pipe connecting the two. The solutions they obtained from both their nonlinear and linear models correlate well with experimental measurements of the stiffness, damping factor, and transmissibility for a reasonable operating range of the suspension. Similar studies were conducted by Quaglia and Sorli (2001) and Porumamilla *et al* (2008). Bhave (1992) investigates the effects of connecting the front and rear air suspensions of a vehicle on the transmissibility of road undulations. A two degree of freedom model is used with linearised mass flow equations. In a study by Theron and Els (2007) they develop a mathematical model of a suspension unit consisting of a two-stage, semi-active, hydro-pneumatic spring, combined with a two-stage, semi-active damper. Here the spring is connected to two accumulators. Abd-El-Tawwab (1997) also looked at the modelling of a twin-accumulator suspension system.

In this study we will try to develop an air spring model that consists of six rolling lobe air springs that includes the mass transfer between the air springs as well as the flow effects in the pipes. Needless to say, that the air spring model has to be able to be integrated into full vehicle simulation models.

3.6.1. Derivation of air spring model

For this model we will assume that the orifice in the levelling valve connecting the left-hand and right-hand side, completely restricts the flow and thus acts as a closed valve. We then choose the control surface in such a way that a control volume is created around each air spring, thus allowing mass to flow between the three air springs on each side. This is illustrated in Figure 3.26. Mass flow out of the air spring is considered to be positive.

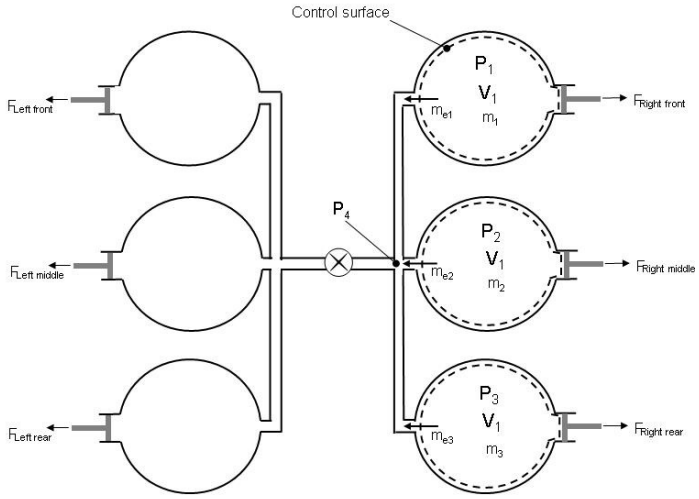

Figure 3.26. Schematic diagram of the air spring system.

The air spring model will receive, as input, the deformations of each air spring from the MBS model for each time step of the simulation. The air spring model will then calculate the forces in each air spring and send this back to the MBS model that will use these forces at the start of the next time step. The procedure the air spring model follows to calculate the forces are described next.

The air spring model starts the calculation by determining the pressure in each air spring due to the volume change induced by the deformation of each air spring. These pressures are calculated from the ideal gas law and the assumption of an isothermal gas compression process:

$$\boxed{PV = mRT}$$

The process is assumed to be isothermal. With some rearrangement and after the volume (V) has been substituted by:

$$V = V_1 + A\Delta x_{ji}$$

we obtain the expression to calculate the pressure in each air spring due to the volume change induced by the deformation of the air spring:

$$P_{ji} = \frac{m_{ji}RT}{V_1 + A\Delta x_{ji}} \qquad \{3.10\}$$

where j represents the three air springs on each side, and i represents the current time step. Thus, Δx_{ji} is the deformation of each respective air spring for the current time step. The

area A is assumed to be a constant based on the findings of section 3.3. V_1 represents the volume of a stand-alone air spring at the ride height position and can be calculated with equation {3.7}. With the process assumed to be isothermal the temperature T stays constant. R is the gas constant of air and m_{ji} is the mass of air present in each air spring at the current time step. For the first time step this value is calculated by:

$$m_{ji} = \frac{P_1 V_1}{RT}$$

where P_1 is the pressure in the system at the ride height position and static equilibrium.

After the pressures have been calculated in each air spring the model then calculates the volume flow (q) in each branch using the Darcy-Weisbach equation (White (2003)) given here as equation {3.11}:

$$h_f = f \frac{L}{d} \frac{v^2}{2g} \qquad \{3.11\}$$

Substituting $v = \frac{q}{A}$, $h_f = \frac{\Delta p}{\rho g}$ into equation {3.11} and rearranging the equation for q, we obtain the following equation:

$$q = \sqrt{\frac{\Delta p}{f\rho \frac{L}{d} \frac{8}{\pi^2 d^4}}}$$

The volume flow in each branch can then be calculated as follows:

$$\boxed{q_{ji} = \sqrt{\frac{(P_{ji} - P_4)}{f\rho \frac{L_j}{d} \frac{8}{\pi^2 d^4}}}} \qquad \{3.12\}$$

Where d is the diameter and L the length of the pipes connecting the air springs. ρ is the density of air. P_{ji} is the pressure in each air spring and is calculated with equation {3.10}. An arbitrary pressure P_4 is chosen that will be changed until the volume flow in the three branches reaches equilibrium. f is the dimensionless parameter known as the *Darcy friction factor*. It is a function of the Reynolds number (Re_d), the relative roughness ($\frac{\varepsilon}{d}$) and the duct shape. The *Darcy friction factor* was obtained experimentally by a trial-and-error process.

Using equation {3.12} the volume flow in each branch is calculated and summed $Q = \sum_{j=1}^{3} q_{ji}$. If the value of Q = 0 then the volume flow in the branches can be used to determine the mass transfer to or from each air spring. If $|Q| >$ *error tolerance* a new value for P_4 is chosen and the volume flow in each branch recalculated. The model repeats this process until $|Q| = 0$ or is within some pre-defined error.

When $|Q| \leq$ *error tolerance* the model will calculate the mass transfer to/from each air spring. In order to catch the transient behaviour of the physical air springs the following is

done in the mathematical model. Each time step of the simulation is divided into smaller time steps:

$$\Delta t_{inner} = \frac{1}{fs \times increments}$$

With *fs* being the sample frequency and *increments* being the number of sub-time steps taken for each time step. The mass transfer calculated here is for each incremental step:

$$m_{e_{ji}} = q_{ji}\rho(P_i)\Delta t_{inner}$$

The density (ρ) of the air in this equation is a function of pressure and thus need to be calculated accordingly:

$$\rho = \frac{P}{RT}$$

After the mass transfer to or from each air spring has been calculated, the pressure in each air spring due to the volume change and the mass transfer can now be calculated:

$$\boxed{P_{ji} = \frac{(m_{ji} - m_{e_{ji}})RT}{V_1 + A\Delta x_{ji}}}$$

With the pressure for each air spring known, the force in each air spring can be calculated using the relation:

$$\boxed{F_{kj} = P_{kj}A}$$ for j = 1, 2, 3. and k = 1, 2.

Before we integrate this air spring model into the full vehicle model, we will first validate the air spring model on its own. The validation of the air spring model will be discussed in the next paragraph.

3.6.2. Validation and refinement of air spring model

As previously mentioned it is of utmost importance to validate mathematical models before they are used in key engineering and business decisions. For this reason we compare the measured forces and pressures with the predictions of the air spring model and hereby verify if the air spring model accurately describes the physical air suspension unit. If we obtain good correlation between the measured and predicted forces and pressures, we will then have confidence in the air spring model and it can then be used in the full vehicle model. In order to generate the predicted forces and pressures, we build an equivalent mathematical model of the experimental setup. The experimental setup is the same as was used in section 3.3. The equivalent mathematical model of the experiment was created in ADAMS/View and is shown in Figure 3.27. The air spring is modelled as a single component force in ADAMS that receives, from SIMULINK, the value of the force for each deformation of the air spring. The signals used in the validation process were of two types:

- Triangular displacement signal with different amplitude and frequency and,
- Random signals.

These signals were used as input to both the experimental setup and the ADAMS model. The correlation between the measured and predicted pressures and forces for the different signals are shown next. In paragraph 3.6.3 we will validate the air spring model for when it hits the bump stop.

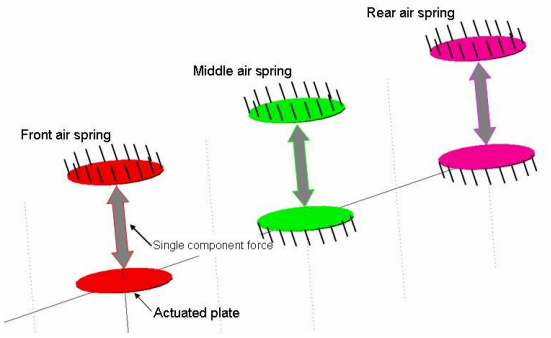

Figure 3.27. ADAMS model of the air spring experimental setup.

Triangular displacement signals

In the following six figures the correlation between the measured and predicted forces and pressures for three different signals can be observed. Three triangular wave shaped signals with different amplitudes and frequencies were used namely:

- Amplitude: 70mm. Frequency: 0.05Hz. (see Figure 3.28 for forces and Figure 3.29 for pressures)
- Amplitude: 70mm. Frequency: 1Hz. (see Figure 3.30 for forces and Figure 3.31 for pressures)
- Amplitude: 35mm. Frequency: 3Hz. (see Figure 3.32 for forces and Figure 3.33 for pressures)

From the figures it is clear that the predictions of the air spring model correlate well with measurements. The only major deviation can be seen in the first graph of Figure 3.28. The model predicts approximately 100kg less than the measurements on the rebound peaks of the front spring. This may be attributed to the same effects that we observed in Figure 3.15. This deviation is not so severe at 1Hz (see Figure 3.30) and may be due to the actuator not being able to closely follow the input signal at the higher excitation frequencies. It can clearly be observed from these figures how the mass transfer to the middle and rear air springs are reduced as the frequency of the input signal is increased. This is a good illustration of the effects stated by Nieto *et al* (2008) that at very fast suspension dynamics the pressure waves will not have time to reach the other air spring. This will lead to the air suspension behaving as if the air springs were not connected.

These comparisons show that the behaviour of the air spring can be predicted quite accurately with the proposed air spring model for triangular displacement inputs. The validation of this air spring model, when subjected to a random signal, will be discussed next.

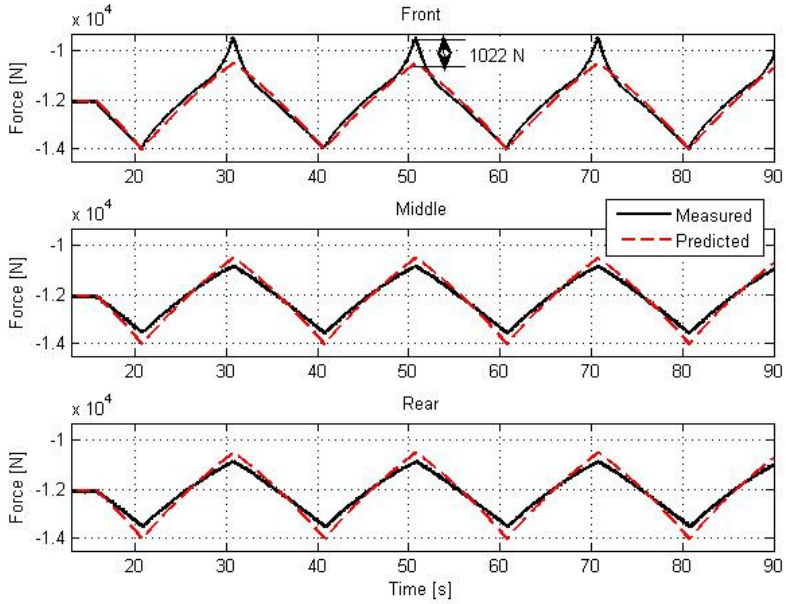

Figure 3.28. Comparison of forces. Input frequency 0.05Hz. Amplitude 70mm. Static pressure 3.2 bar.

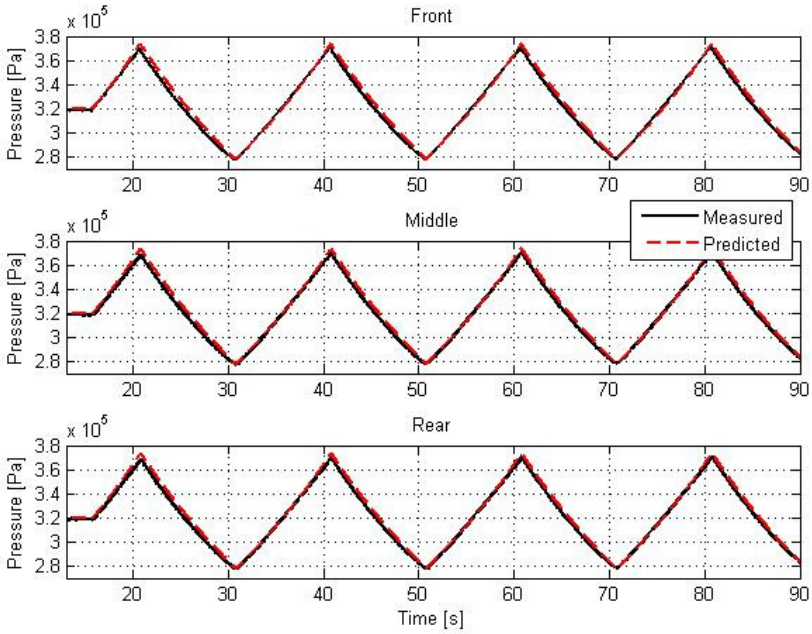

Figure 3.29. Comparison of pressures. Input frequency 0.05Hz. Amplitude 70mm. Static pressure 3.2 bar.

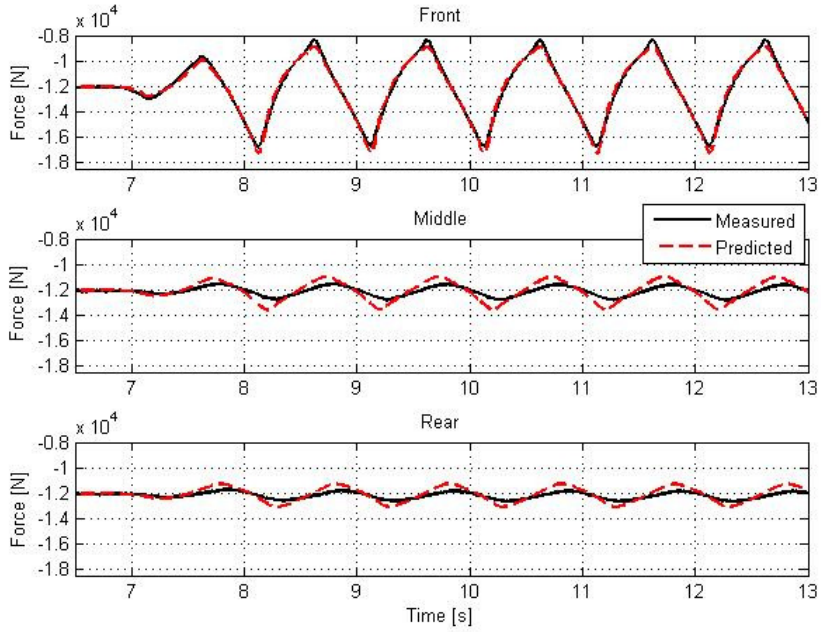

Figure 3.30. Comparison of forces. Input frequency 1Hz. Amplitude 70mm. Static pressure 3.2 bar.

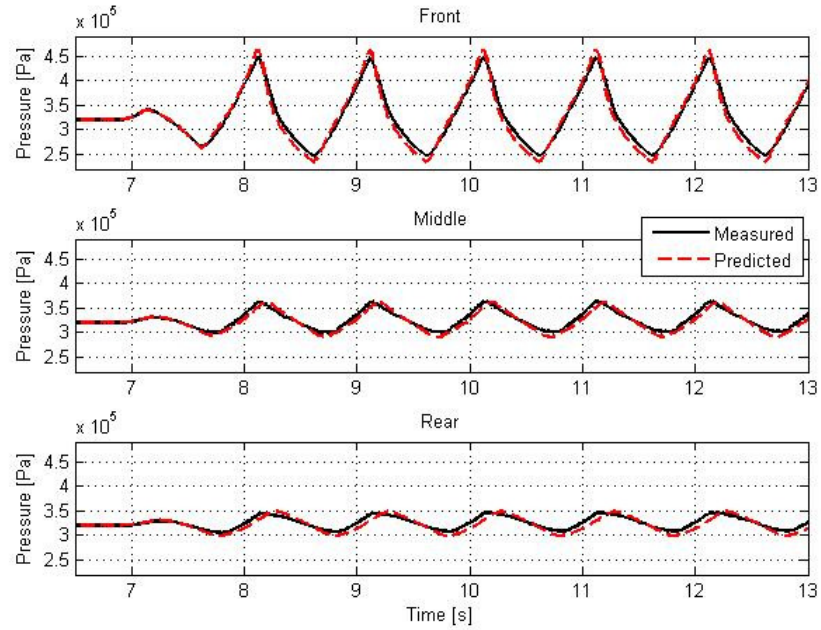

Figure 3.31. Comparison of pressures. Input frequency 1Hz. Amplitude 70mm. Static pressure 3.2 bar.

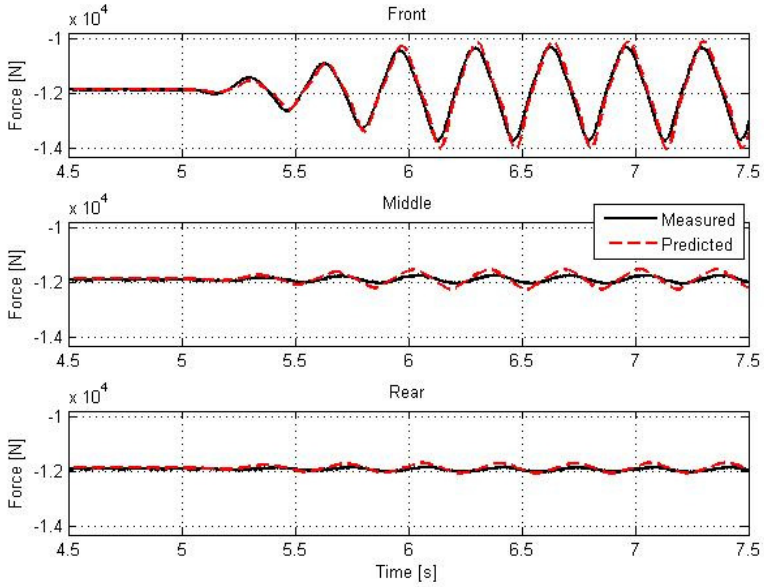

Figure 3.32. Comparison of force. Input frequency 3Hz. Amplitude 35mm. Static pressure 3.2 bar.

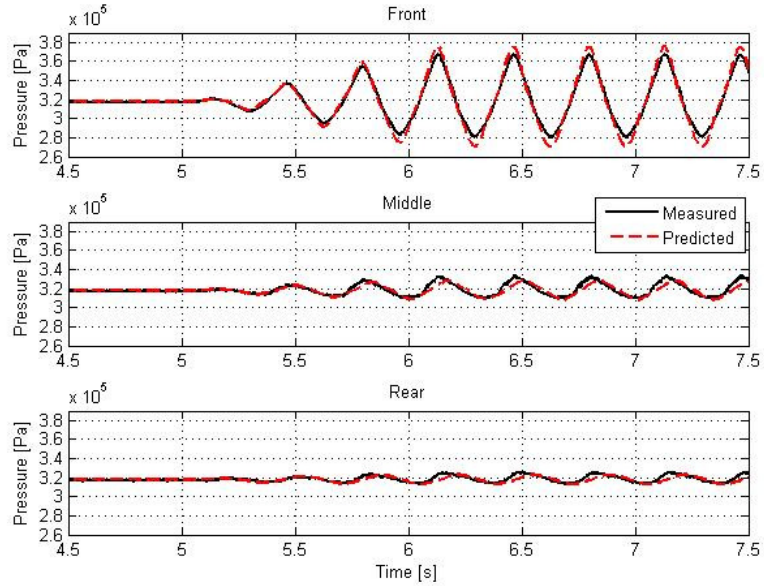

Figure 3.33. Comparison of pressures. Input frequency 3Hz. Amplitude 35mm. Static pressure 3.2 bar.

Random signal

The random signal that was used had a bandwidth of 5Hz and rms amplitude of 30mm. A 10 second section of the correlation between the measured and predicted forces and pressures are shown in Figure 3.34 and Figure 3.35, respectively. The correlation between these two sets of data is excellent.

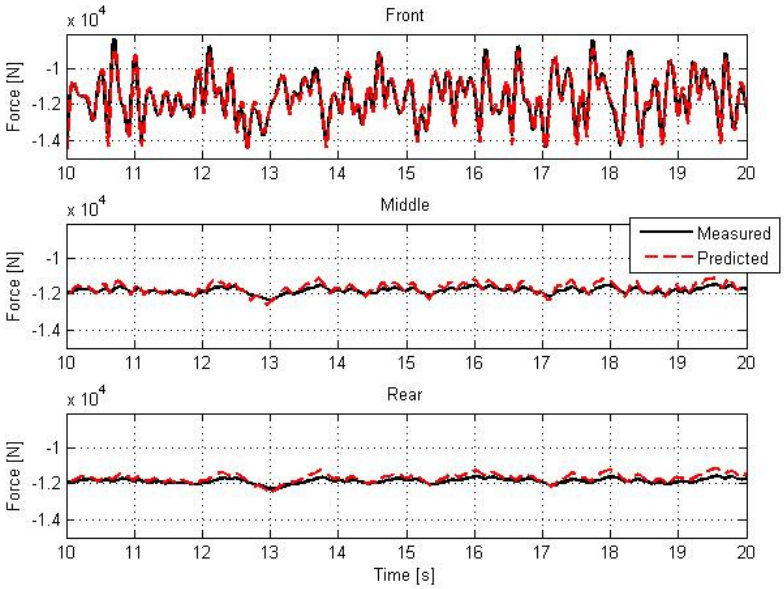

Figure 3.34. Comparison of forces for random input.

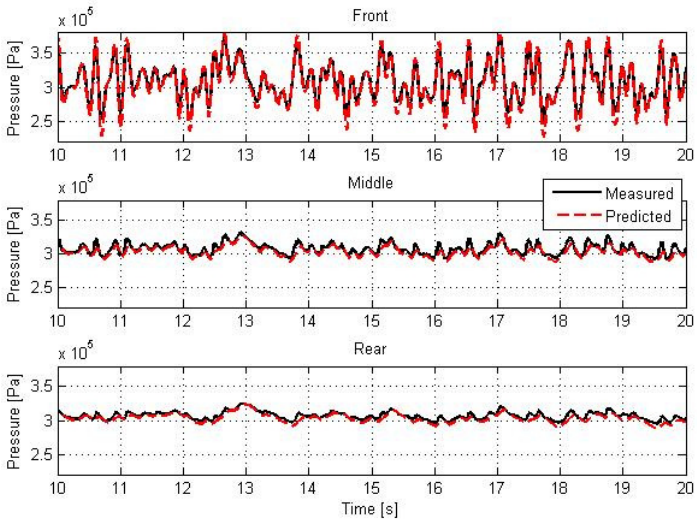

Figure 3.35. Comparison of pressure for random input.

3.6.3. Addition of bump stops to air spring model

We added the non-linear bump stop characteristic that was obtained in Chapter 2, to the air spring model by adding an additional spring (having the characteristics of the non-linear bump stop) in parallel with each air spring. As soon as the maximum allowable travel is exceeded the spring force is obtained from the spring representing the bump stop, and no longer from the air springs themselves. We verified that the air spring model can predict both the pressures and forces when the suspension exceeds its allowable travel and hit the bump stops. Figure 3.36 and Figure 3.37 show the correlation between the measured and predicted forces and pressures when the bump stops are hit, and it can be observed form these figures that there is very good correlation.

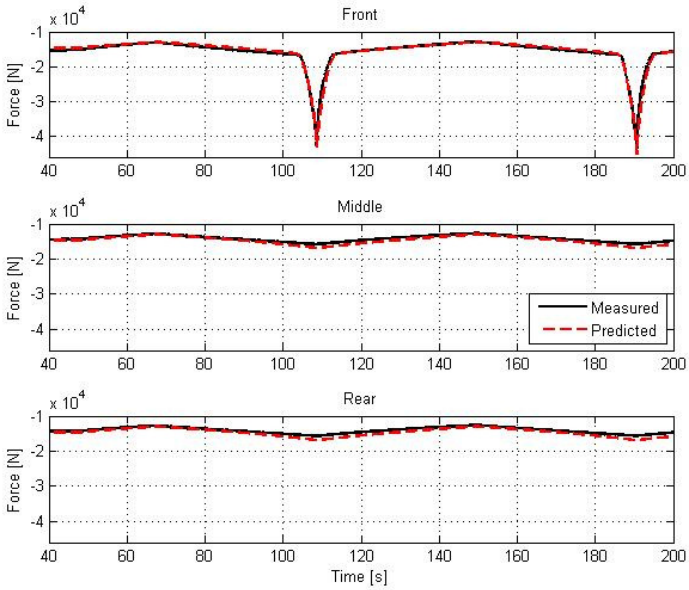

Figure 3.36. Comparison of predicted and measured forces.

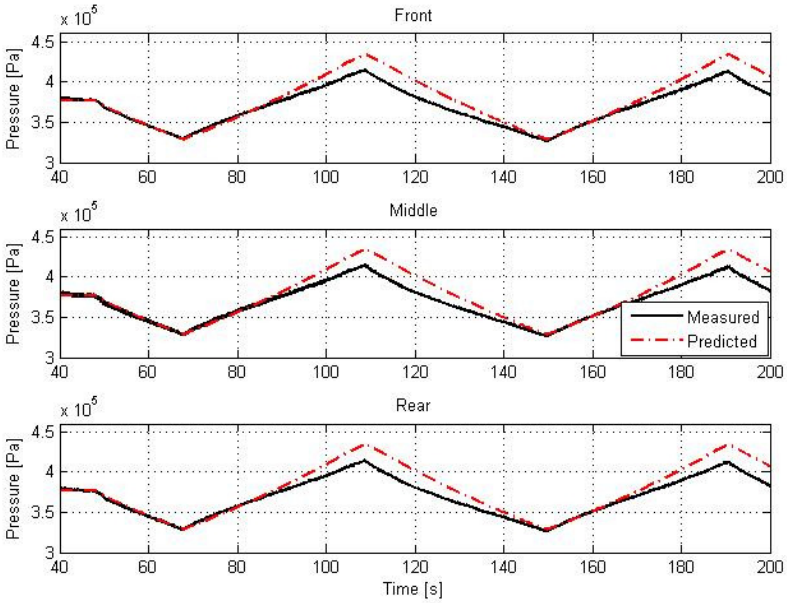

Figure 3.37. Comparison of predicted and measured pressures.

3.7. Summary

After some doubt arose regarding the validity and accuracy of the initial assumptions made about the air spring model we set out in this chapter to obtain a validated air spring model. We compared different air spring models and found that none of them could accurately represent the physical air suspension unit. We concluded that the major reason for the air spring models not being able to give accurate predictions was due to the fact that we have to include mass transfer between the air springs and the effects of the flow in the connecting pipes.

The air spring model derived in section 3.6 allowed for mass transfer between the air spring and the flow effects in the pipes. This model was validated by comparing the

predicted forces and pressures to measured forces and pressures for different inputs on the laboratory test rig. The correlation obtained between the predicted and measured data indicates that the air spring model accurately describes the behaviour of the air springs in the air suspension unit even when the bump stops are hit.

This air spring model was integrated into the full vehicle model to check if it had an improvement in the predicted pressures. If we look at Figure 3.38, which shows the comparison between the measured pressures and the pressures predicted by two of the models over a discrete symmetric obstacle, it can be observed that the improved air spring model indeed gives a significant improvement on the predicted pressures. It is difficult to say if there is an improvement when we look at Figure 3.39 which shows the comparison when the vehicle drives over a discrete asymmetric obstacle. This might be due to suspension kinematics and will be investigated Chapter 4.

The predictions obtained from the full vehicle model, with the improved air spring model, seem to have had a positive effect on the correlation compared to the other air spring models presented in this study. The deviation in the prediction, of the full vehicle model, from the measured pressures may be due to other parameters of the vehicle, i.e. suspension kinematics, speed, etc. These aspects will be investigated in the next chapter when we will perform a thorough validation of the full vehicle model.

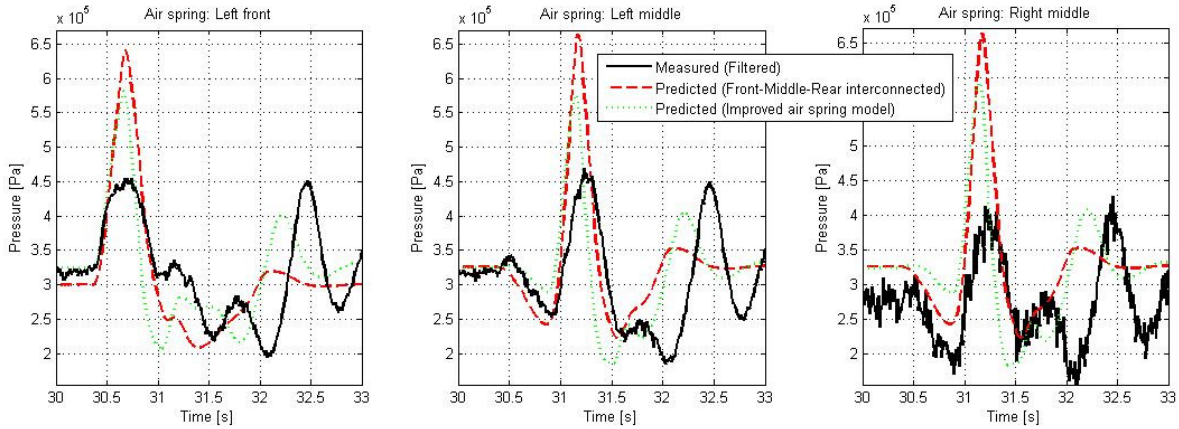

Figure 3.38. Comparison of pressures over discrete symmetric obstacle.

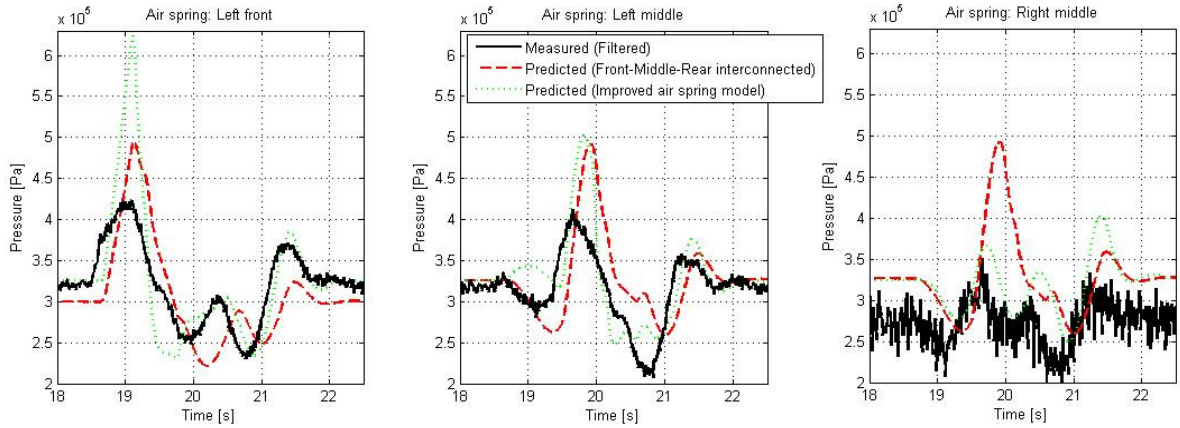

Figure 3.39. Comparison of pressures over discrete asymmetric obstacle.

Chapter 4

The Multi-Body Simulation Model

A multi-body simulation (MBS) model is usually a simplified mathematical representation of the physical vehicle that represents the most important dynamic properties and characteristics of the vehicle. The MBS model, being a simplification, will cause some deviation from the dynamic behaviour of the physical vehicle. If, however, the dynamic model is created thoughtfully the deviation between the MBS model and the physical vehicle can be minimized. As mentioned previously it is necessary to find a compromise between complexity (accuracy) and simplicity (computational efficiency) of the MBS model for its intended use. Therefore, a few assumptions were made at the start to simplify the modelling of some of the physical characteristics of the trailer. In Chapter 3 we saw that we had to discard the assumption made about the air springs not being connected in order to obtain better accuracy from the MBS model. A more accurate air spring model was developed and will be coupled with the MBS model as shown in Figure 4.1. The air spring model was created in SIMULINK and will receive as input the deformations of the air spring from the MBS model. The air spring model will then solve for the forces in the air springs and send this information back to the MBS model.

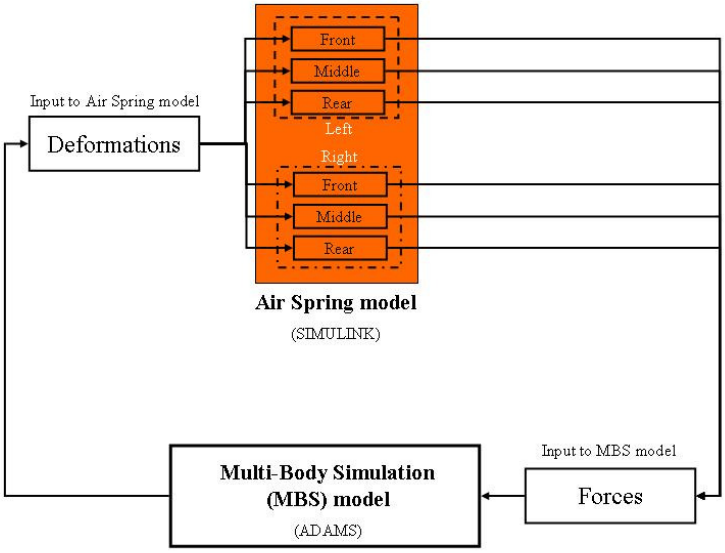

Figure 4.1. Schematic of the data flow between the air spring model and the MBS model.

There are still two more assumptions that remain in order to simplify the present model. The assumptions are:

- all bodies are rigid,
- inputs (displacements, accelerations and forces) from the truck towing the trailer are ignored.

In this chapter we will look at the creation of the MBS model of the trailer, and the validation process that was followed to ensure that the full vehicle model can indeed be used to predict the suspension forces. The emphasis of this chapter will however be on the validation of the full vehicle model and not the creation of the model.

4.1 The initial multi-body simulation model

A multi-body simulation model basically consists of four building blocks namely,

- bodies (in most cases assumed to be rigid),
- force elements,
- constraints (or joints) and,
- drivers (e.g. speed or steering controllers)

The **bodies** are the various components of the trailer that are mathematically described by mass, moments of inertia, centre of gravity and geometry. The required parameters are usually obtained from CAD software. **Force elements** connect bodies without removing any degrees of freedom from either connected body. The force elements include dampers, air springs, bump stops, tyres, etc. Their characteristics are obtained experimentally or from supplier data (see *Chapter 2 - Experimental Work*). **Constraints (or joints)** connect bodies and limit the relative motion of the bodies depending on which types of constraints are used. This implies that constraints remove certain degrees of freedom from a pair of bodies. The type of constraint used is important as it affects the kinematics and kinetics of a pair of bodies. The use of the correct constraints between bodies is of great importance when modelling for instance the suspension of a vehicle as the choice of constraints will affect the kinematics of the suspension system. **Drivers** may be added to the MBS model to for example control the speed of the vehicle or to steer the model through a pre-defined track.

The trailer body, as shown in Figure 4.2, is modelled as a rigid body with its mass, moment of inertia, centre of gravity position and geometry all obtained from CAD. The “truck” is modelled as a body which is restricted to move only in the horisontal plane. The “truck” and trailer is connected with a spherical joint and a force element that counters the body roll of the trailer and attempts to represent the roll stiffness of the fifth wheel.

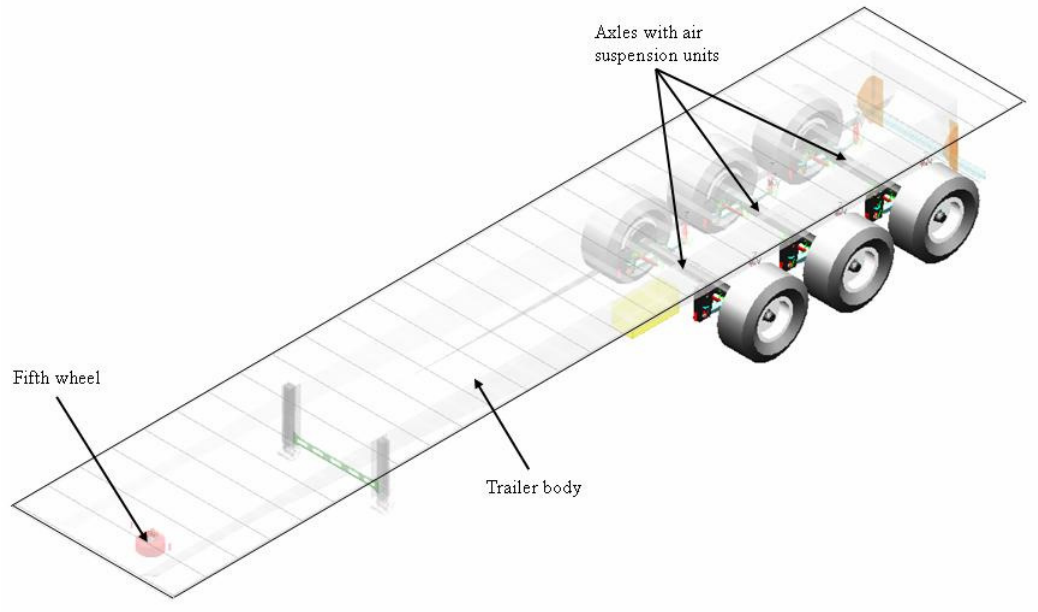

Figure 4.2. Model of trailer.

The model of the suspension unit is shown in Figure 4.3. The dampers are modelled as non-linear splines, and represent the force elements between the hangers and the axles. The air springs are modelled as single component forces, between the trailing arm and trailer body, that receives its force from the air spring model developed in Chapter 3. The non-linear bump stops are included in the air spring model. The bushings between the trailing arms and hangers are modelled as linear bushing elements. This MBS model uses the non-linear ADAMS Pacejka '89 handling tyre model that was fitted to the manufacturer tyre data (see paragraph 2.1.3). A schematic of how all the bodies are connected in the MBS model is shown in Figure 4.4.

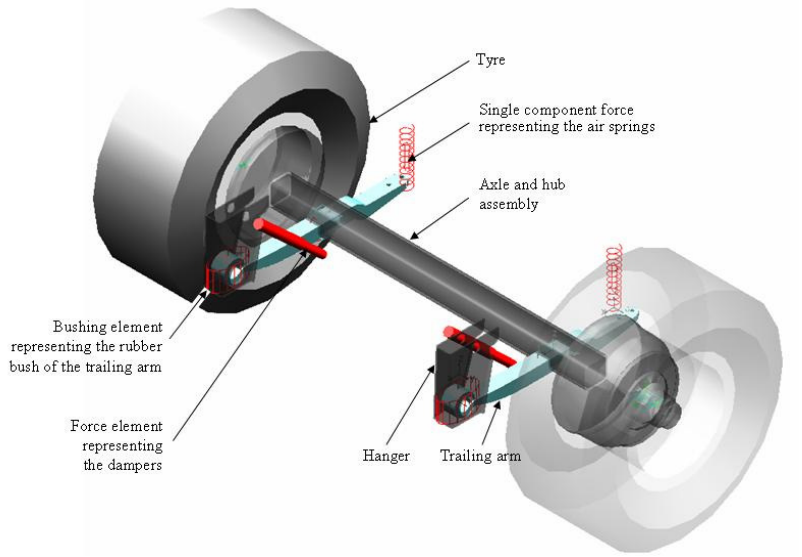

Figure 4.3. Model of suspension unit.

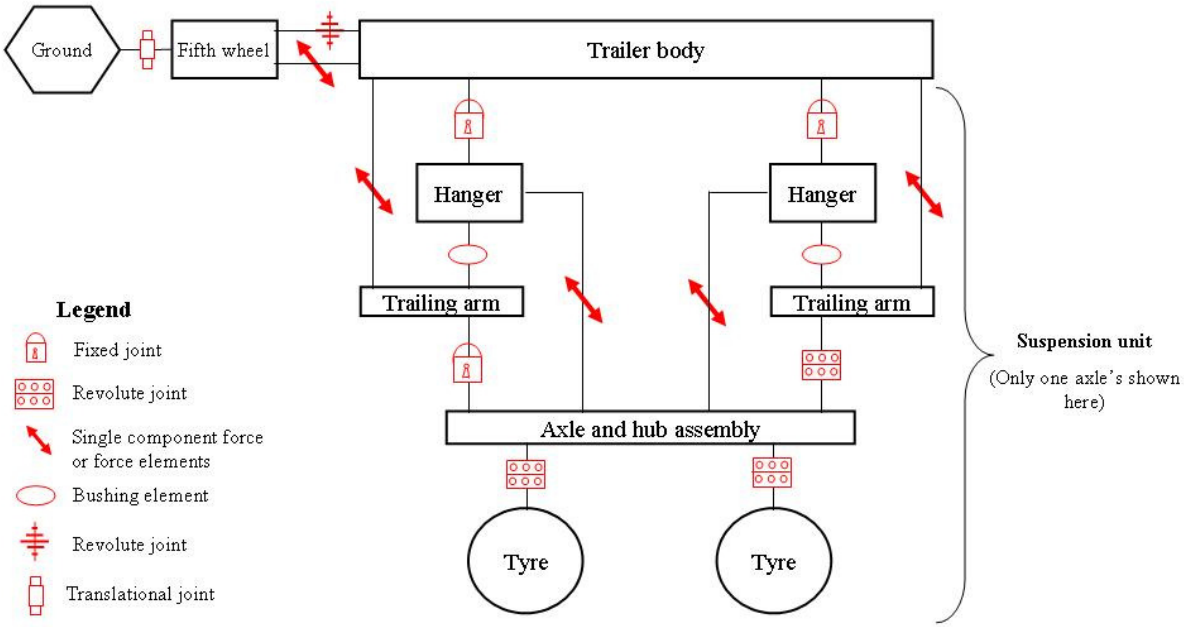

Figure 4.4. Schematic of MBS model

One characteristic that is known to have a large effect on the dynamic behaviour of a vehicle is the speed. This sensitivity towards speed is shown in Figure 4.5 and Figure 4.6 where the speed difference, at which the MBS model hits the obstacle, is only 0.5km/h. From Figure 4.6 it can be observed that the phase difference that exists in Figure 4.5 is no longer present. It can also be observed that there is an improvement in the trend of the predicted data in Figure 4.6.

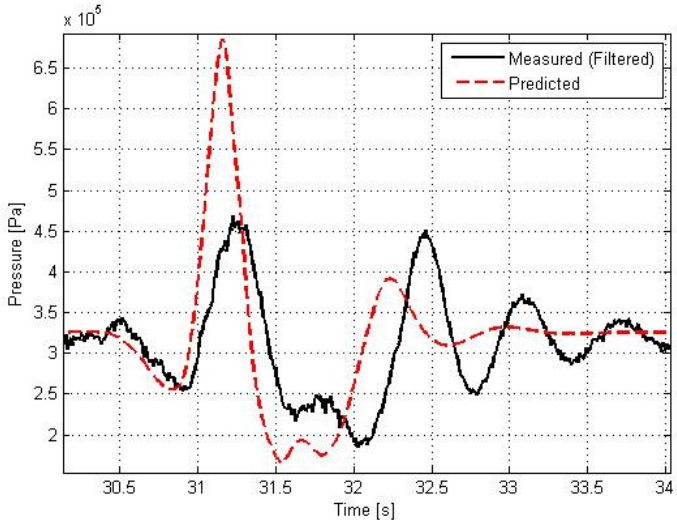

Figure 4.5. Phase shift due to speed difference.

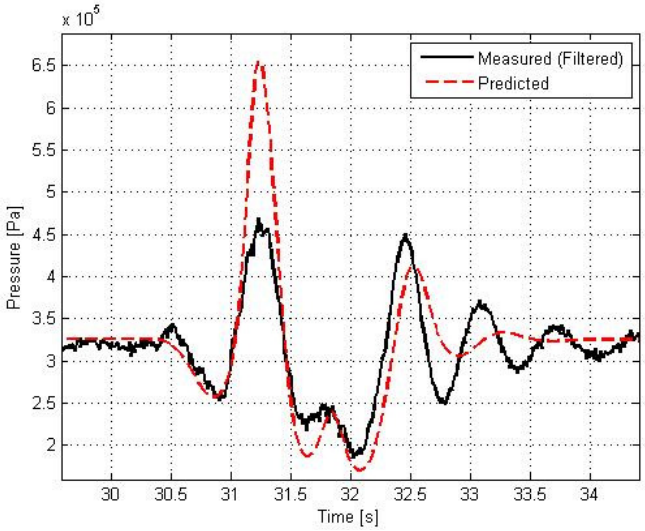

Figure 4.6. Adjusted speed eliminated phase shift and improved trend.

To ensure that the MBS model travels at the same speed as the physical vehicle, a speed controller is added to the MBS model. The physical vehicles' measured speed, for a certain manoeuvre, will be used as input to the speed controller. The speed controller will then aim to keep the MBS model's speed as close to the physical trailer's speed by trying to minimize the error between the desired speed and the actual speed of the MBS model. A comparison between the measured speed of the physical vehicle with that of the MBS model is shown in Figure 4.7. The gain parameter is tuned by trial-and-error until small enough speed errors are achieved. The speed controller is implemented in the MBS model by applying a longitudinal force on the joint representing the fifth wheel of the truck. The magnitude of the force is:

Force on fifth wheel = Gain*(Desired speed-Current speed)

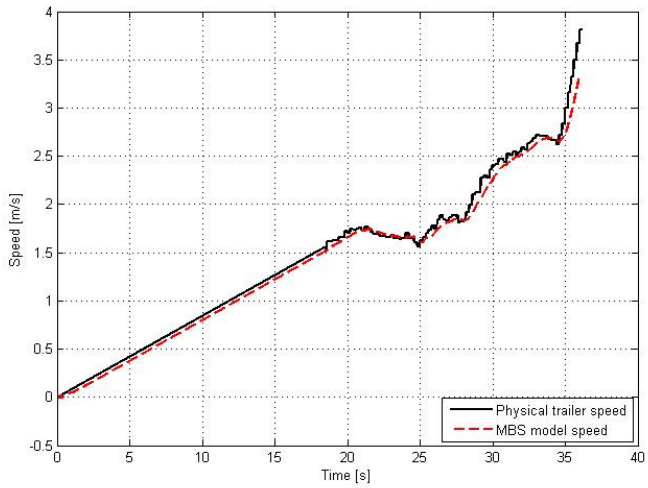

Figure 4.7. Comparison between the physical trailer and the MBS model's speed.

4.2 Validation and refinement of the MBS model

The validation of the MBS model is very important, as mathematical models that are not validated can only be used to do relative comparison studies and even then great care should be taken in the use of these results. The validation process used in this study is similar to the process suggested by Heydinger *et al* (1990) and is indicated in Figure 4.8.

The validation process consists of two branches namely the experimental process and the simulation process. The experimental testing in sub-process a. was done in Chapter 2. In completing this sub-process we obtained the measurements of the behaviour of the physical trailer. The data reduction in sub-process b. includes transforming measured electrical signals into engineering units and digital filtering. The road profiles of the terrains that were used in sub-process a. were obtained (Becker (2008)) and are used as the experimental inputs into the simulations of sub-process e. To validate the simulation model's predictions against the experimentally measured data it is vital to subject the MBS model to the same inputs. With the experimental inputs determined, we then obtained the physical trailer's parameters in order to be able to create the MBS model. These parameters were also obtained in Chapter 2. When we have created the MBS model we can use it in sub-process e. to generate the predictions over the same terrains that were used during the experimental tests.

With the test data and simulation predictions available we can then compare these to verify if the MBS model's predictions are accurate (sub-process f.). These comparisons of sub-process f. will be shown and discussed in this section. If the correlation is good, the validation process is finished and we have a simulation model that can accurately predict the trailer's behaviour. If not, we will have to revisit the assumptions and make the necessary model refinements in sub-process g. The refinements made to the model will also be discussed in this chapter.

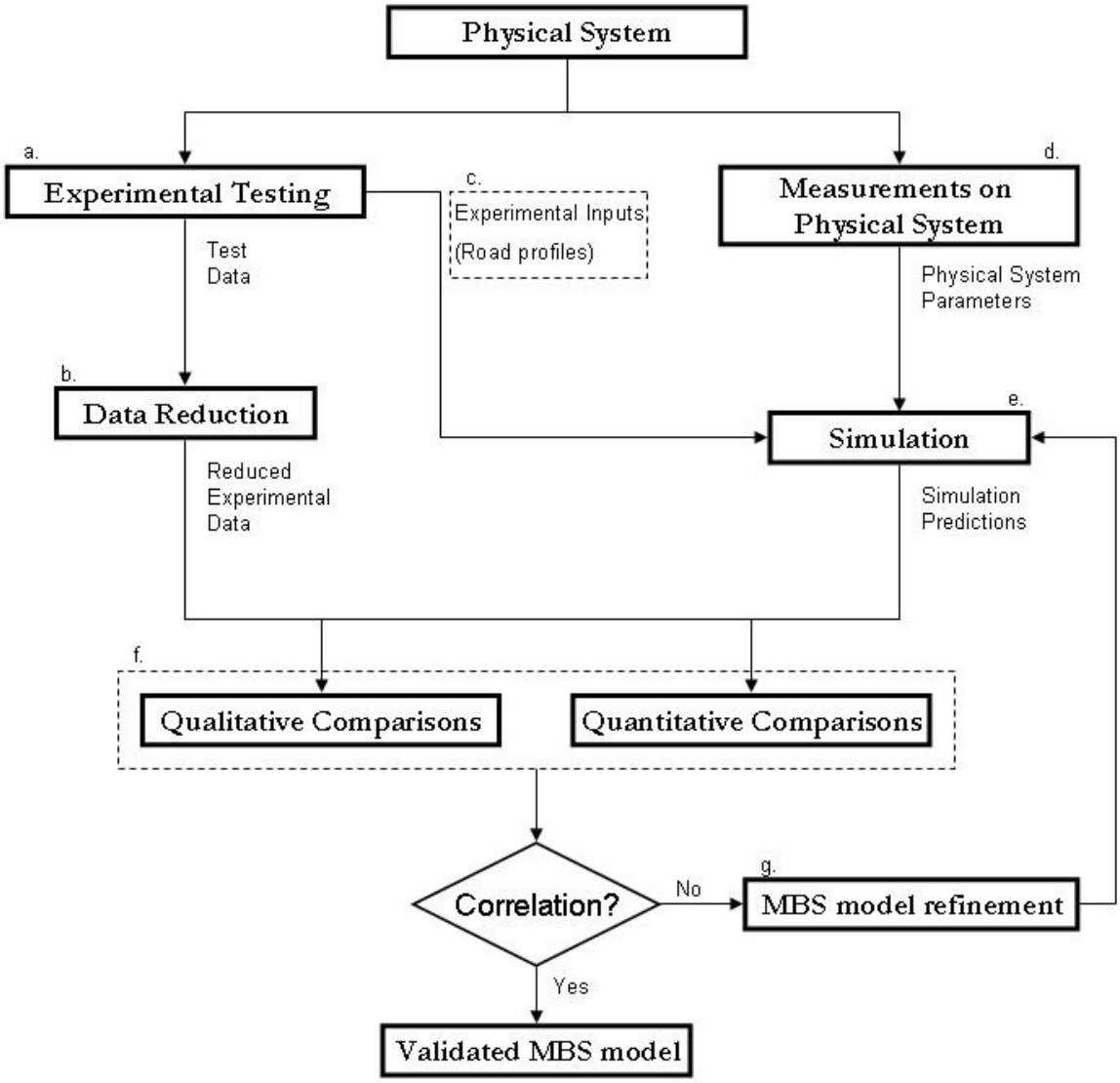

Figure 4.8. Simulation validation process data flow. (Adapted from Heydinger *et al* (1990))

In order to validate the MBS model for a wide operating range we will compare the measured and predicted data over different terrains. These terrains include:

- a discrete symmetric obstacle,
- a discrete asymmetric obstacle and,
- a rough road.

We start the validation process by comparing measured and predicted data over a discrete symmetric obstacle. After we obtained the required correlation over the symmetric discrete obstacle we will then look at an asymmetric discrete obstacle and then at a rough road. The next three paragraphs will determine the correlation over these terrains.

4.2.1. Correlation over symmetric discrete obstacle

The discrete obstacle represents a speed bump that the vehicle may encounter during operation and was defined earlier in Figure 2.16. A photograph of the vehicle driving over the symmetric discrete obstacle is shown in Figure 4.9. We start with the discrete symmetric obstacle as it is easier to analyze the results and to check for correlation. The symmetric obstacle may also minimise certain suspension kinematic effects like for example the auxiliary roll stiffness of the suspension system.

Figure 4.10 and Figure 4.11 show the correlation for the vertical acceleration of the body and the roll and pitch angular velocities respectively. The correlation between the measured and predicted data of these parameters is good (note that the values of the angular velocities are very small). The yaw angular velocity is not included here as it is not a relevant indicator for this type of test.

Figure 4.9. The symmetric discrete obstacle.

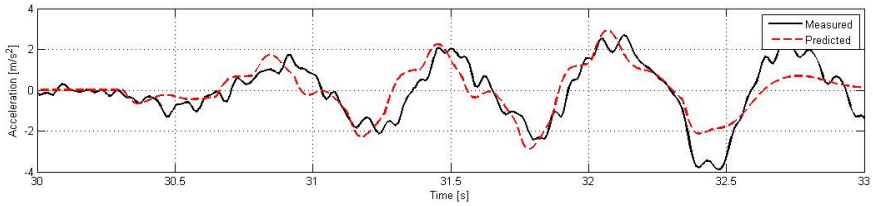

Figure 4.10. Body vertical acceleration over a discrete symmetrical obstacle.

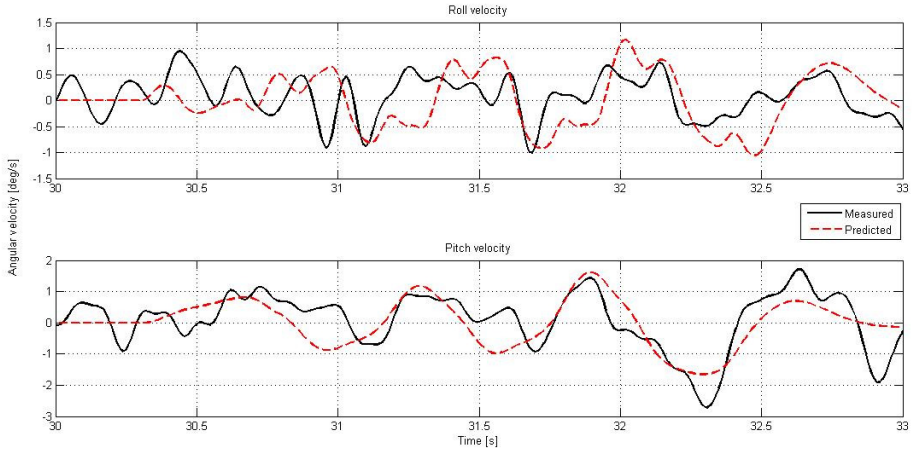

Figure 4.11. Body angular velocities over a discrete symmetrical obstacle.

Figure 4.12 shows the correlation for the damper forces. The predicted tension forces are a bit higher than the measured forces for some of the peaks. If we go back to chapter two we will remember that the correlation of the damper forces, during the calibration process, was not very good in tension. This may be a possible reason for the predicted tension forces being a bit higher than the measured tension forces. Figure 4.13 shows the correlation of the damper deformations and are very good, except for the first peak of the predicted data for the right front damper.

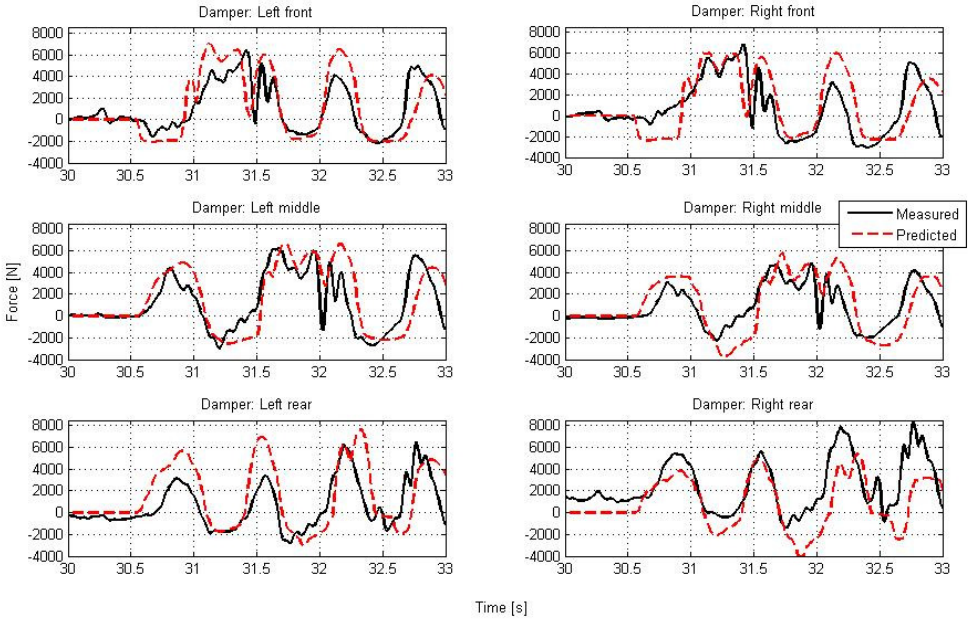

Figure 4.12. Damper forces over a discrete symmetrical obstacle.

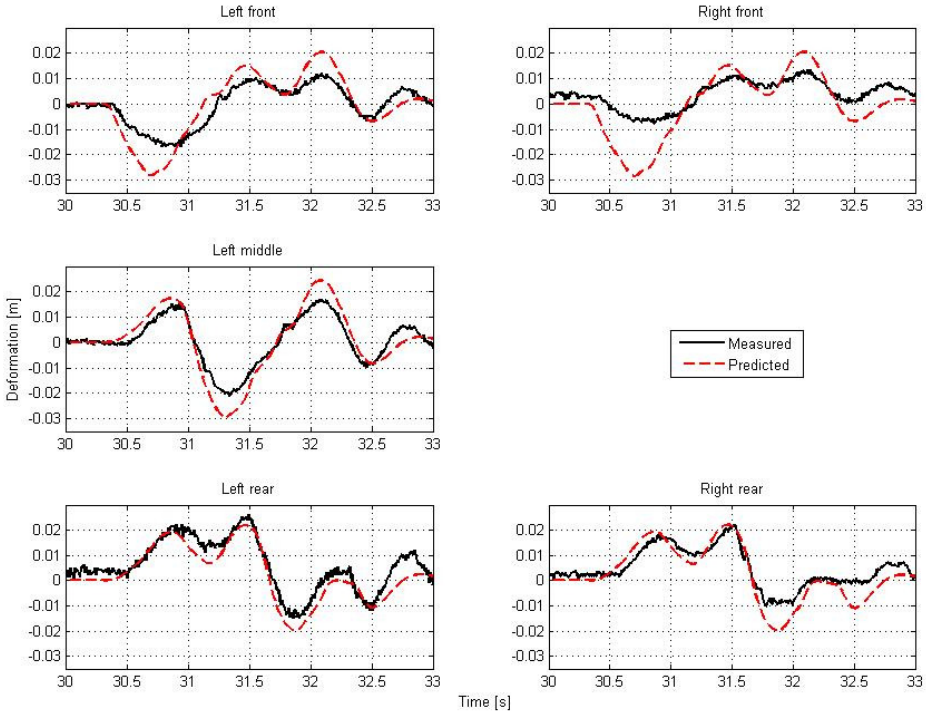

Figure 4.13. Damper deformations over a discrete symmetrical obstacle.

The predicted pressures in the air springs, shown in Figure 4.14, correlate very well with the measured data. The correlation of the pressure of the right middle air spring is not as good, but with closer inspection it can be observed that the measured static pressure in this air spring differs from the other measured static pressures. The increase noise in the measurement is due to the fact that a pressure transducer with a higher pressure rating was used for this measurement. This has the effect of magnifying the noise on the signal. This might also explain the small offset as this transducer, with the higher pressure rating, is much more sensitive to small offsets in the signal.

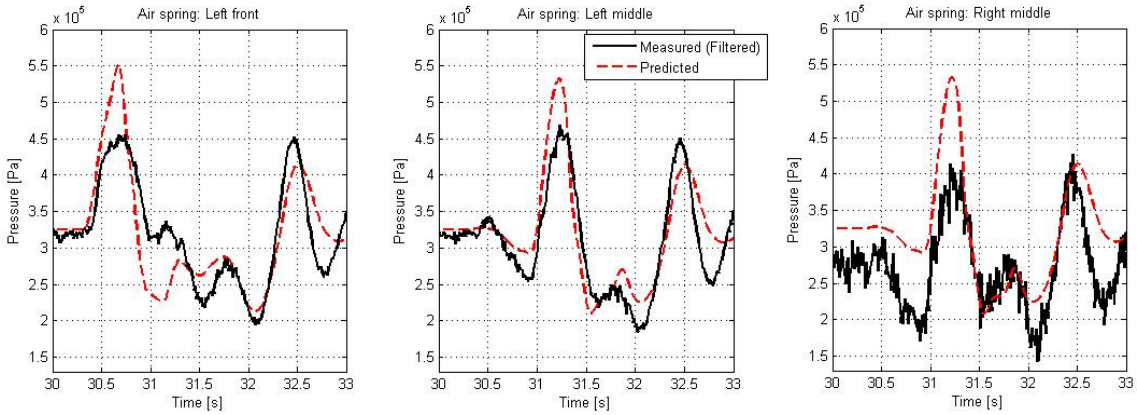

Figure 4.14. Air spring pressures over a discrete symmetrical obstacle.

4.2.2. Correlation over asymmetric discrete obstacle

The asymmetric discrete obstacle is used as a further check for the suspension kinematics in the MBS model. The asymmetric discrete obstacle is shown in Figure 4.15. We suspect that the suspension kinematics will start playing a bigger roll than it did in the symmetric obstacle's case and these effects will be more easily observable. The picture in Figure 4.15 was taken with the trailer empty and it can be observed that both the 1st and 3rd axles lift off the ground when the 2nd axle goes over the obstacle. This indicates that the roll stiffness of the suspension is an important parameter.

Figure 4.15. The asymmetrical discrete obstacle.

One suspension element that has a very significant effect on the suspension forces are the bushings found between the trailing arm and hanger. It has an effect on the suspension forces over both the symmetric and asymmetric obstacle. This effect can clearly be

observed in Figure 4.16. The result obtained with Susp1v2, which has the bushings in place of the revolute joints (see Figure 4.17), shows an improvement in the predicted air spring pressures.

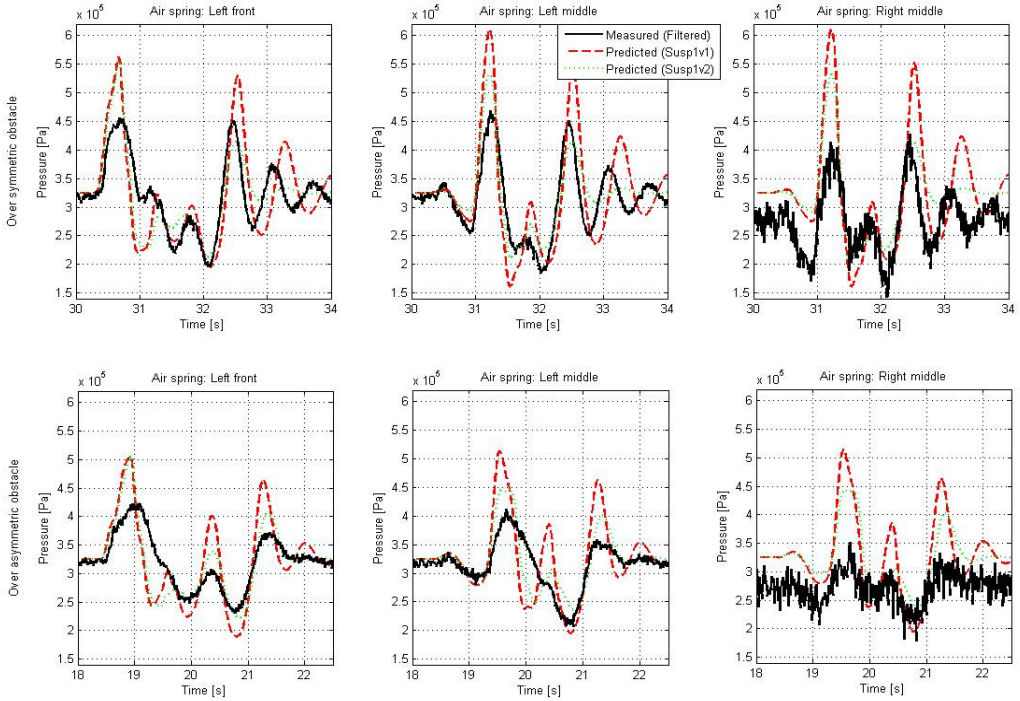

Figure 4.16. Effects of suspension bushings on the suspension forces.

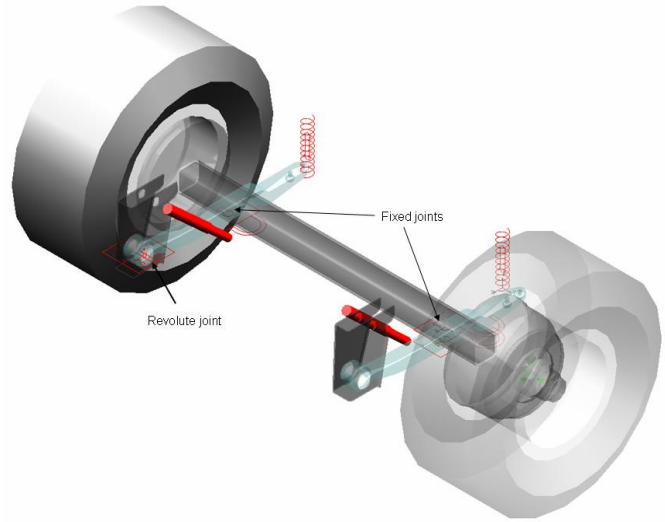

Figure 4.17. Constraints used in modelling the kinematics of the suspension system denoted as Susp1v1.

The constraints as used in Susp1v1 causes the suspension to be rigid around the x-axis, thus preventing the left and right hand wheels to move independently in the vertical direction. If we compare the measured pressures of the left middle and right middle air springs, we can see that the air spring that does not go over the obstacle (in this case the right hand side) has a lower pressure. This effect might be due to the auxiliary roll stiffness of the suspension system. The addition of the bushings in Susp1v2 allows the axle to roll

but does not capture the roll stiffness of the suspension unit. To try and model this effect we replaced one of the fixed joints, between the trailing arm and the axle in Susp1v2, with a revolute joint and a torsion spring shown in Figure 4.18. The torsion spring represents the torsional stiffness of the axle. The torsional stiffness is calculated in Appendix E. The effect of using Susp5 is shown in Figure 4.19 were we can see that this configuration does decrease the pressure in the air spring that does not go over the obstacle. The correlation obtained using Susp5, for the rest of the data, is shown in Figure 4.20 to Figure 4.24. The reader should note that the predicted values in the previous paragraph were obtained from the full vehicle model using Susp5.

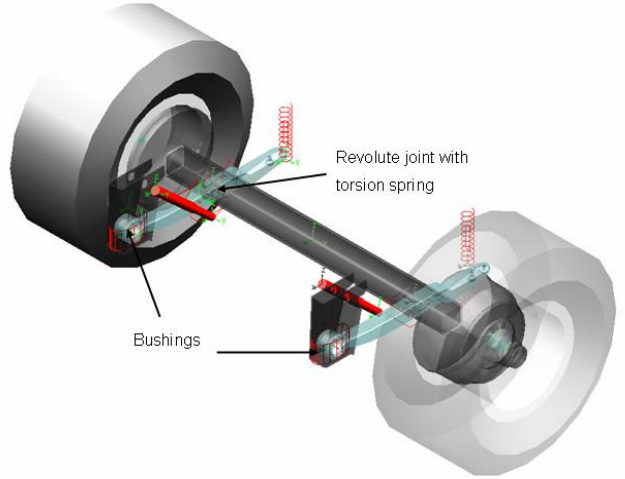

Figure 4.18. Constraints used in modelling the kinematics of the suspension system denoted as Susp5.

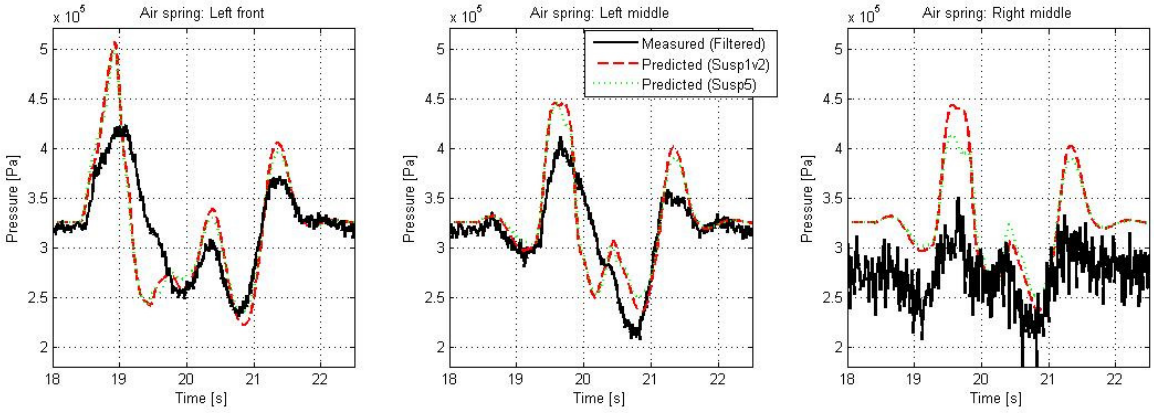

Figure 4.19. Comparison of the predictions of Susp1v2 and Susp5.

Figure 4.20 and Figure 4.21 show the correlation of the vertical acceleration of the body and the roll-and pitch angular velocities respectively. The correlation of these parameters over the asymmetric obstacle is just as good as for the symmetric obstacle, although a higher frequency component is clearly visible in the measured results but absent in the simulation results. This is due to the limitation of the tyre model that will be discussed in the next paragraph.

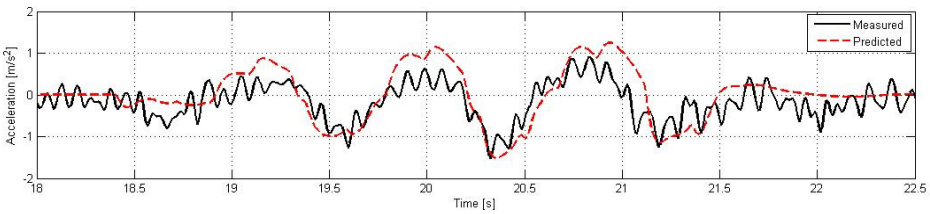

Figure 4.20. Body vertical acceleration over a discrete asymmetrical obstacle.

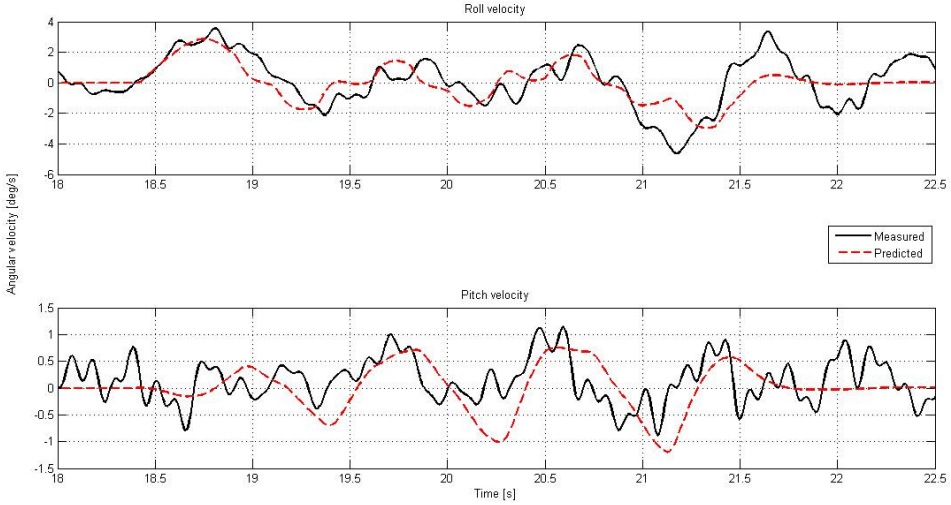

Figure 4.21. Body angular velocities over a discrete asymmetrical obstacle.

Figure 4.22 shows the correlation of the damper forces over the asymmetric obstacle. The correlation over the asymmetric obstacle is not as good as the correlation of the damper forces over the symmetric obstacle. The damper deformations, shown in Figure 4.23, are much better than the correlation obtained for the damper forces.

If one were only to look at the correlation of the body vertical acceleration and the body angular velocities over both the symmetric and asymmetric obstacle, it would have seemed that the MBS model accurately predicts the behaviour of the physical trailer. This would also have been the conclusion if one looked at the damper deformation correlations. However, it is clear from the damper forces that the model does not give the same accuracy over the symmetric and asymmetric obstacle. This observation emphasis the remark made by Bernard and Clover (1994) noted in section 1.1.3, that using vehicle test data to validate the MBS model may lead to certain shortfalls of the simulation model not being detected. It is because of this that it is considered to be very risky to validate one's model against accelerations and/or displacements alone, and then to use the MBS model to predict forces.

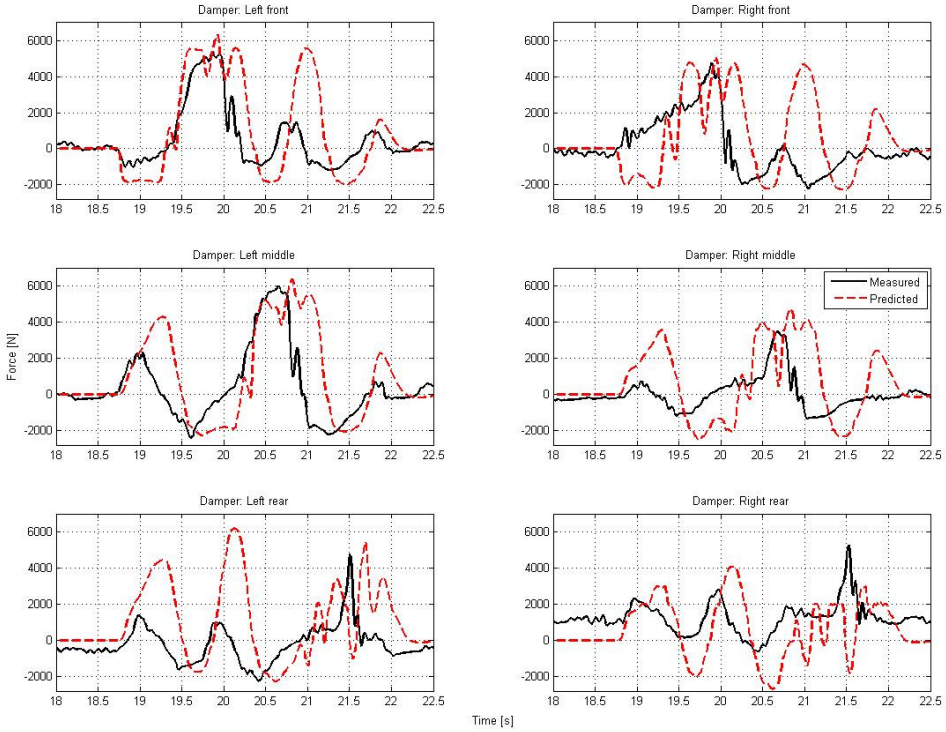

Figure 4.22. Damper forces over a discrete asymmetrical obstacle.

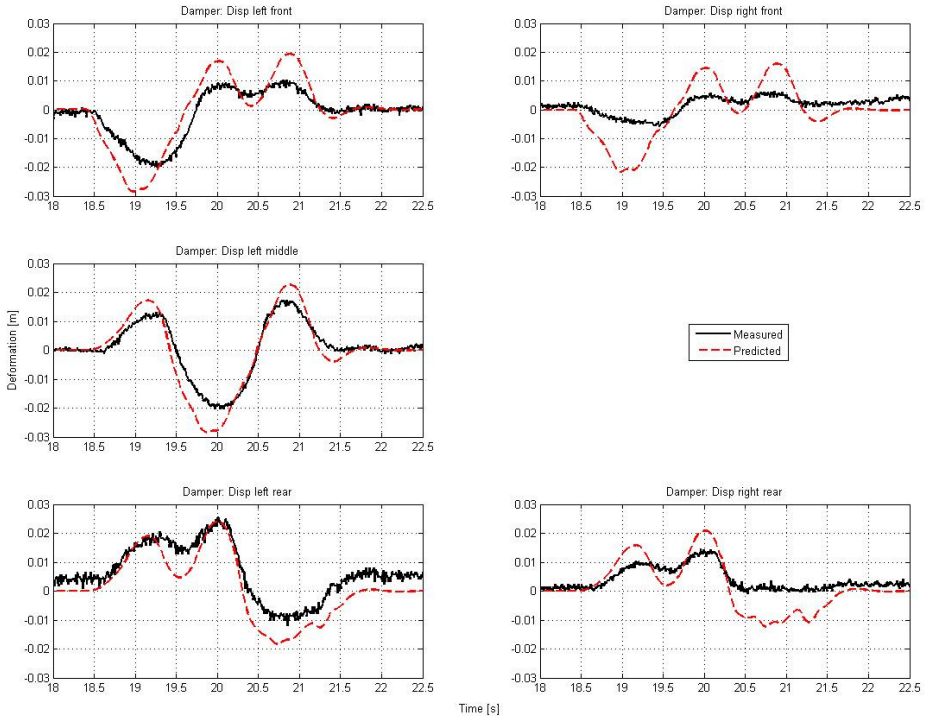

Figure 4.23. Damper deformations over a discrete asymmetrical obstacle.

The predicted pressures in the air springs over the asymmetric obstacle, shown in Figure 4.24, correlate very well with the measured pressures. The same observation is made here regarding the measured static pressure of the right middle air spring that was made for this air spring over the symmetric obstacle.

The correlation obtained for the other two load cases over the discrete obstacle, can be seen in Appendix F and Appendix G.

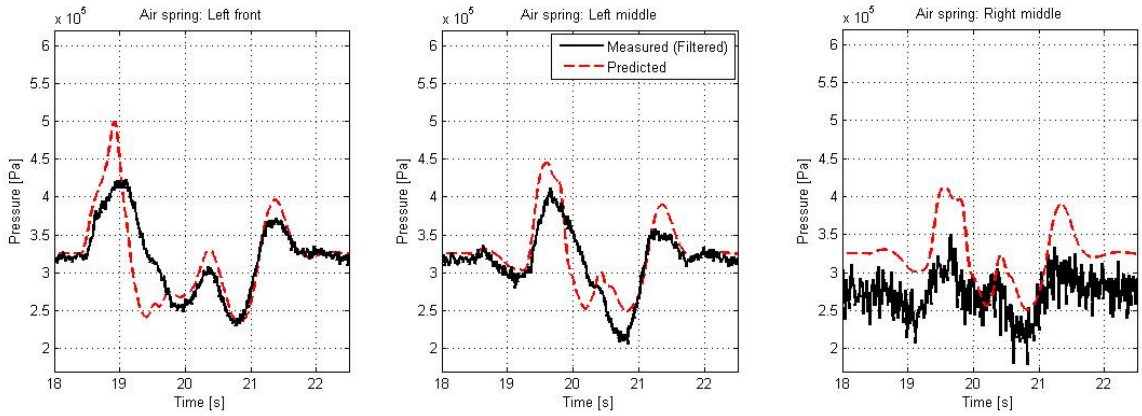

Figure 4.24. Air spring pressures over a discrete asymmetrical obstacle.

4.2.3 Correlation over rough terrain

The terrain used to validate the model over a rough road is the Belgian paving and is shown in Figure 4.25. The Belgian paving was used for two reasons, 1) the Belgian paving stays the same (makes repeatable test possible) and 2) the profile was known (important as it needed as experimental input into the simulation model).

Figure 4.25. Belgian paving.

The correlation between the measured and predicted data for the rough road will be done by comparing the root-mean-square (rms) value of each data set. The results will be compared in this statistical form as it is difficult to compare data that tend to be random in the time-domain. We will also compare the data in the frequency domain and with histograms of the measured and predicted data. The results for load case 2 over the Belgian paving are shown in Table 4.1. The mean percentage difference of all the data is 21.9% with a standard deviation of 18.8%. The data of the right middle damper's forces were ignored in the calculation of the mean and standard deviation as the measured data seemed suspect. Excellent correlation for the body acceleration and the air spring pressures are obtained. The percentage difference in the damper force correlation is bigger at 27%, but

the damper forces are significantly lower than the spring forces and will therefore have a smaller effect on the overall dynamics.

The comparisons between the measured and predicted data in the frequency-domain and as histograms seem to be better than when the percentage difference between the rms values are considered. The FFT's and histograms for some of the parameters in Table 4.1 are shown in Figure 4.26 to Figure 4.32 to illustrate this comment. Figure 4.26 to Figure 4.32 each indicate three graphs namely: 1) comparison of time domain values on the graph on the left, 2) frequency domain comparisons of FFT's on the middle graph and 3) histograms on the right hand graph. Direct comparisons of the time domain data (left hand graph) is difficult as the vehicle doesn't travel on exactly the same lateral position on the three-dimensional Belgian paving road. This should therefore rather be compared in terms of the rms values indicated in Table 4.1. The FFT's in the middle graph gives the frequency content of the parameters and indicate the natural frequency contained in the measurements. The histogram in the right hand graph indicates the time (or number of data points) that the parameters spend in a specific range. Figure 4.26 shows the body vertical acceleration correlation. It is clear from the FFT in this figure that the natural frequency of the trailer bodies' vertical motion compares well.

Table 4.1. Statistical representation of the correlation over a rough road.

	Measured	Predicted	% difference
RMS of Body vertical acceleration [m/s^2]	0.734	0.739	0.68
RMS of Axle vertical acceleration [m/s^2]	2.717	2.299	-15.38
RMS of Air spring pressures [Pa]			
Left front	321225.98	316565.12	-1.45
Left middle	315364.51	312642.44	-0.86
Right middle	282481.49	283089.6	0.22
RMS of Damper forces [N]			
Left			
Front	2079.77	2607.8	25.39
Middle	2023.99	2568.38	26.90
Rear	2091.73	2748.72	31.41
Right			
Front	1947.52	2463.39	26.49
Middle	1386.72	2218.18	*59.96*
Rear	2429.53	2121.04	-12.70
RMS of Damper displacements [m]			
Left			
Front	0.00215	0.0031207	45.15
Middle	0.0024	0.0031176	29.90
Rear	0.00303	0.00316	4.29
Right			
Front	0.00144	0.00322	*123.61*
Middle	0.00671	0.00319	-52.46
Rear	0.00209	0.00323	54.55
Mean			**21.85**
Standard deviation			**18.84**

Note: Values in italics are not used in the calculation of the mean and standard deviation.

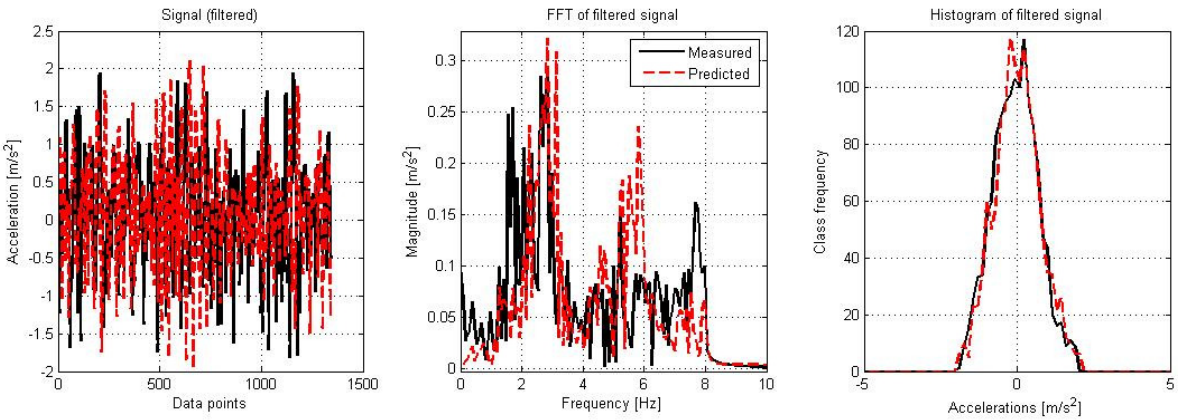

Figure 4.26. Time-and frequency domain representation and histogram of body vertical acceleration.

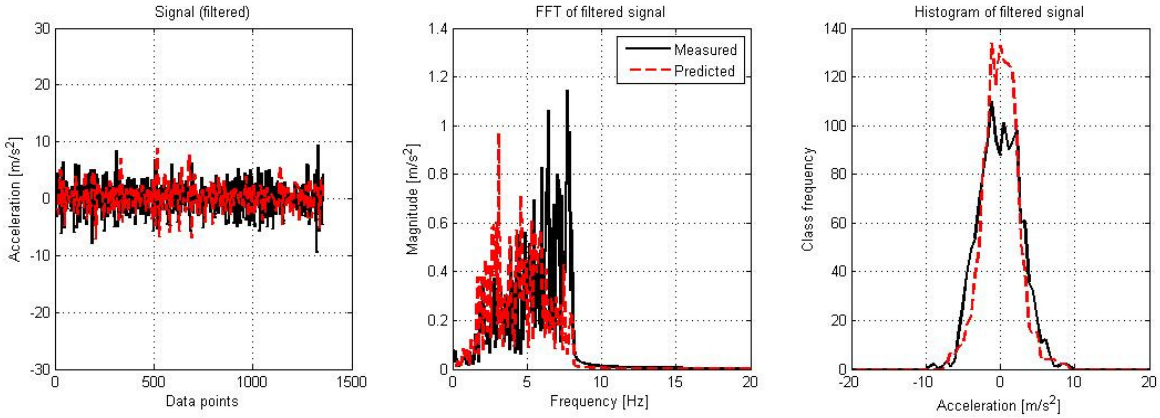

Figure 4.27. Time-and frequency domain representation and histogram of axle vertical acceleration.

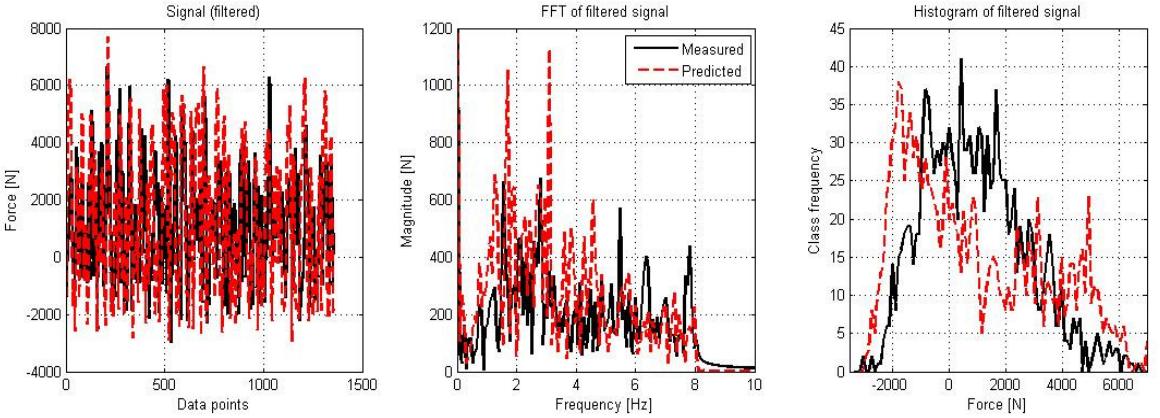

Figure 4.28. Time-and frequency domain representation and histogram of left middle damper forces.

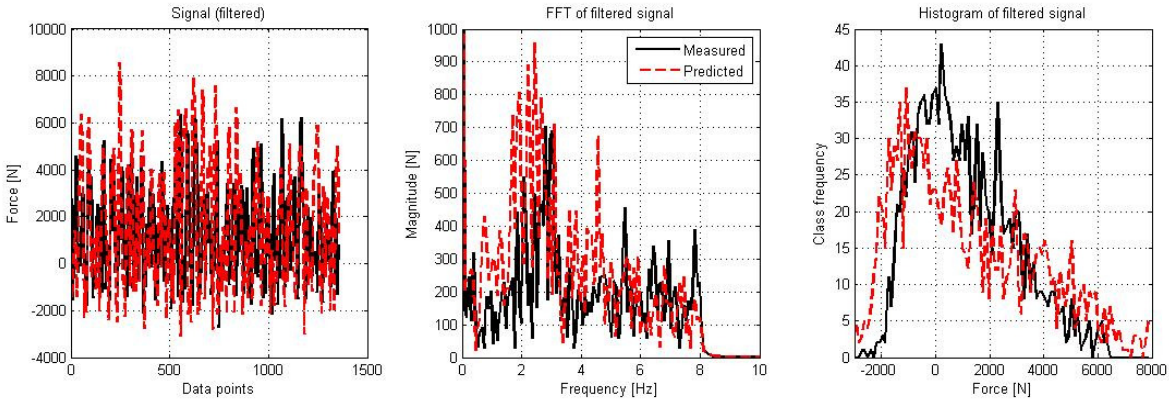

Figure 4.29. Time-and frequency domain representation and histogram of left rear damper forces.

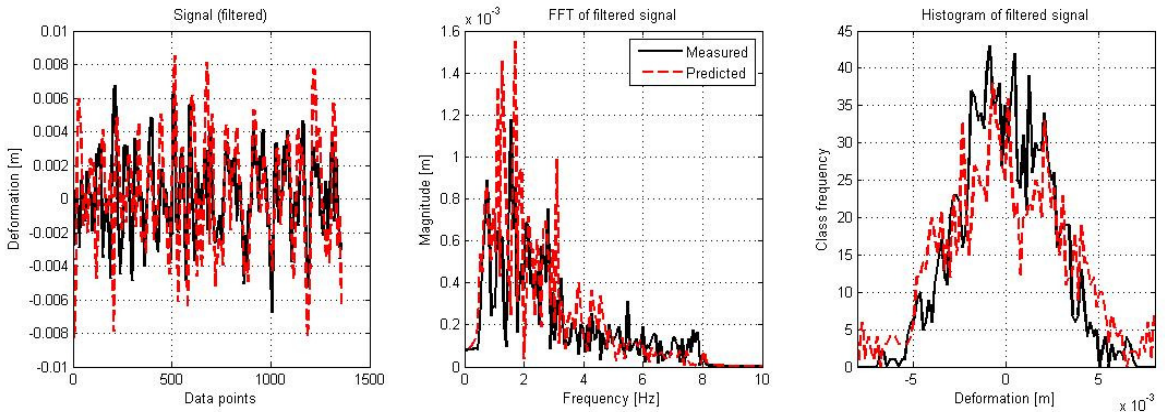

Figure 4.30. Time-and frequency domain representation and histogram of left middle damper deformation.

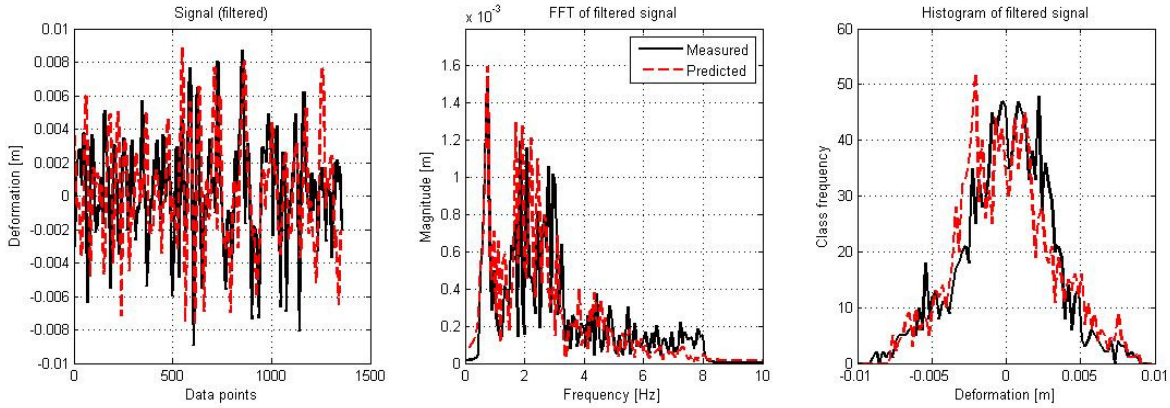

Figure 4.31. Time-and frequency domain representation and histogram of left rear damper deformation.

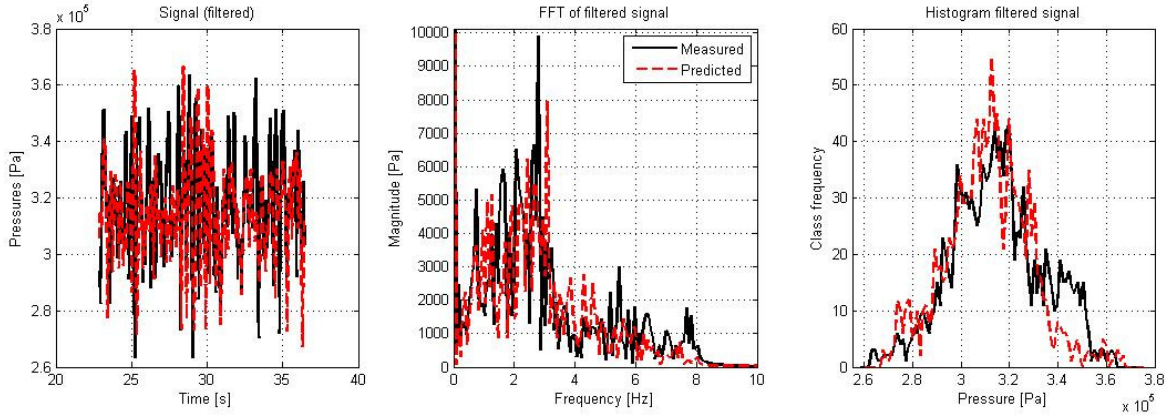

Figure 4.32. Time-and frequency domain representation and histogram of left middle air spring pressure.

Table 4.2 shows the percentage difference between the measured and predicted data for all three load cases. The best overall correlation is obtained for load case three with a mean percentage difference of 11.3% and a standard deviation of 13.3% between the measured and predicted data. The quality in the correlation then decreases as the load is decreased.

Table 4.2. Summary of the correlation over a rough road for the three load cases.

	% difference		
	Load case 1	**Load case 2**	**Load case 3**
RMS of Body vertical acceleration [m/s^2]	4.71	0.68	-49.45
RMS of Axle vertical acceleration [m/s^2]	-35.08	-15.38	-11.59
RMS of Air spring pressures [Pa]			
Left front	-18.79	-1.45	-0.36
Left middle	-12.93	-0.86	-0.30
Right middle	-63.29	0.22	-0.95
RMS of Damper forces [N]			
Left			
Front	-31.46	25.39	14.24
Middle	-27.02	26.90	16.53
Rear	-28.52	31.41	10.00
Right			
Front	No measurement	26.49	0.32
Middle	-17.93	*59.96*	*38.59*
Rear	-42.25	-12.70	-17.96
RMS of Damper displacements [m]			
Left			
Front	-11.49	45.15	-1.09
Middle	-31.02	29.90	-5.22
Rear	-45.89	4.29	-23.18
Right			
Front	20.15	*123.61*	*58.43*
Middle	*-80.00*	-52.46	No measurement
Rear	-34.66	54.55	-6.92
Mean	**28.35**	**21.85**	**11.29**
Standard deviation	**15.06**	**18.84**	**13.32**

Note: Values in italics are not used in the calculation of the mean and standard deviation.

The effect of the tyre model's limitation can clearly be seen in the correlation obtained for the three load cases. If we look at the FFT of the vertical acceleration of the trailer body and axle for the three load cases, shown in Figure 4.33, the reason for the decrease in correlation as the load on the trailer is decreased becomes evident. The first row of figures shows the natural frequency of the body and axle for their vertical motions. From these three graphs it can be seen that the natural frequency of the body decreases and the natural frequency of the axle increases as the load on the trailer is increased. The graphs in the second row show the correlation of the vertical acceleration of the axle after it has been filtered with an 8Hz low-pass filter. It can be seen in these graphs that with the lighter load cases there tends to be more activity near 8Hz in the measured data than for the heavier load cases. This is due to the natural frequency of the unsprung mass i.e. the axle, being lower than for the heavier load cases. As previously stated, the tyre model is not able to go above 8 Hz and thus the predicted data starts to roll off as it nears 8 Hz. This implies that

the measured data has more higher frequencies in their data than the predicted data. This means that the tyre model has a greater effect on the correlation at lower loads. This effect of the tyre model's limitation demonstrated here by using the axle's vertical acceleration, is seen in the other data as well. This implies that the predictions obtained with the Pacejka '89 tyre model will be good as long as the unsprung mass's natural frequency is significantly above 8Hz.

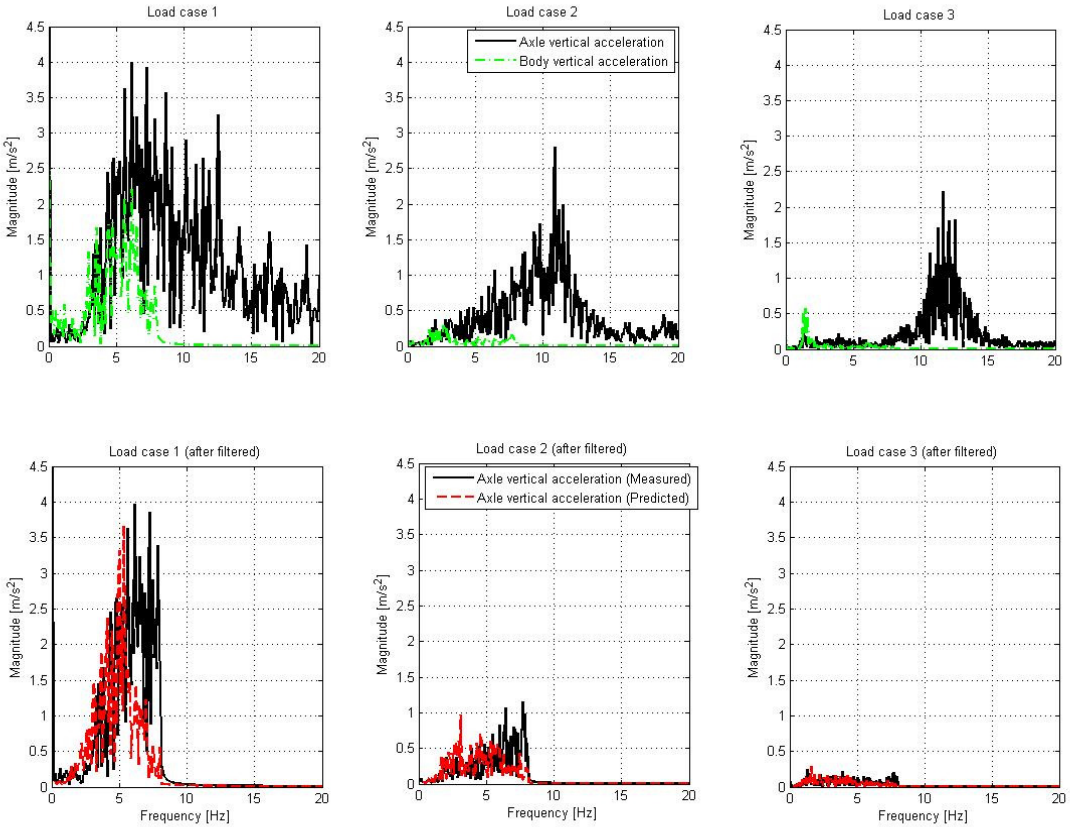

Figure 4.33. Effect of tyre model on data.

4.3. Details of validated MBS model.

The MBS model that we have validated in the previous section was created in ADAMS/view. This MBS model uses the non-linear ADAMS Pacejka '89 handling tyre model that was fitted to the supplier tyre data (see paragraph 2.1.3). The dampers are modelled as non-linear splines, and represent the force elements between the hangers and the axles. The air springs are modelled as single component forces, between the trailing arm and trailer body, that receives its force form the air spring model developed in chapter 3. The non-linear bump stops are included in the air spring model. The bushing between the trailing arm and hanger is modelled as linear bushing elements. The "truck" is modelled as a body which is restricted to move only in the horisontal plane. The "truck" and trailer is connected with a spherical joint and with a force element that counters the body roll of the trailer and attempts to represent the roll stiffness of the fifth wheel.

The complete MBS model consists of 23 bodies, 9 revolute joints, 1 spherical joint, 1 translational joint and 9 fixed joints and one motion defined by the speed controller. Thus

the unconstrained degrees of freedom of the MBS model can be calculated by the Gruebler count:

Gruebler count = (Number of bodies x 6) – (Number of joints x DOF each joint removes) – (Number of motions defined)

The Gruebler count is calculated in Table 4.3. The associated motion of each body is given in Table 4.4.

Table 4.3. Gruebler count of validated MBS model.

	Number of	Degrees of freedom	Total degrees of freedom
Bodies	23	6	138
Joints			
Revolute	9	5	-45
Spherical	1	3	-3
Translational	1	5	-5
Fixed	9	6	-54
Defined motions	1	1	-1
Unconstrained DOF's			**30**

Table 4.4. MBS model's degrees of freedom.

Body	Amount	Unconstrained Degrees of freedom	Associated motions
Trailer body	1	5	Lateral, vertical, roll, pitch and yaw
Axle and hub sub-assembly	3	6 x 3	Longitudinal, lateral, vertical, roll, pitch and yaw
Trailing arm	6	1 x 3	Roll
Wheels	6	1 x 6	Pitch

4.4. Summary

The correlation shown up to now in this chapter was for the second load case (see section 2.2.2 for load case details). The correlations over the symmetric and asymmetric discrete obstacle as well as over the rough road for the other two load cases are shown in Appendix F and G respectively.

Correlation over the discrete obstacle for all three load cases is very good and it seems that the MBS model can accurately predict the behaviour of the vehicle over a discrete road event. The correlation achieved over the rough road is not as good as the correlation over the discrete obstacle. The major reason for this is due to the limitation brought on by the tyre model with it not being able to function over 8Hz as discussed in paragraph 4.2.3. From the correlation achieved in the validation process it would seem that the air spring model that was created in Chapter 3, coupled with the MBS model, is an accurate representation of the physical trailer. Furthermore it is evident that it is possible to obtain

quite accurate prediction of the suspension forces over discrete road events and rough roads using the Pacejka ’89 handling tyre model.

The importance of validating the MBS model for the parameters that will be used in further analyses, or in key business and engineering decisions, were also shown. The conclusion along with the limitations of the current model and the recommendations for future work, are given in Chapter 5.

The second road event, the rough road also called the Belgian paving, represents a road with higher frequency content. Validation of the MBS model over this road ensures that the MBS model can in fact predict the dynamic behaviour of the vehicle over rough roads like for example gravel roads and bad secondary roads. Figure 2.18 shows the Belgian paving. Tests over both of these two road events are done at different speeds for the three load cases discussed in Table 2.7 and Figure 2.15.

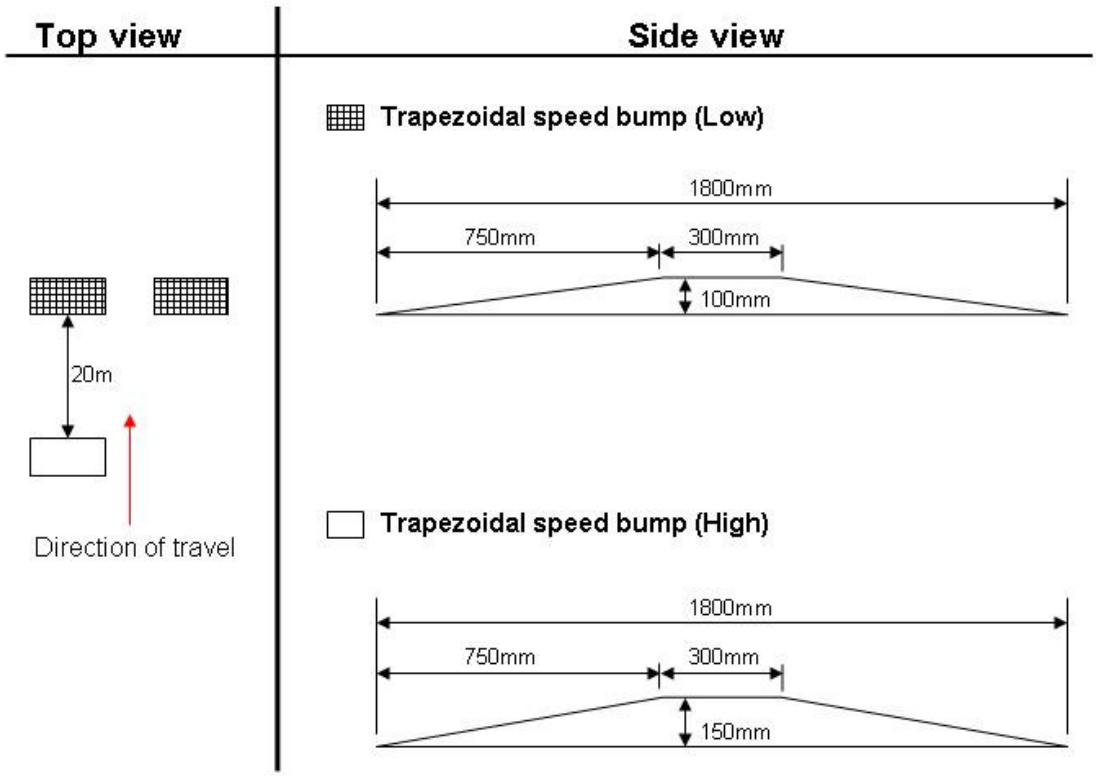

Figure 2.16. Configuration and dimension of the trapezoidal speed bumps.

Figure 2.17. Trailer driving over the trapezoidal speed bump.

Figure 2.18. Trailer driving over Belgian paving.

2.3. Summary

At this point we have successfully obtained the vehicle parameters that are needed for the creation of the MBS model except for the characteristics of the air springs. We have also obtained the required data for the validation of the MBS model. This data will enable us to validate the MBS model for discrete road events and roads which contain higher frequencies. We can also validate the MBS model over these roads with different payloads. The correlation between the measured and predicted data will be discussed in Chapter 4.

However, before we get to the correlation we need to create the MBS model in order to generate the predicted data, we also still have to characterise the air springs. The characterisation of the air springs and the resulting model of the air suspension unit is the subject of the next chapter.

Chapter 5

Conclusions and Recommendations

In this study we attempted to determine the feasibility of using a Multi-Body Simulation model to predict the suspension forces of a 40 ton flat bed tri-axle air suspended semi-trailer. We started the study by obtaining the physical vehicle parameters and the measured behaviour of the physical trailer. One of the major challenges en route to creating an accurate full vehicle simulation model, was to obtain a model of the air springs able to accurately describe the behaviour of the air springs. A lot of time and effort went into the air spring model and in the end it seems that the air spring model was successful in accurately describing the behaviour of the air springs. Both the air spring model and the full vehicle model were validated and the importance of validating a mathematical model was again made evident.

In this chapter we will look at the final conclusions of the results obtained in this study. The limitations and shortfalls of the full vehicle model will be discussed as well as the recommendations for future work that need to be done to improve the accuracy of the full vehicle model.

5.1. Conclusions

In this study we have created a validated MBS model of a 40 ton flat bed tri-axle air suspended semi-trailer that can predict the vertical dynamics and more importantly the suspension forces quite accurately. A validated mathematical model of the air springs used on the experimental trailer that can accurately predict the behaviour was also developed. Two assumptions that were made at the start of the study to simplify the mathematical model still hold and are:

- all bodies are rigid,
- inputs (displacements, accelerations and forces) from the truck towing the trailer are ignored.

These assumptions does place certain limitations on the use of the MBS model, as discussed in section 5.2, but the advantages of these two assumptions may be greater than the drawbacks. The assumption that the inputs of the truck towing the trailer are ignored implies that the MBS model can accurately predict the suspension forces independent of the truck used. The correlation obtained with this assumption is good news for trailer manufacturers as different trucks are used to tow the same trailer. The correlation also seems to indicate that the assumption that all bodies are rigid greatly simplifies the model but still gives reasonably good accuracy.

Bibliography

Abd-El-Tawwab A.M. (1997), "Twin-Accumulator Suspension System.", *SAE Technical paper* 970384.

ADAMS/Tire (2007) help documentation, 2007r1

Anderson D., Schade G., Hamill S. and O'Heron P. (2001), "Development of a Multi-Body Dynamic Model of a Tractor-Semitrailer for Ride Quality Prediction", *SAE Technical Paper* 2001-01-2764.

Bakker E., Pacejka H.B. and Lidner L. (1989),"A New Tire Model with an Application in Vehicle Dynamics Studies", *SAE Technical Paper Series*, 890087.

Becker C.M. (2008), *Obtained information on Belgian paving***.** [e-mail] (Personal communication, 5 February 2008).

Bernard J.E. and Clover C.L. (1994), "Validation of Computer Simulations of Vehicle Dynamics", *SAE Technical Paper* 940231.

Bernard J.E. and Shannan J.E. (1990), "Simulation of Heavy Vehicle Dynamics", *SAE Technical Paper* 902270.

Bhave S.Y. (1992), "Effect of Connecting the Front and Rear Air Suspension of a Vehicle on the Transmissibility of Road Undulation Inputs", *Vehicle System Dynamics*, 21:1, pp.225-245.

Broek D. (1988). "The practical use of fracture mechanics.", Dordrecht: Kluwer Academic Publishers.

Captain K.M., Boghani A.B. and Wormley D.N. (1979),"Analytical Tire Models for Dynamic Vehicle Simulations", *Vehicle System Dynamics*, Vol. 8, Issue 1, pp. 1-32.

Chandrasekaran A.K., Rizzoni G., Soliman A., Josephson J. and Carroll M. (2002), "Design Optimization of Heavy Vehicles by Dynamic Simulations.", *SAE Technical Paper* 2002-01-3061.

Chase E. (2001), "Truck Durability Evaluation through Computer Simulation", *SAE Technical Paper* 2001-01-2763.

Chen D., Shahidi B., Stuhec U., Song Y., Chang Y.P. and Palmer T. (2006), "Correlation of Explicit Finite Element Road Load Calculations for Vehicle Durability Simulations", *SAE Technical Paper* 2006-01-1980.

Conle F.A. and Chu C.C. (1997), "Fatigue analysis and the local stress–strain approach in complex vehicular structures", *International Journal of Fatigue*, Vol. 19, Supp. No. 1, pp. S317–S323.

Cosme C., Ghasemi A. and Gandevia J. (1999), "Application of Computer Aided Engineering in the Design of Heavy-Duty Truck Frames", *SAE Technical Paper* 1999-01-3760.

Dietz S., Netter H. and Sachau D. (1998), "Fatigue Life Prediction of a Railway Bogie under Dynamic Loads through Simulation", *Vehicle System Dynamics*, 29:6, pp.385 – 402.

Dressler K. and Kottgen V.B. (1999), "Synthesis of realistic loading specifications", *European journal of mechanical engineering*, 41(3).

Edara R. and Shih S. (2004), "Effective Use of Multibody Dynamics Simulation in Vehicle Suspension System Development", *SAE Technical Paper* 2004-01-1547.

Edara R., Shih S., Tamini N., Palmer T. and Tang A. (2005), "Heavy Vehicle Suspension Frame Durability Analysis Using Virtual Proving Ground", *SAE Technical Paper* 2005-01-3609.

Els P.S. (1993), "Die Hitteprobleem op Hidropneumatiese veer-en-demperstelsels" ("The heat problem on Hydro pneumatic spring and damper systems"), University of Pretoria.

Els P.S. and Grobbelaar B. (1993), "Investigation of the Time- and Temperature Dependency of Hydro-Pneumatic Suspension Systems", *SAE Technical Paper Series*, 930265.

Els P.S., Uys P.E., Snyman J.A. and Thoresson M.J. (2006), "Gradient-based approximation methods applied to the optimal design of vehicle suspension systems using computational models
with severe inherent noise**",** *Mathematical and Computer Modelling*, 43, p.787–801

Faria L.O., Oden J.T., Yavari B., Tworzydlo W.W., Bass J.M. and Becker E.B (1992),"Tyre modeling by finite elements.", *Tyre Science Technology*, 20.

Ferry W.B., Frise P.R., Andrews G.T. and Malik M.A. (2002), "Combining virtual simulation and physical vehicle test data to optimize durability testing", *Fatigue & Fracture of Engineering Materials and Structures*, Volume 25, Issue 12, pp.1127-1134.

Fox M.N., Roebuck R.L. and Cebon D. (2007), "Modelling rolling-lobe air springs", *International Journal of Heavy Vehicle Systems*, Vol. 14 , No. 3, pp.254-270.

Gere J.M. (2004), "Mechanics of Materials", 6th edition, Brooks/Cole.

Gerotek, (2008), Gerotek Test Facilities. Available at: http://www.armscorbusiness.com/SubSites/Gerotek/Gerotek01_landing.asp [Accessed 14 October 2008].

Gipser M. (2007), "FTire - the tire simulation model for all applications related to vehicle dynamics", *Vehicle System Dynamics*, 45:1, pp. 139 – 151.

Gopalakrishnan G., Agrawal H.N. (1993), "Durability Analysis of Full Automotive Body Structures", *SAE Technical Paper* 930568.

Haiba M., Barton D.C., Brooks P.C., Levesley M.C. (2002), "Review of life assessment techniques applied to dynamically loaded automotive components.", *Computers and Structures*, Vol. 80, pp.481-494.

Haiba M., Barton D.C., Brooks P.C., Levesley M.C. (2003), "The development of an optimisation algorithm based on fatigue life", *International Journal of Fatigue*, Vol. 25, pp.299-310.

Heydinger G.J., Garrott W.R., Chrstos J.P. and Guenther D.A. (1990), "A Methodology for Validating Vehicle Dynamics Simulations", *SAE Technical Paper* 900128.

Huizinga F. T. M. J. M., Van Ostaijen R. A. A. and Slingeland A. Van Oosten (2002), "A practical approach to virtual testing in automotive engineering", *Journal of Engineering Design*, 13:1, 33-47.

Kuo E.Y., Kelkar S.G. (1995), "Vehicle Body Structure Durability Analysis", *SAE Technical paper* 951096.

Luque P. and Mántaras D.A. (2003), "Pneumatic suspensions in semi-trailer: Part II Computer simulation.", *Heavy Vehicle Systems*, A Special Issue of the *International Journal of Vehicle Design*, Vol. 10, No.4, pp. 309-320.

McBeath S. (2000), "Virtually physical." Testing Technology International, February 2000, UK and International Press, Surrey, UK.

Mousseau C.W., Laursen T.A., Lidberg M., Taylor R.L. (1999), "Vehicle dynamics simulations with coupled multibody and finite element models", *Finite elements in analysis and design*, 31, 295-315.

Nieto A.J., Morales A.L., González A., Chicharro J.M., Pintado P. (2008), "An analytical model of pneumatic suspensions based on an experimental characterization.", *Journal of Sound and Vibration* 313 (2008) 290-307.

Porumamilla H., Kelkar A.G., Vogel J.M. (2008), "Modelling and Verification of an Innovative Active Pneumatic Vibration Isolation System.", *Journal of Dynamic Systems, Measurement, and Control*, Vol. 130, 031001, pp. 1-12.

Quaglia G. and Sorli M. (2001), "Air Suspension Dimensionless Analysis and Design Procedure.", *Vehicle System Dy*namics, 35:6, p443 — 475.

Socie D.F. and Pompetzki M.A. (2004), "Modeling variability in service loading spectra", *Journal of ASTM International*, Vol 1, No.2.

Svensson T. (1997), "Prediction uncertainties at variable amplitude fatigue", *International journal of fatigue*, 19(1).

Theron N.J., Els P.S. (2007), "Modelling of a semi-active hydropneumatic spring-damper unit.", *International Journal of Vehicle Design*, Vol.45, Num 4, pp501-521.

Uys P.E., Els P.S., Thoresson M.J. (2007), "Suspension settings for optimal ride comfort of off-road vehicles travelling on roads with different roughness and speeds**",** *Journal of Terramechanics*, 44, p.163–175.

Wannenburg J. (2007), "A study on fatigue loading on automotive and transport structures", PhD thesis, University of Pretoria.

White F.M. (2003), "Fluid Mechanics", McGrawHill.

Zhang Y., Stawiarski T., Subramanian M., Yung D., Farahani A.D., Zhang X. (2005), "Full Vehicle Finite Element Model 4-Post Durability Analysis", *SAE Technical paper* 2005-01-1402.

With the mathematical models of the sub-systems such as the air suspension unit and other critical elements such as the dampers and tyres validated, any trailer using the same suspension unit, dampers and tyres can be modelled with good reliability as the other parameters can be easily and accurately obtained from CAD.

5.2. Limitations

The limitations and shortfalls of the full vehicle model in this study are:

- Tyre model

The biggest shortfall of the present MBS model is the limitation brought on by the tyre model that is used. The Pacejka '89 handling tyre model does not let higher frequencies go through and thus acts as a low-pass filter with a cut-off frequency at around 8Hz. The effect of the tyre model on the data over the rough road was discussed in paragraph 4.2.3. Even though the tyre model did have a big influence on the predicted forces, acceptable correlation was still obtained for the rough road. The tyre model did not seem to present any problems over the discrete road event.

- Truck omitted from MBS model

One of the important assumptions made was with respect to the interaction between the truck and the trailer at the fifth wheel. It was assumed that there is no input from the truck on the trailer. This assumption was made partly because we were not able to measure the forces acting on the fifth wheel, but mainly because we did no have the characteristics available to model the truck. The major limitation of not having the truck included is that the forces acting on the fifth wheel cannot be predicted with this model. But, the implications that this assumption has as mentioned in section 5.1, outweighs the limitations.

- MBS model validated only for vertical dynamics

The MBS model developed in this study has only been validated for the vertical dynamics and not handling.

5.3. Recommendations and future work

Recommendations for further work are cantered around three aspects namely:

- Tyre model

  The tyre model will be the first place to start in order to improve the prediction of the suspension forces especially for the unladen case over the rough road. A possible substitute for the Pacejka '89 tyre model is FTire (Gipser (2007)).

- Addition of flexible bodies

  From the correlation achieved between the predicted and measured data it seems that the assumption that all bodies are rigid greatly simplifies the model but still gives reasonably good accuracy. However, the addition of flexible bodies may increase the accuracy as the effects of the mode shapes of the vehicle structure can be included. Comparison of strains measured on the trailing arms can then also be compared with the predicted values and give further confidence in the MBS model.

- Including the truck in the MBS model

  The addition of the truck in the MBS model will allow for the prediction of the forces acting on the fifth wheel. The addition of the truck will also make it possible to check other aspects of the truck-trailer combination i.e. roll-over, braking ability, rearward amplification, etc.

Appendix A – Calibration of strain gauges on dampers.

In Appendix A the correlation between the compression forces, as measured by the strain gauges and the load cell, for the left front, left middle, left rear, right front and right middle dampers are shown here graphically.

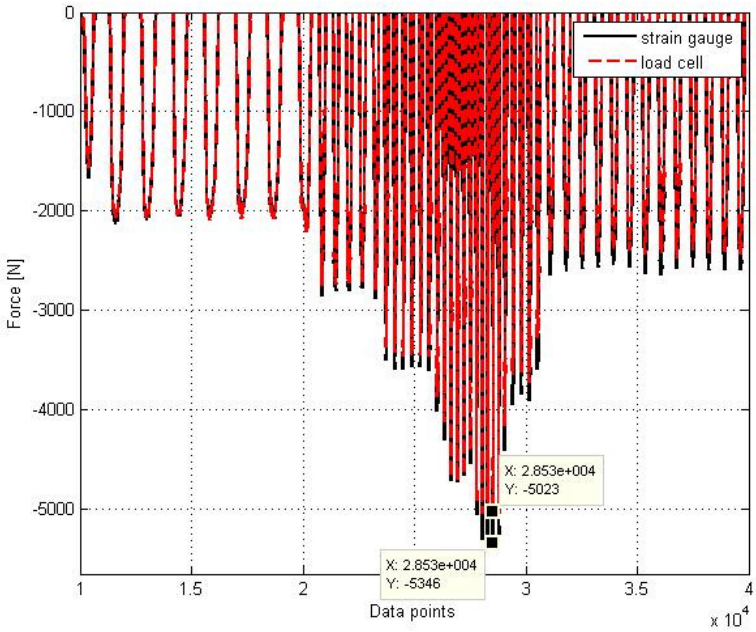

Figure A.1. Comparison of compression forces as measured by strain gauge and load cell for left front damper.

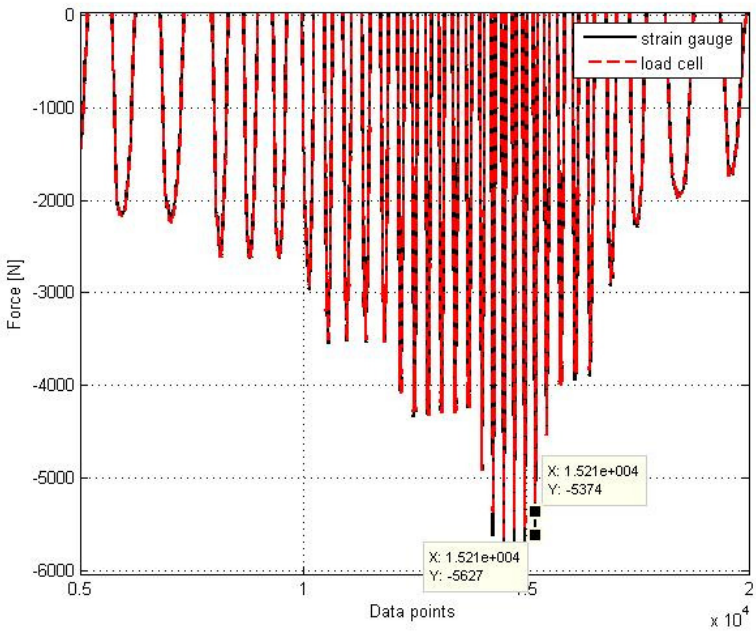

Figure A.2. Comparison of compression forces as measured by strain gauge and load cell for left middle damper.

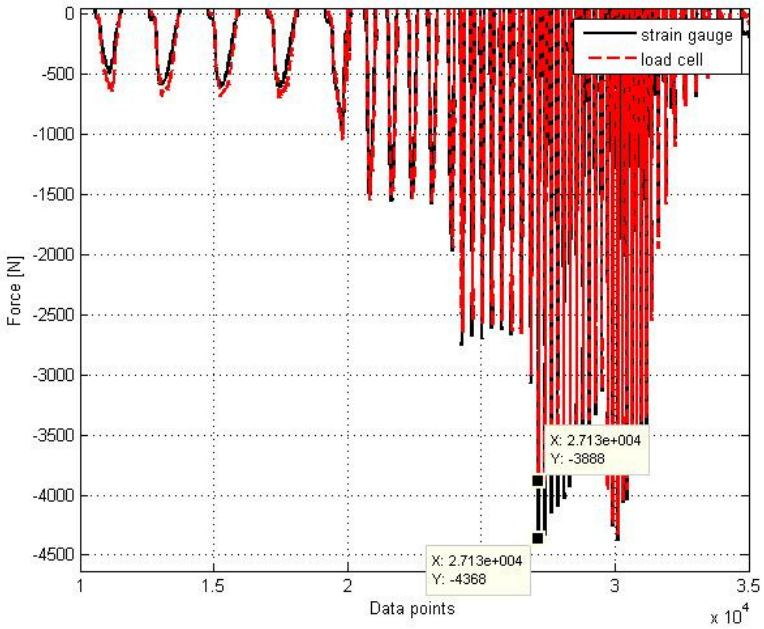

Figure A.3. Comparison of compression forces as measured by strain gauge and load cell for left rear damper.

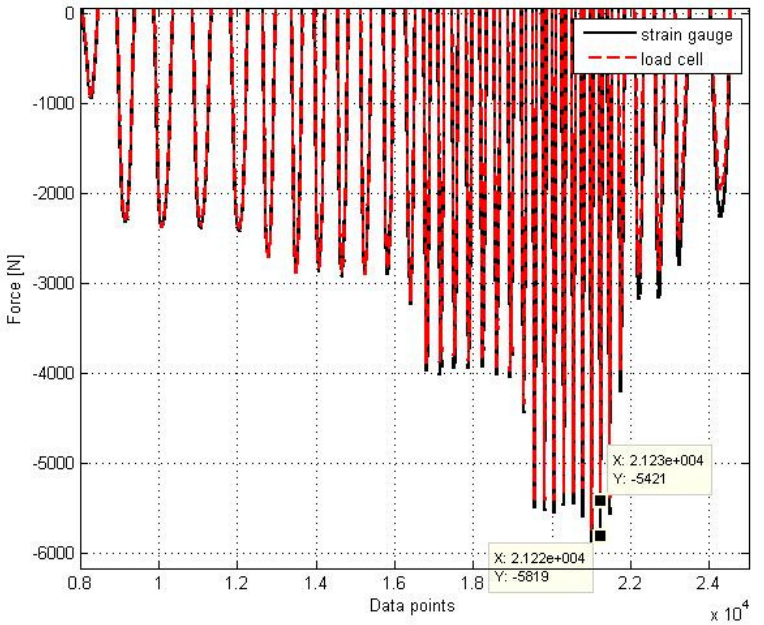

Figure A.4. Comparison of compression forces as measured by strain gauge and load cell for right front damper.

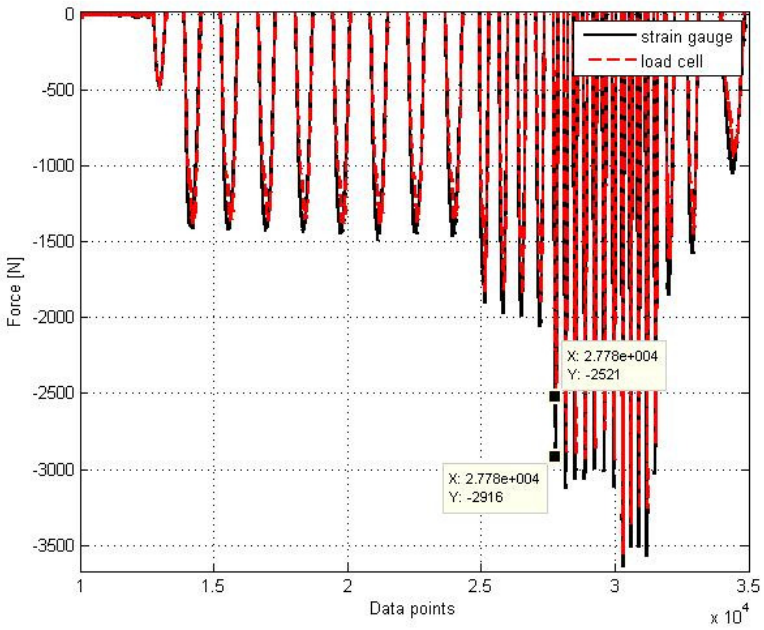

Figure A.5. Comparison of compression forces as measured by strain gauge and load cell for right middle damper.

Appendix B – Analytical methods for calculating the stand-alone air spring's characteristics

In Appendix B we will look at the derivation of the analytical expression for calculating the force-displacement characteristics of the air spring. We will also compare the results of the analytical expressions obtained with the both the assumption of an isothermal and an adiabatic gas compression process, with the experimentally obtained characteristics.

B.1. Isothermal gas compression process

To obtain the characteristics of the air spring by analytical means the static length x_{os}, which relates the area of the air spring to its volume, must first be determined. From the ideal gas law and the isothermal gas compression processes, as in Els (1993) and Els & Grobbelaar (1993), it is known that:

$$P_1 V_1 = P_2 V_2 \qquad \{B.1\}$$

Where subscript 1 denotes state 1 and subscript 2 represents any other state. With:

$$P_1 = \frac{F_1}{A_1} \qquad V_1 = A_1 x_{o1}$$

$$P_2 = \frac{F_2}{A_2} \qquad V_2 = A_2 x_{o2}$$

we can substitute these into equation {B.1} and cancelling A_1 and A_2 (area assumed to stay constant) gives:

$$F_1 x_{o1} = F_2 x_{o2}$$

With $x_{o2} = x_{o1} + \Delta x$ and some manipulation and rearrangement we can obtain an expression for x_{o1}:

$$\boxed{x_{o1} = \frac{F_2 \Delta x}{F_1 - F_2}} \qquad \{B.2\}$$

Where $\Delta x = x_2 - x_1$. To calculate the non-geometrical length (x_{o1}) of the air spring from equation {B.2}, the values on the right-hand side of this equation is obtained from Figure B.1.

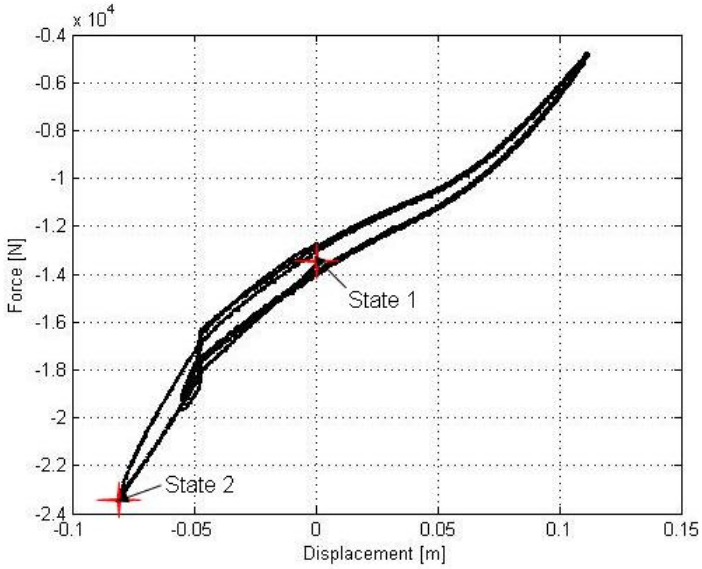

Figure B.1. Air spring characteristic at gage static pressure of 3.9bar. Values read off for the variables at state 1 and state 2.

With x_{o1} known and starting again with the ideal gas law in equation {B.1}, the analytical expression can be obtained that gives the force as a function of displacement:

$$\boxed{F_2 = \frac{F_1 x_{o1}}{x_{o1} + x}}$$

Where x is any displacement relative to the displacement of the air spring at state 1.

B.2. Adiabatic gas compression process

From the ideal gas law and assuming an adiabatic gas compression process:

$$P_1 V_1^{1.4} = P_2 V_2^{1.4}$$

we obtain equation {B.3} when the following substitutions are made:

$$P_1 = \frac{F_1}{A_1} \qquad V_1 = A_1 x_{o1}$$

$$P_2 = \frac{F_2}{A_2} \qquad V_2 = A_2 x_{o2}$$

$$\frac{F_1}{A_1}(A_1 x_{o1})^{1.4} = \frac{F_2}{A_2}(A_2 x_{o2})^{1.4} \qquad \{B.3\}$$

$A_1 = A_2$ (area assumed to stay constant) implies that the areas can be eliminated from equation {B.3} giving

$$F_1 x_{o1}^{1.4} = F_2 x_{o2}^{1.4}$$

Substituting $x_{o2} = x_{o1} + \Delta x$ and rearranging gives

$$x_{o1} = \frac{\sqrt[1.4]{F_2}\,\Delta x}{\sqrt[1.4]{F_1} - \sqrt[1.4]{F_2}}$$

Where $\Delta x = x_2 - x_1$ and the values for state 1 and state 2 are again read off from the graph as indicated in Figure B.1.

With x_{o1} known and starting again with the ideal gas law the analytical expression can be obtained that gives force as a function of displacement, this analytical expression is given by equation {B.4}:

$$F_2 = \frac{F_1 x_{o1}^{1.4}}{(x_{o1} + x)^{1.4}} \qquad \{C.4\}$$

Where x is any displacement relative to the displacement of the spring at state 1.

B.3. Comparison of analytical methods

Figure B.2 to Figure B.7 shows the comparison between the analytical characteristics and the experimentally obtained characteristic. From these figures it seems that the isothermal gas compression process gives better correlation than the adiabatic gas compression process. Nieto *et al* (2008) monitored the suspension air temperature during working conditions and their results supported the hypothesis of an isothermal process. Therefore for all analytical derivations an isothermal gas compression process will be assumed.

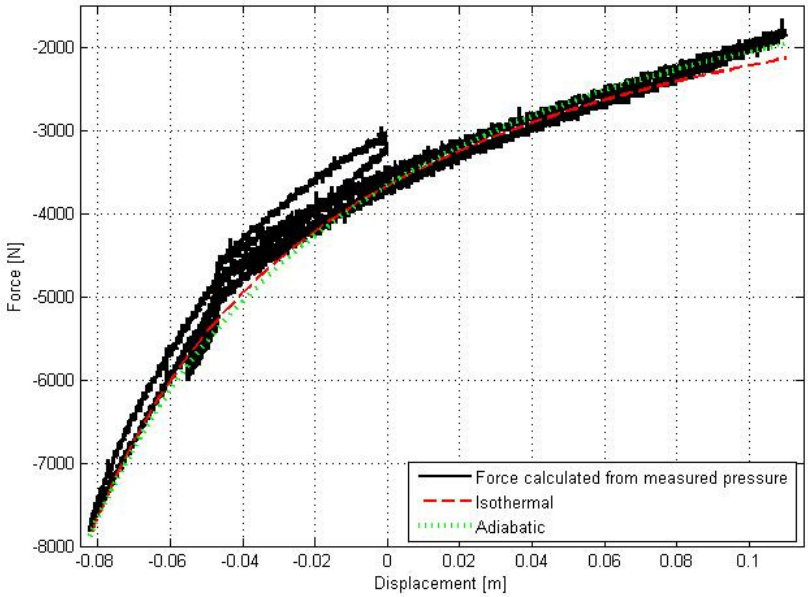

Figure B.2. Comparison of measured and analytical characteristics at 1bar (gage pressure) internal pressure.

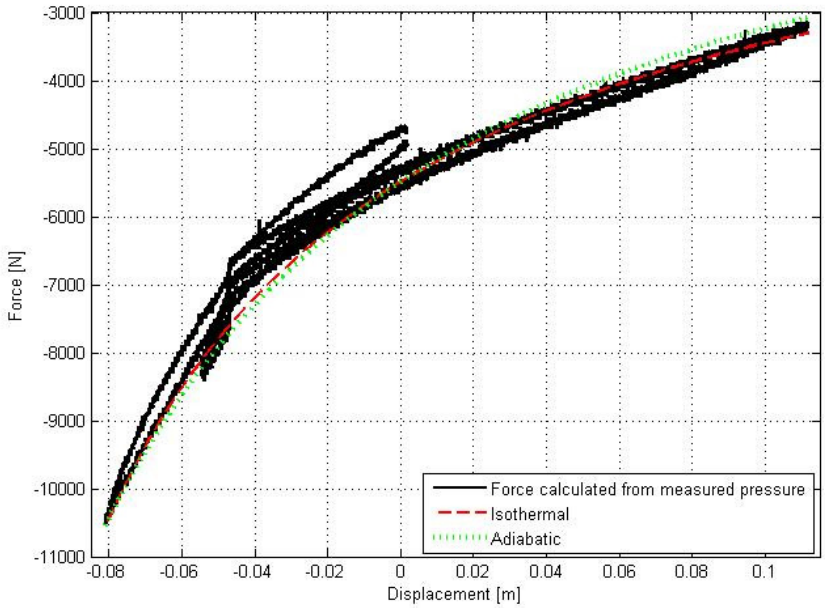

Figure B.3. Comparison of measured and analytical characteristics at 1.5bar (gage pressure) internal pressure.

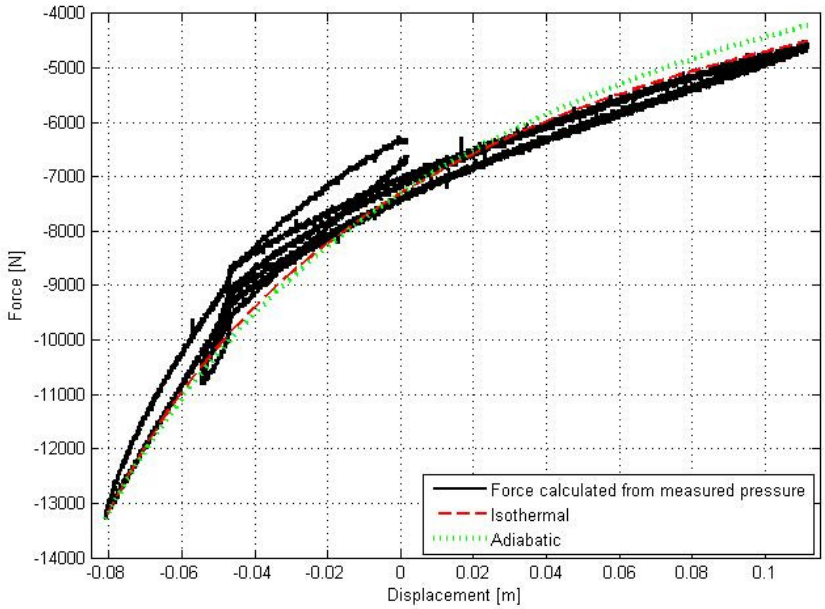

Figure B.4. Comparison of measured and analytical characteristics at 2bar (gage pressure) internal pressure.

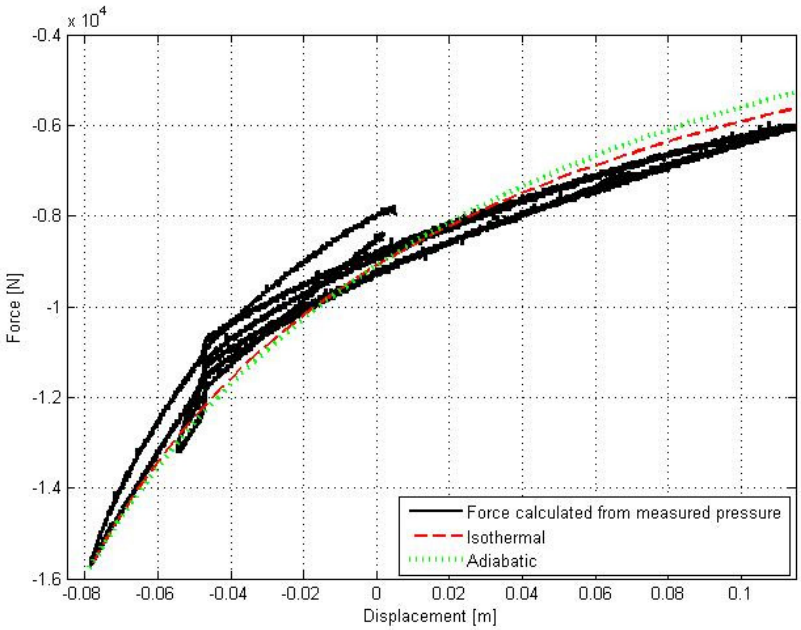

Figure B.5. Comparison of measured and analytical characteristics at 2.5bar (gage pressure) internal pressure.

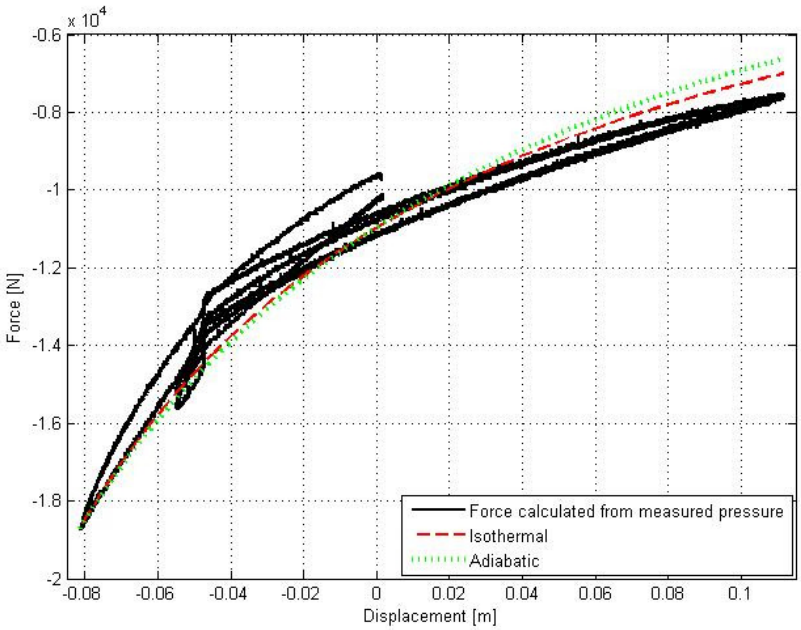

Figure B.6. Comparison of measured and analytical characteristics at 3bar (gage pressure) internal pressure.

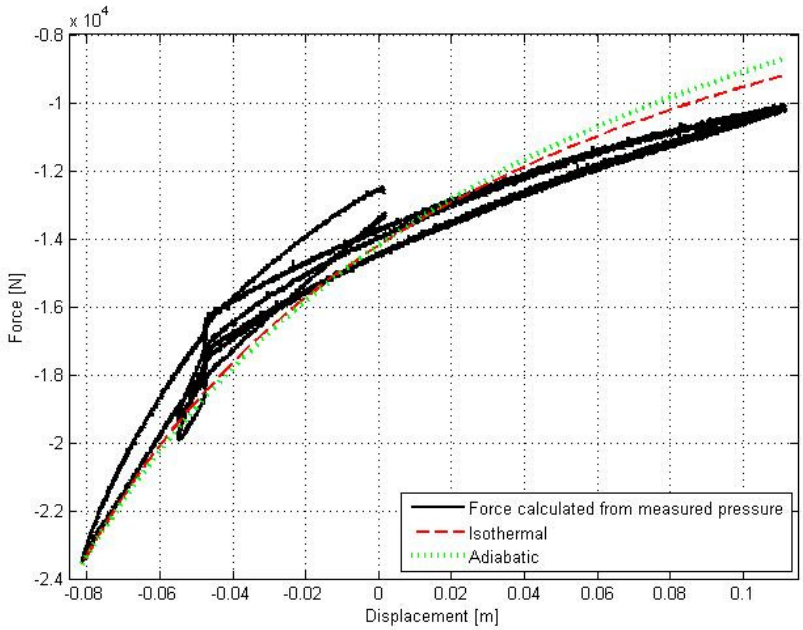

Figure B.7. Comparison of measured and analytical characteristics at 3.9bar (gage pressure) internal pressure.

Appendix C – Interconnected air spring model: An adiabatic process

In this section we will model the six air springs as being connected with each other as was done in paragraph 3.5.2. The same procedure and assumptions are used but with the difference being that we now assume an adiabatic gas compression process.

The ideal gas law with the assumption of an adiabatic gas compression process is:

$$ {}_{sys}P_1 {}_{sys}V_1^{1.4} = {}_{sys}P_2 {}_{sys}V_2^{1.4} \qquad \{C.1\} $$

The same steps that were followed in the isothermal process in paragraph 3.5.2 are followed here to obtain an expression for ${}_{sys}P_2$:

$$ \boxed{ {}_{sys}P_2 = \frac{ {}_{sys}P_1 {}_{sys}V_1^{1.4}}{[{}_{sys}V_1 + \sum_{i=1}^{6} A\Delta x_i]^{1.4}} } \qquad \{C.2\} $$

With i representing the six air springs. The variables on the right hand side of equation {C.2} are calculated exactly the same as was done for equation {3.2} in paragraph 3.5.2. With the static pressure of the system at state 2 known, the force in each air spring can be calculated.

$$ \boxed{F_i = {}_{sys}P_2 A} \qquad \text{for i = 1,2 ,…,6} $$

The two air spring models using the isothermal and adiabatic gas compression process are compared in figure C.1 and figure C.2. There is a bigger difference in the prediction over the symmetric obstacle than over the asymmetric obstacle, but we still have the problem that the pressures for all six the air springs are the same.

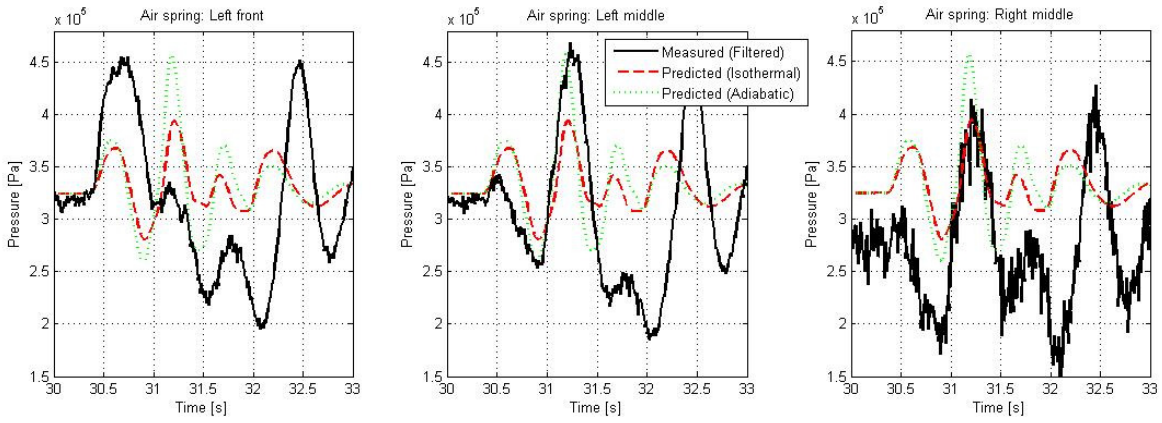

Figure C.1. Comparison of pressures over discrete symmetric obstacle.

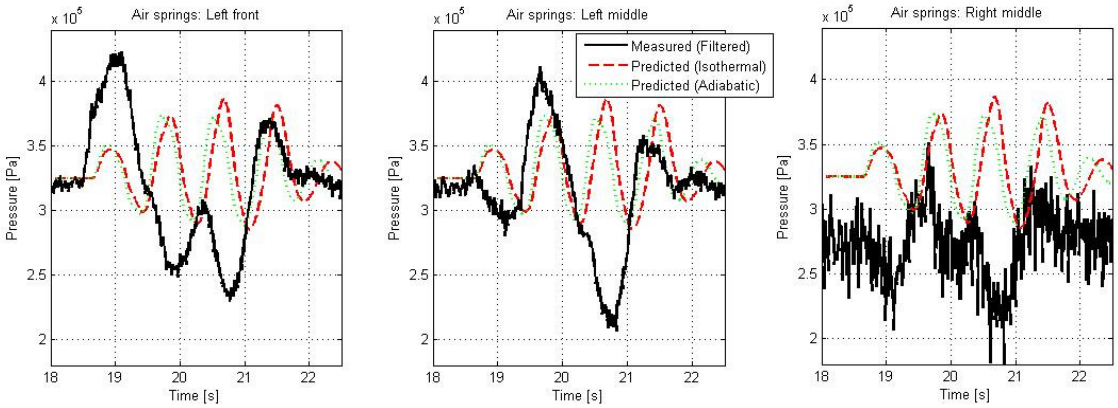

Figure C.2. Comparison of pressures over discrete asymmetric obstacle.

Appendix D – Front-Middle-Rear interconnected air spring model

In Appendix D we will derive an air spring model where the two front, middle and rear air springs are connected. A schematic diagram of the Front-Middle-Rear interconnected air spring model is shown in Figure D.1.

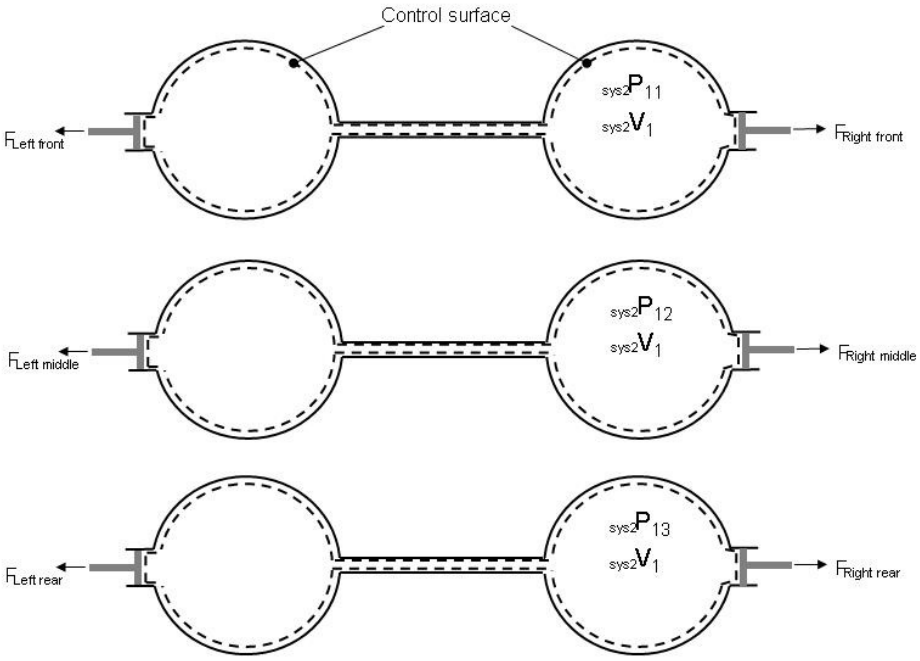

Figure D.1. Schematic diagram of Front-Middle-Rear interconnected system.

We proceed in a similar manner as for the Left-right interconnected air spring model in paragraph 3.5.3 and start with the ideal gas law assuming an isothermal gas compression process:

$$_{sys2}P_{1,j}\ {}_{sys2}V_1 = {}_{sys2}P_{2,j}\ {}_{sys2}V_{2,j} \qquad \text{for } j = 1,2,3.$$

Where j represents the three axles of the trailer. If we substitute $_{sys2}V_{2,j}$ with:

$$_{sys2}V_{2,j} = {}_{sys2}V_1 + \Delta V_{sys2,j}$$

we obtain an expression for calculating the pressure present in each of the three systems representing each axle:

$$_{sys2}P_{2,j} = \frac{{}_{sys2}P_{1,j}\ {}_{sys2}V_1}{{}_{sys2}V_1 + \Delta V_{sys2,j}}$$

The change in volume of each of the three systems is calculated as follows:

$$\Delta V_{sys2,j} = \sum_{i=1}^{2} A\Delta x_{ij}$$

Where *i* represents the two air springs on each axle. Substituting this equation into the equation for ${}_{sys2}P_{2,j}$ gives:

$$\boxed{{}_{sys2}P_{2,j} = \frac{{}_{sys2}P_{1,j}\,{}_{sys2}V_1}{{}_{sys2}V_1 + \sum_{i=1}^{2} A_{ij}\Delta x_{ij}}} \qquad \{D.1\}$$

The variables and the right-hand side of equation {D.1} is calculated exactly the same as was done in paragraph 3.5.2. and 3.5.3 for equation {3.2} and equation {3.9} respectively. The only difference is in the calculation of the static volume of the system consisting out of two air springs ${}_{sys2}V_1$ and is equal to two times the volume of one of the air springs:

$${}_{sys2}V_1 = 2 \times V_1$$

Where V_1 is calculated from equation {3.7} that was derived in paragraph 3.5.2. With all the variables known the pressure present in each of the three systems at state 2 can now be calculated with equation {D.1}. These pressures can then be used in the following equation to calculate the forces in each air spring:

$$\boxed{F_{ij} = {}_{sys2}P_{2,j}A}$$

for i = 1,2.
and j = 1,2,3.

Appendix E – Calculation of torsional stiffness of axle

The torsional stiffness of the axle is calculated here and is used as the stiffness of the torsion spring in Susp5 described in section 4.2.2. The axle's torsional stiffness is calculated from (Gere (2004)):

$$k_T = \frac{GI_P}{L} \qquad \{E.1\}$$

With G being the shear modulus of elasticity, I_P being the polar moment of inertia of the cross-sectional area of the axle and L is the length. I_P for a solid rectangular section is:

$$I_P = \frac{bh}{12}(h^2 + b^2)$$

Because the axle is hollow the polar moment of inertia of the cross-sectional area is calculated by subtracting the value of the inner area from the outer area:

$$I_P = I_{P,outer} - I_{P,inner}$$

$$I_P = \frac{(0.12)^2}{12}(0.12^2 + 0.12^2) - \frac{(0.1)^2}{12}(0.1^2 + 0.1^2)$$

The dimensions of the axle are shown in figure E.1.

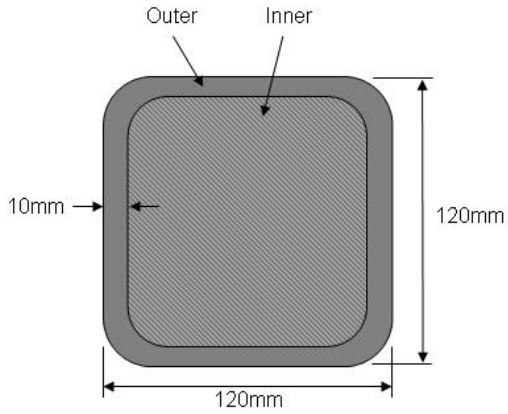

Figure E.1. Cross sectional view of axle.

The shear modulus of elasticity is calculated from Young's modulus of elasticity and poisons ratio.

$$G = \frac{E}{2(1+\upsilon)}$$

The length L is the length between the two attachment points of the trailing arms and axle. With these variables now known equation {E.1} can be used to calculate the torsional stiffness of the axle. The torsional stiffness is calculated as 1 187 267 N.m/rad.

Appendix F – Validation of MBS model: Load case 1

The correlation for load case 1 over the symmetric discrete obstacle, the asymmetric discrete obstacle and the rough road are shown in this appendix.

F.1. Correlation over symmetric discrete obstacle.

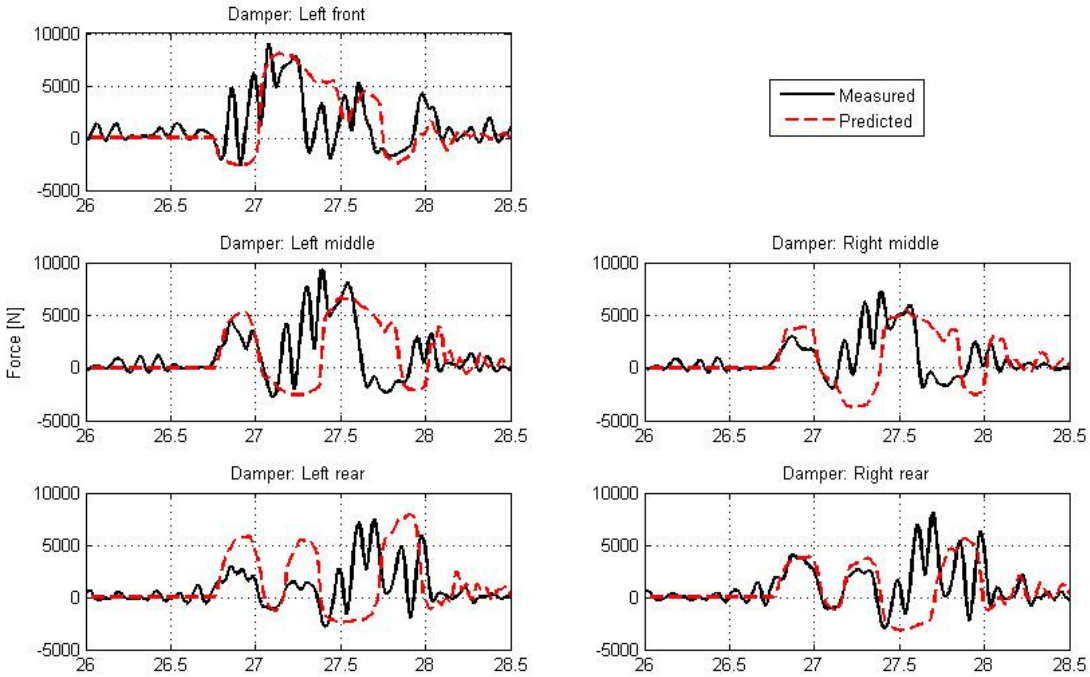

Figure F.1. Damper forces over symmetric discrete obstacle for load case 1.

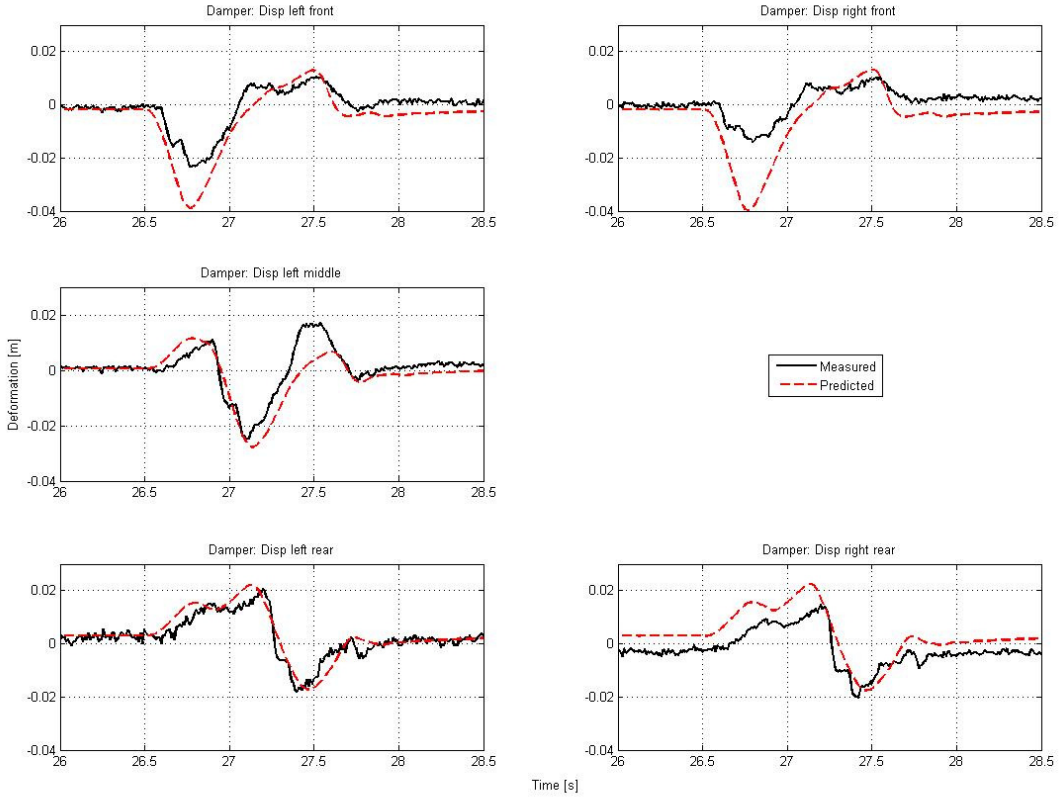

Figure F.2. Damper deformations over symmetric discrete obstacle for load case 1.

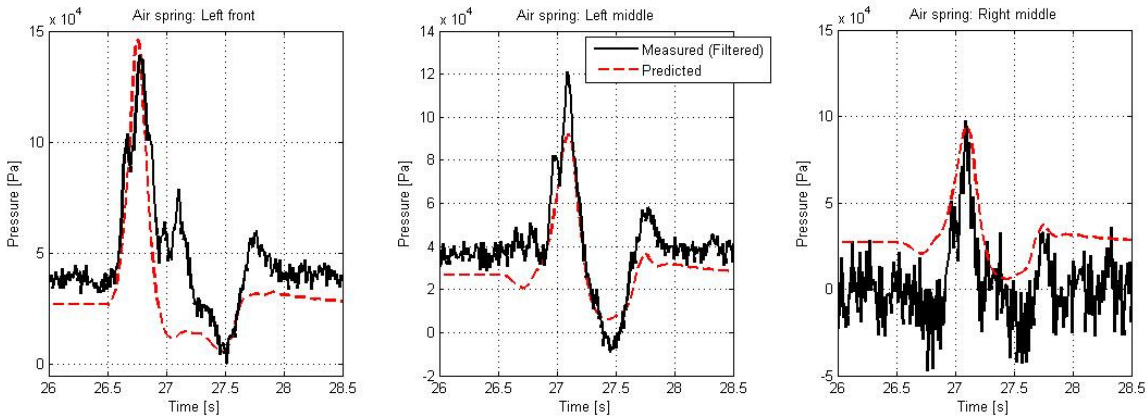

Figure F.3. Air spring pressures over symmetric discrete obstacle for load case 1.

F.2. Correlation over asymmetric discrete obstacle.

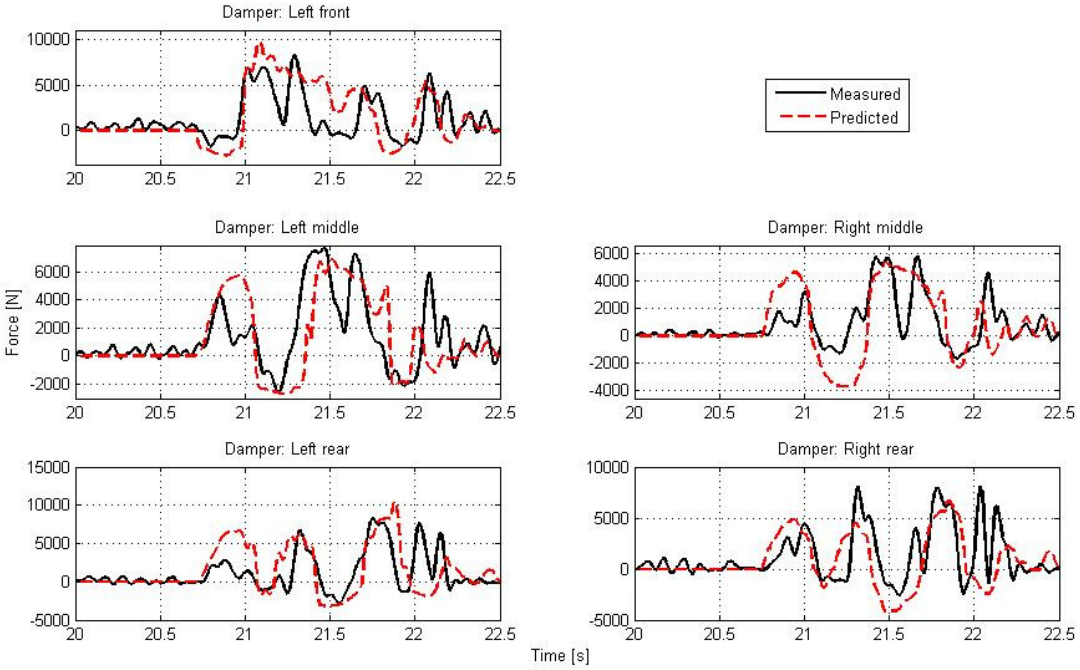

Figure F.4. Damper forces over asymmetric discrete obstacle for load case 1.

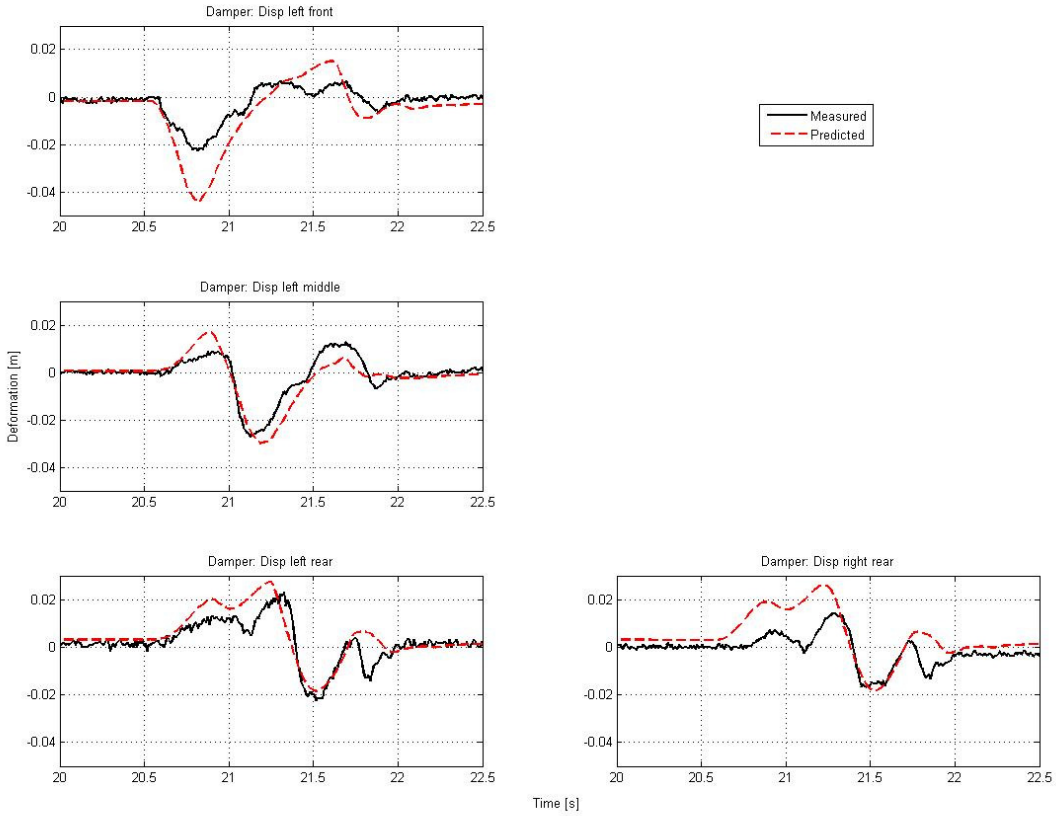

Figure F.5. Damper deformations over asymmetric discrete obstacle for load case 1.

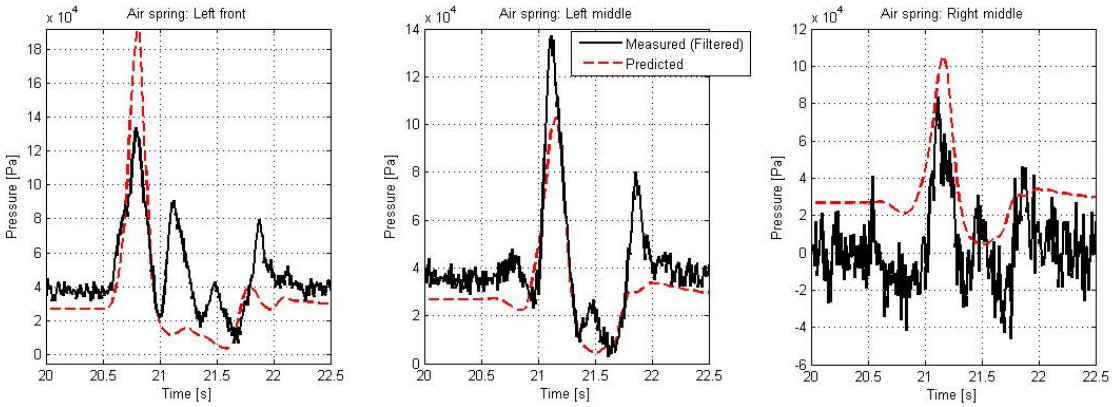

F.6. Air spring pressures over asymmetric discrete obstacle for load case 1.

F.3. Correlation over rough terrain

Table F.1. Statistical representation of the correlation over a rough road for load case 1.

	Measured	Predicted	% difference
RMS of Body vertical acceleration	5.95	6.23	4.71
RMS of Axle vertical acceleration	10.89	7.07	-35.08
RMS of Air spring pressures			
Left front	53331.2	43312.18	-18.79
Left middle	48467.13	42202.43	-12.93
Right middle	17562.49	6447.92	-63.29
RMS of Damper forces			
Left			
Front	3713.65	2545.5	-31.46
Middle	3723.56	2717.54	-27.02
Rear	3328.32	2379.13	-28.52
Right			
Front	No measurements		
Middle	2904.78	2383.91	-17.93
Rear	3162.53	1826.33	-42.25
RMS of Damper displacements			
Left			
Front	0.00348	0.00308	-11.49
Middle	0.00403	0.00278	-31.02
Rear	0.00475	0.00257	-45.89
Right			
Front	0.00263	0.00316	20.15
Middle	0.0144	0.00288	*-80.00*
Rear	0.00401	0.00262	-34.66
Mean			**28.35**
Standard deviation			**15.06**

Note: Values in italics are not used in the calculation of the mean and standard deviation.

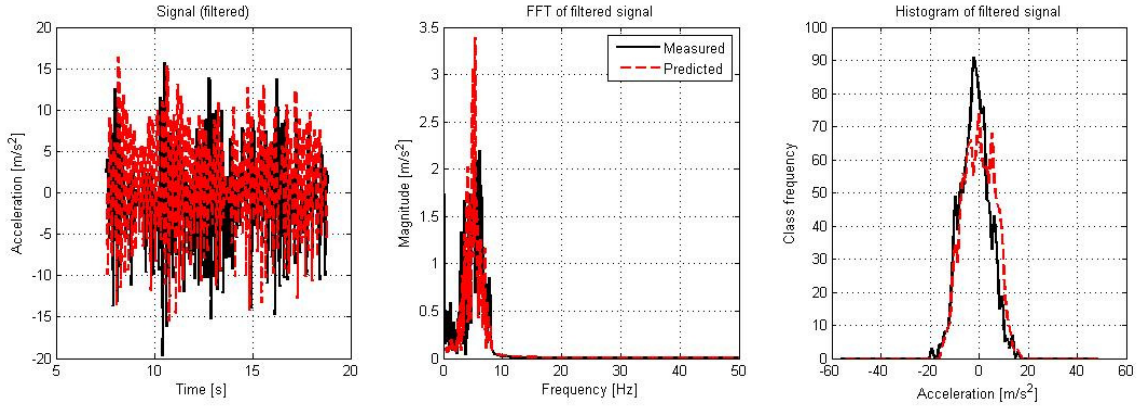

Figure F.7. Time-and frequency domain representation and histogram of body vertical acceleration for load case 1.

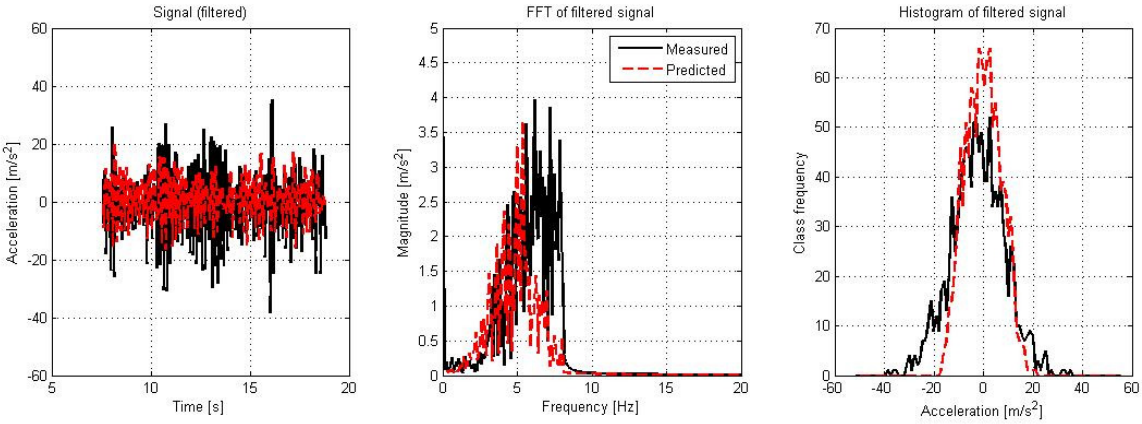

Figure F.8. Time-and frequency domain representation and histogram of axle vertical acceleration for load case 1.

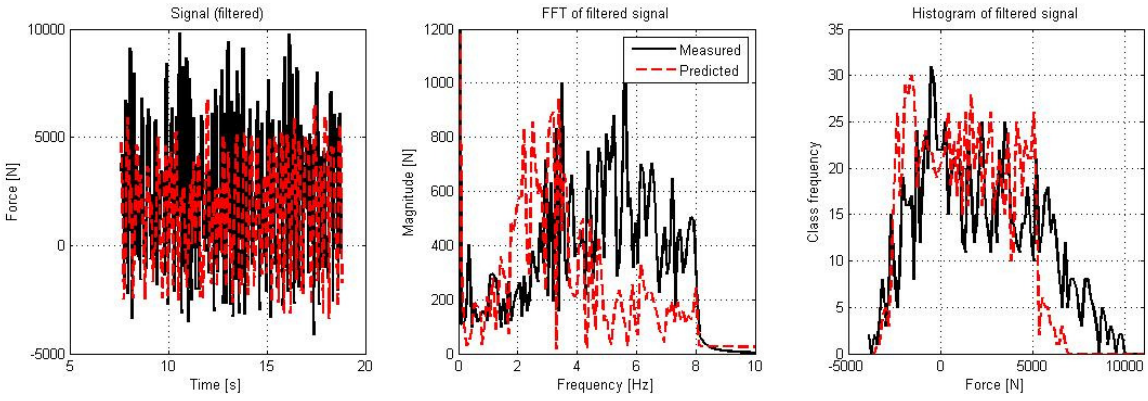

Figure F.9. Time-and frequency domain representation and histogram of left middle damper forces for load case 1.

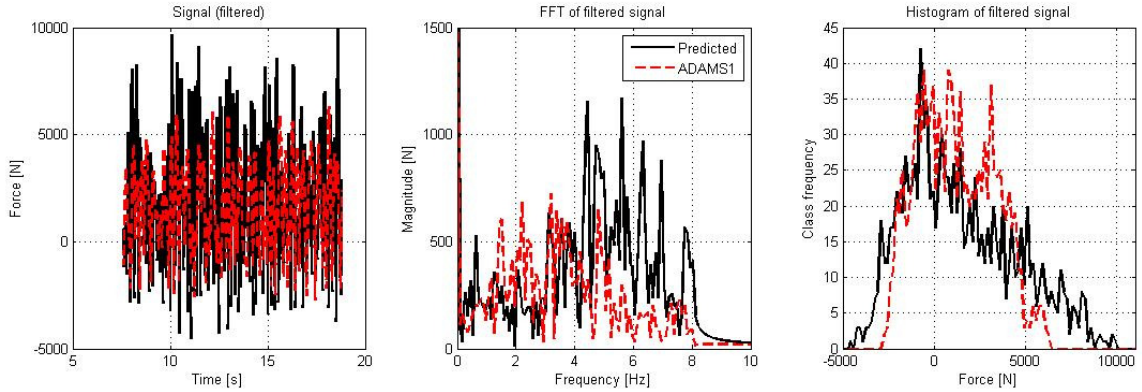

Figure F.10. Time-and frequency domain representation and histogram of left rear damper forces for load case 1.

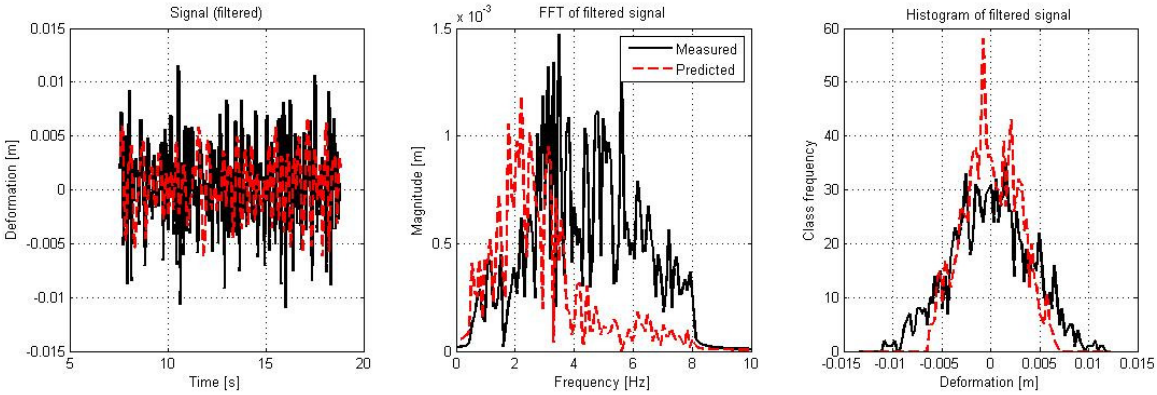

Figure F.11. Time-and frequency domain representation and histogram of left middle damper displacement for load case 1.

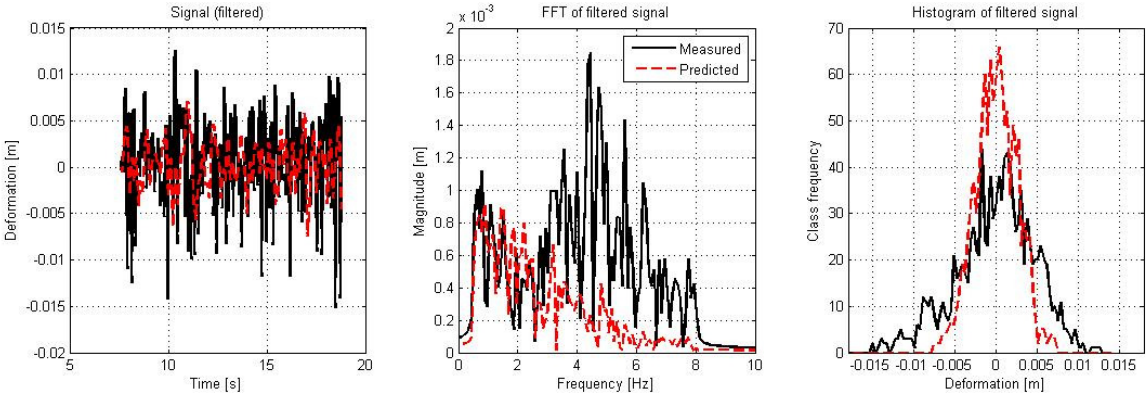

Figure F.12. Time-and frequency domain representation and histogram of left rear damper deformations for load case 1.

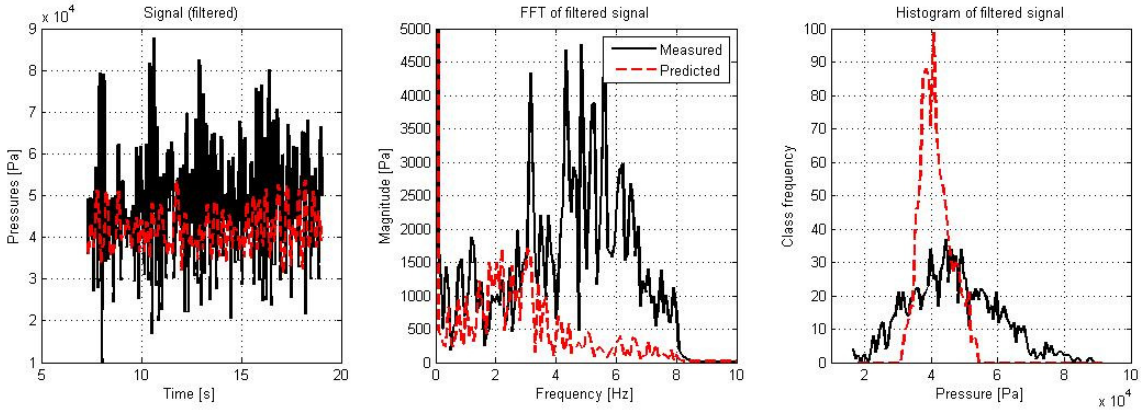

Figure F.13. Time-and frequency domain representation and histogram of left middle air spring pressure for load case 1.

Appendix G – Validation of MBS model: Load case 3

The correlation for load case 3 over the symmetric discrete obstacle, the asymmetric discrete obstacle and the rough road are shown in this appendix.

G.1. Correlation over symmetric discrete obstacle

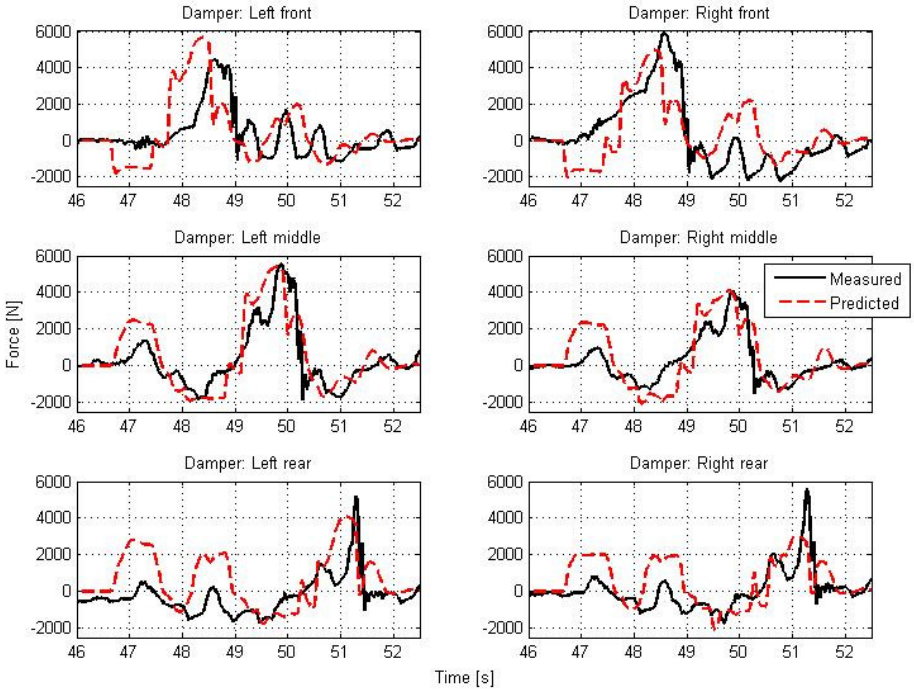

Figure G.1. Damper forces over symmetric discrete obstacle for load case 3.

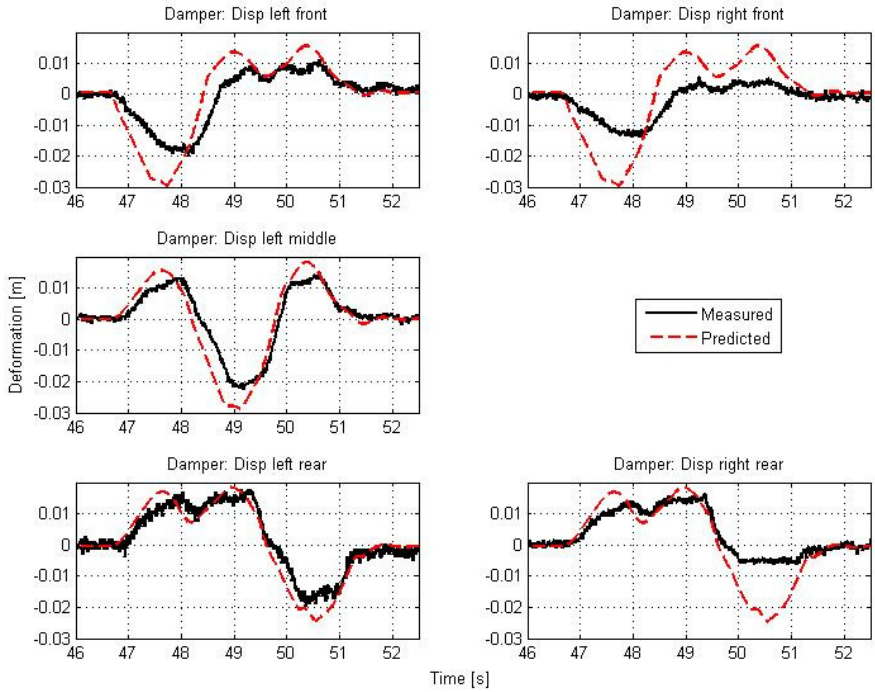

Figure G.2. Damper deformations over symmetric discrete obstacle for load case 3.

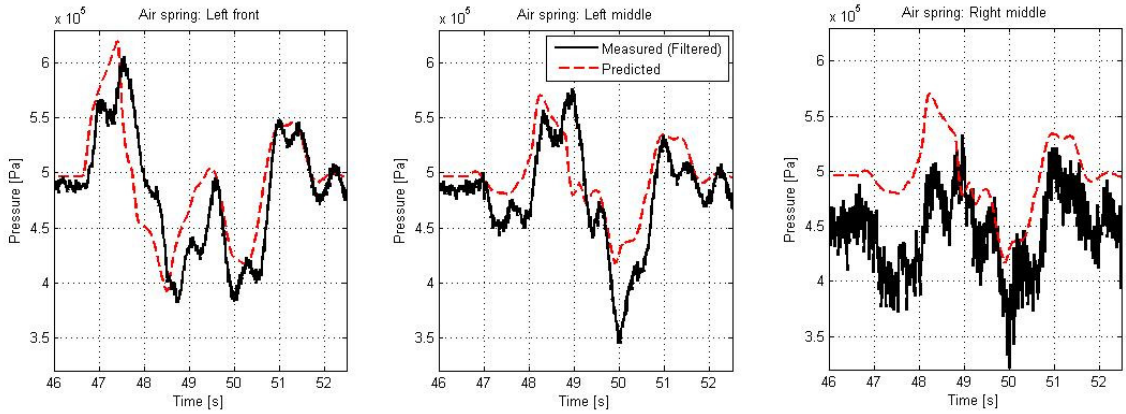

Figure G.3. Air spring pressures over symmetric discrete obstacle for load case 3.

G.2. Correlation over asymmetric discrete obstacle

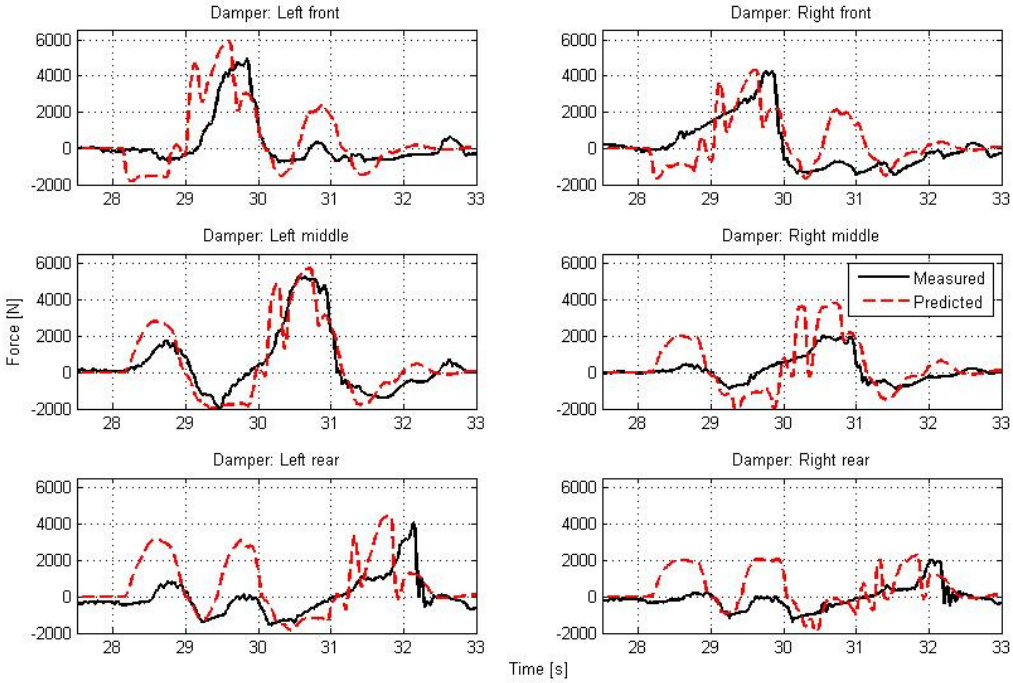

Figure G.4. Damper forces over asymmetric discrete obstacle for load case 3.

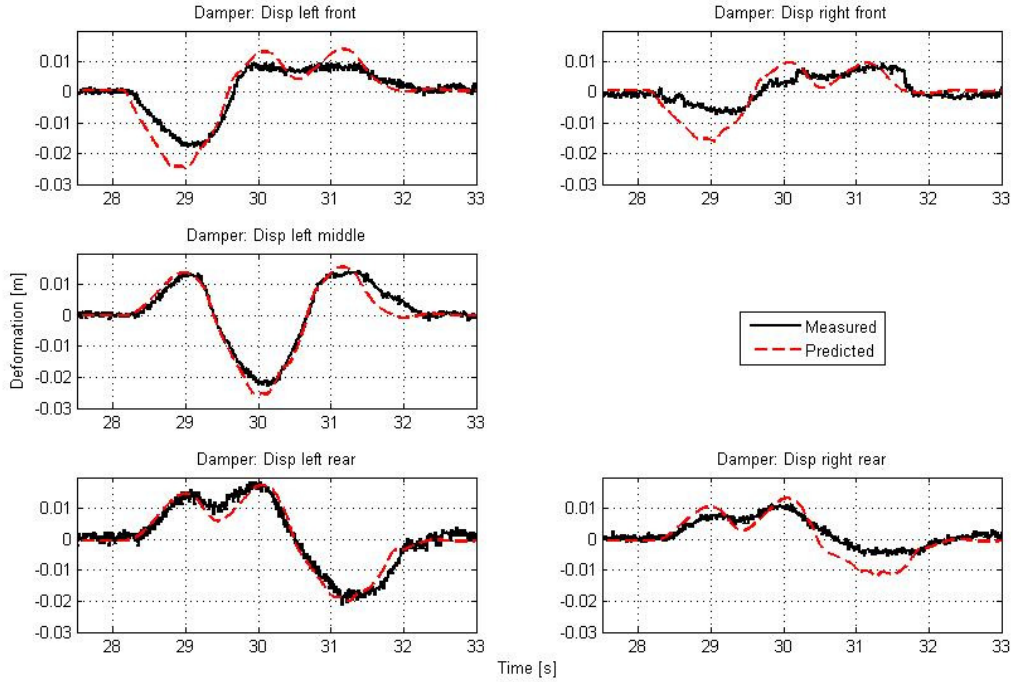

Figure G.5. Damper deformations over asymmetric discrete obstacle for load case 3.

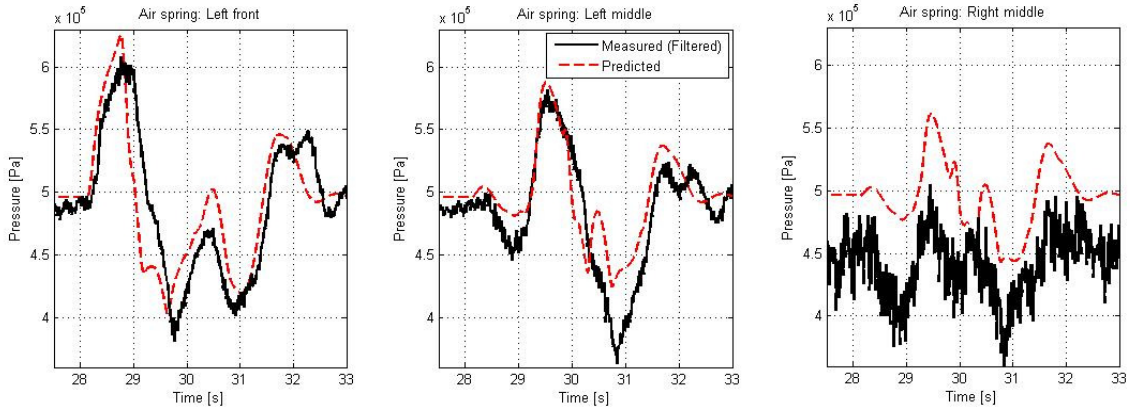

Figure G.6. Air spring pressures over asymmetric discrete obstacle for load case 3.

G.3. Correlation over rough terrain

Table G.1. Statistical representation of the correlation over a rough road for load case 3.

	Measured	Predicted	% difference
RMS of Body vertical acceleration	0.993	0.502	-49.45
RMS of Axle vertical acceleration	0.863	0.763	-11.59
RMS of Air spring pressures			
Left front	493658.34	491860.99	-0.36
Left middle	487553.03	486106.09	-0.30
Right middle	455505.02	451191.52	-0.95
RMS of Damper forces			
Left			
Front	1560.17	1782.35	14.24
Middle	1685.54	1964.09	16.53
Rear	1661.64	1827.87	10.00
Right			
Front	1649.41	1654.64	0.32
Middle	1202.88	1667.1	*38.59*
Rear	1702.31	1396.57	-17.96
RMS of Damper displacements			
Left			
Front	0.00275	0.00272	-1.09
Middle	0.00345	0.00327	-5.22
Rear	0.00361	0.0027731	-23.18
Right			
Front	0.00166	0.00263	*58.43*
Middle	No measurement	0.003125	
Rear	0.00289	0.00269	-6.92
Mean			**11.29**
Standard deviation			**13.32**

Note: Values in italics are not used in the calculation of the mean and standard deviation.

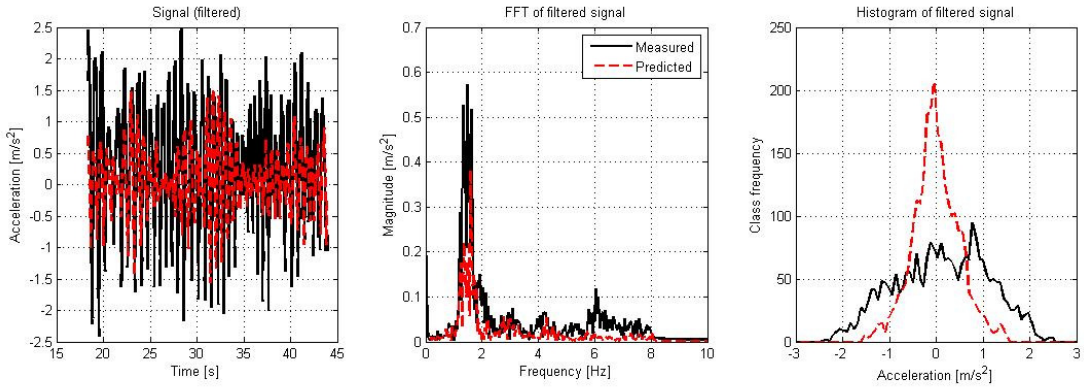

Figure G.7. Time-and frequency domain representation and histogram of body vertical acceleration for load case 3.

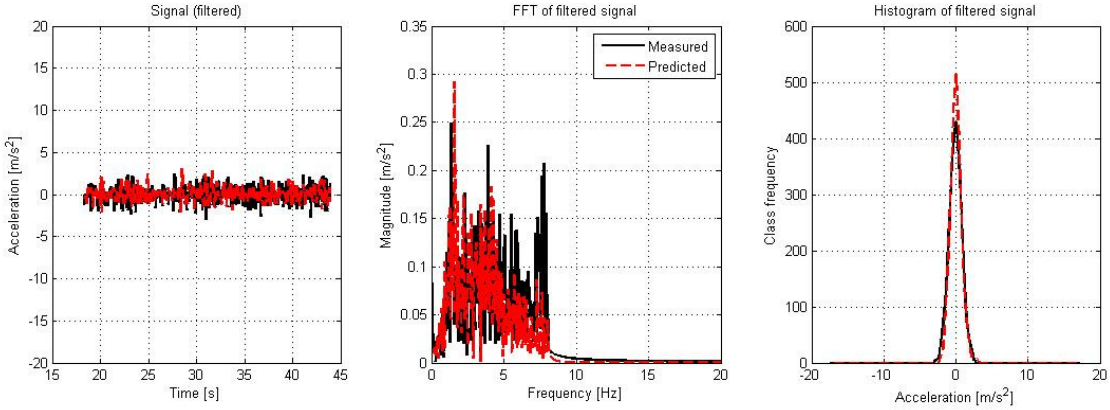

Figure G.8. Time-and frequency domain representation and histogram of axle vertical acceleration for load case 3.

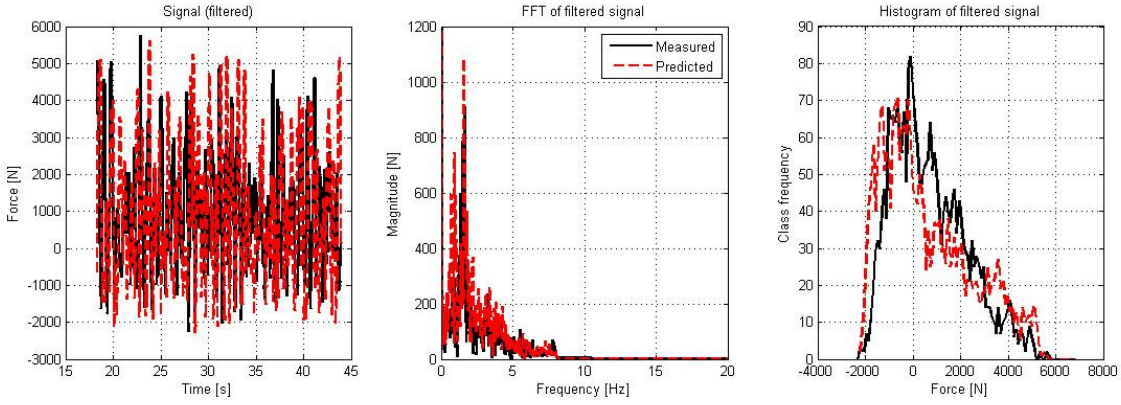

Figure G.9. Time-and frequency domain representation and histogram of left middle damper forces for load case 3.

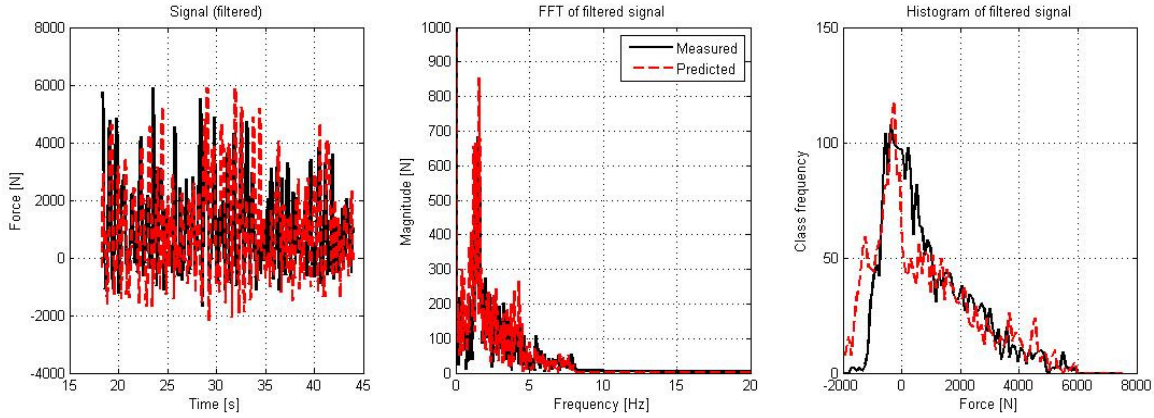

Figure G.10. Time-and frequency domain representation and histogram of left rear damper forces for load case 3.

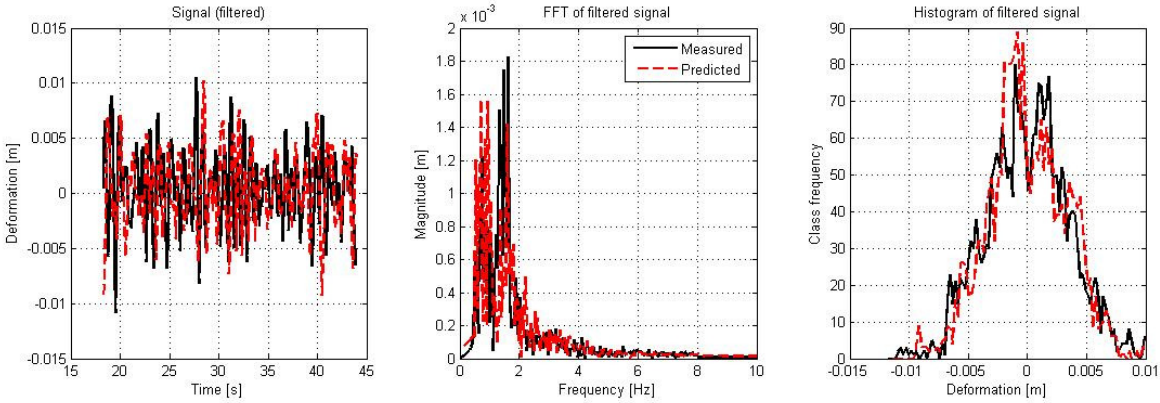

Figure G.11. Time-and frequency domain representation and histogram of left middle damper displacement for load case 3.

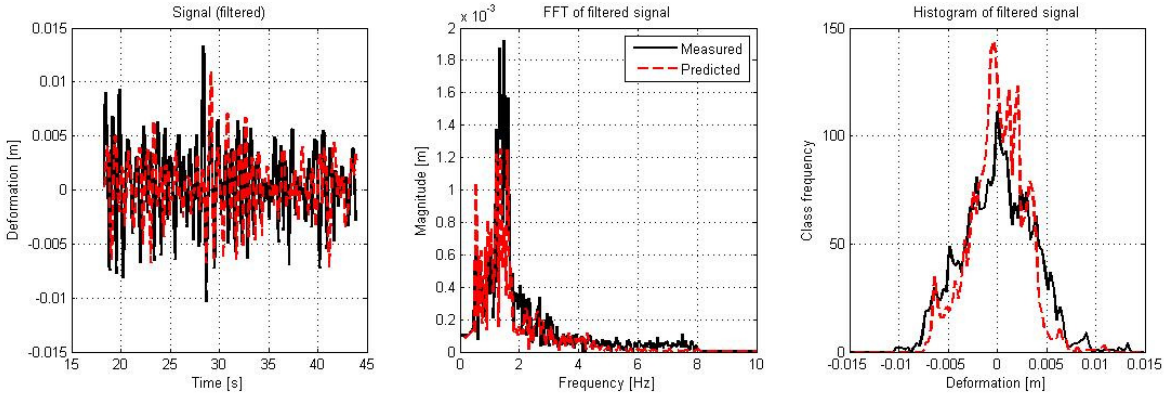

Figure G.12. Time-and frequency domain representation and histogram of left rear damper deformations for load case 3.

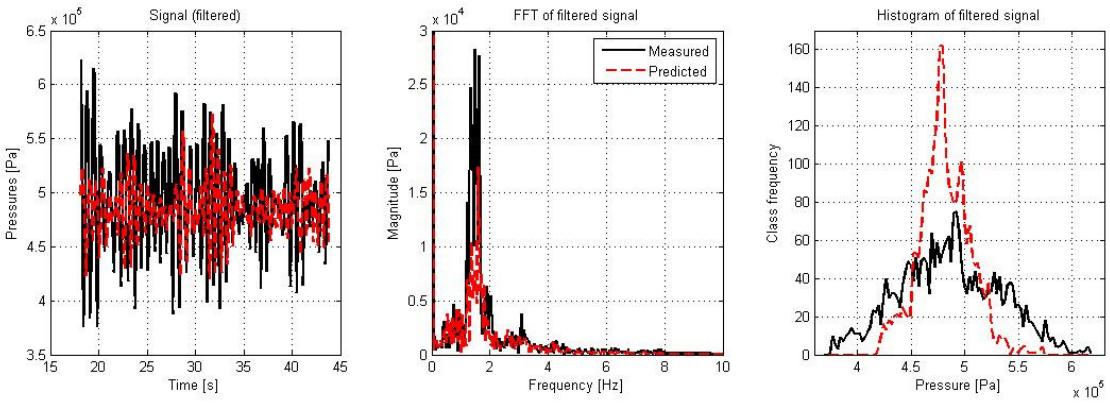

Figure G.13. Time-and frequency domain representation and histogram of left middle air spring pressure for load case 3.